Exploring the Applications of PBPK Modelling to Optimise HIV-1 Treatment

Thesis submitted in accordance with the requirements of the University of Liverpool for the degree of Doctor in Philosophy

By Fazila Sadik Bunglawala

March 2022

This thesis is the results of my own work. The material contained within the thesis has not been presented, either wholly or in part, for any other degree or qualification.

Fazila Bunglawala

This research was carried out in the

Department of Pharmacology and Therapeutics

Institute of Systems, Molecular and Integrative Biology

University of Liverpool, UK.

Table of Contents

Acknowledgements

As I sit here trying to articulate my words, I realise they might possibly fail in expressing my gratitude to you all, so I'll keep this short and sweet. To begin, I would like to thank the University of Liverpool for funding my PhD studentship. I would also like to extend my sincerest thanks to my primary supervisor Dr Marco Siccardi and my secondary supervisor Prof Andrew Owen, it has been a privilege to work alongside you both. The completion of this thesis could not have been possible without the constant support of my supervisor, mentor, friend and critic, Marco. The past 4 years have been fun, challenging (mostly for Marco), knowledgeable and most importantly, one of the best experiences. I have missed and will miss knocking on your door with my 'annoying' questions, be them about science or just life. You truly have been a great supervisor. I would also like to thank all the colleagues-now-turned-friends I have made over my years at 'H-block'. I will cherish the memories and friendships I have made during my time here.

Lastly, to my family and friends, thank you for listening to me 'passionately' discuss my PhD a countless number of times and for always encouraging and motivating me. I have appreciated it more than you know. To my mother, thank you for your kindness, generosity, endless love, and patience, I love you more than words could express.

Abbreviations

3TC	Lamivudine
AAFE	Absolute Average-Fold Error
ABS	Absorption
ADME	Absorption, Distribution, Metabolism And Excretion
AIDS	Acquired Immune Deficiency Syndrome
ART	Antiretroviral Therapy
ARV	Antiretroviral
AUC	Area Under The Curve
AUC_{av}	Average AUC over 28-day simulations
AUC_{24}	AUC over 24 hours
BIC	Bictegravir
BID	Twice Daily
BMI	Body Mass Index
BSA	Body Surface Area
CAB	Cabotegravir
C_{avg}	Average Plasma Concentration
CL	Clearance
CL/F	Apparent Oral Clearance
CL_{gut}	Gut Clearance
$CL_{int,CYP}$	Cytochrome P450 Enzyme Intrinsic Clearance
$CL_{int,CYP3A4}$	CYP3A4 Intrinsic Clearance
$CL_{int,E}$	Enzyme Intrinsic Clearance
$CL_{int,liver}$	Total Metabolic Intrinsic Clearance
CL_{sys}	Systemic Clearance

C_{max}	Maximum Plasma Concentration
C_{min} /C_{trough}	Minimum Plasma Concentration
C_{SI}	Small Intestine Concentration
$Conc_{soluble}$	Soluble Concentration
CV	Coefficient Of Variation
CYP	Cytochrome P450
CYP2C9	Cytochrome P450 2C9
CYP3A4	Cytochrome P450 3A4
D	Dose
D_{sol}	Solubility of Drug
$D^*_{vo:w}$	Olive Oil:Buffer Partition Coefficient Of Nonionised And Ionised Species at pH 7.4
DDI	Drug-Drug Interaction
DDI_R	Drug-Drug Interaction Ratio
DNA	Deoxyribonucleic Acid
DTG	Dolutegravir
E	Experimentally Determined
EFV	Efavirenz
F	Bioavailability
F_a	Fraction Of Drug Absorbed Across The Gi Tract
FDA	U.S Food And Drug Administration
F_g	Fraction Of Drug Escaping Metabolism In The GI Tract
F_h	Fraction Of Drug Escaping First-Pass Metabolism In The Liver
FTC	Emtricitabine
f_u	Fraction Of Unbound Drug In Plasma
$f_{u,b}$	Fraction Unbound In Blood

$f_{u,g}$	Fraction Unbound In The Gut
$fu_{Paediatric}$	Fraction Unbound in Paediatric Patients
$f_{u,t}$	Fraction Unbound In Tissue
GI	Gastrointestinal
gp120	Glycoprotein 120
gp41	Glycoprotein 41
HBD	Hydrogen Bond Donor
HBV	Hepatitis B
HCV	Hepatitis C
HIV	Human Immunodeficiency Virus
IC_{50}	Half Maximal Inhibitory Concentration
IM	Intramuscular
IV	Intravenous
IVIVE	In Vitro-In Vivo Extrapolation
K_a	Absorption Rate Constant
K_c	Colon Transit Rate Constant
K_m	Michaelis Constant
K_s	Transit Rates For Stomach
K_t	Small Intestine Transit Rate Constant
Log $P_{O:W}$	Partition Coefficient Between Octanol And Water
LPV	Lopinavir
LPV/r	Ritonavir Boosted Lopinavir
MDCK	Madin-Darby Canine Kidney
MDZ	Midazolam
MPPGL	Microsomal Protein Per Gram Of Liver
mRNA	Messenger RNA

NNRTI	Non-Nucleoside Reverse Transcriptase Inhibitor
NRTI	Nucleoside Reverse Transcriptase Inhibitor
NVP	Nevirapine
OATP	Organic Anion Transporting Polypeptides
OATP1B1	Organic Anion Transporting Polypeptides 1B1
PA-IC_{90}	Protein Adjusted 90% Inhibitory Constant
P_{app}	Apparent Permeability
P_{eff}	Effective Permeability
PBPK	Physiologically-Based Pharmacokinetic Modelling
PCR	Polymerase Chain Reaction
P-gp	P-Glycoprotein
PI	Protease Inhibitor
pK_a	Logarithmic Value Of The Dissociation Constant
pK_a1	Logarithmic Value Of The Dissociation Constant For Acid
pK_a2	Logarithmic Value Of The Dissociation Constant For Base
PLWH	People Living With HIV
PMTCT	Prevention of mother to child transmission
$P_{o:w}$	Partition Coefficient Between Octanol And Water
PrEP	Pre-Exposure Prophylaxis
PSA	Polar Surface Area
$P_{t:p}$	Adipose And Non-Adipose Tissue:Plasma Partition Coefficient
$P_{vo:w}$	N-Octanol:Buffer Partition Coefficient Of Nonionised Species at pH 7.4
PXR	Pregnane X Receptor
QD	Once Daily
Q_{gut}	Blood Flow To The Gut

Q_{3mo}	Every 3 months
Q_{mo}	Once Monthly
R	Blood-To-Plasma Ratio
RAL	Raltegravir
RIF	Rifampicin
RNA	Ribonucleic Acid
RPV	Rilpivirine
SD	Standard Deviation
SI	Small Intestine
ST	Stomach
TAF	Tenofovir Alafenamide
TB	Tuberculosis
TDF	Tenofovir Disoproxil Fumarate
TFV	Tenofovir
TFV-DP	Tenofovir Diphosphate
T_{max}	Time Of Maximum Concentration
UGT	Uridine 5'-Diphospho-Glucuronosyltransferase
UGT1A1	Uridine 5'-Diphospho-Glucuronosyltransferase 1A1
UGT1A3	Uridine 5'-Diphospho-Glucuronosyltransferase 1A3
UGT1A9	Uridine 5'-Diphospho-Glucuronosyltransferase 1A9
UNAIDS	Joint United Nations Programme On HIV/Aids
V_{nl}	Neutral Lipid Volume Fraction Of Wet Tissue Weight
V_p	Fractional Volumes Of Plasma
V_{ph}	Phospholipid Volume Fraction Of Wet Tissue Weight
V_{ss}	Volume Of Distribution
V_t	Fractional Volumes Of Tissue

V_w	Water Volume Fraction Of Wet Tissue Weight
WHO	World Health Organisation
W_{Liver}	Weight Of The Liver

Publications

Bunglawala, F., Rajoli, R.K.R., Mirochnick, M., Owen, A., Siccardi, M. Prediction of dolutegravir pharmacokinetics and dose optimization in neonates via physiologically based pharmacokinetic (PBPK) modelling. J Antimicrob Chemother. 2020;75(3):640-7.

Montanha, M.C., Fabrega, F., Howarth, A., Cottura, N., Kinvig, H., Bunglawala, F., Lloyd, A., Denti, P., Waitt, C., Siccardi, M. Predicting Drug–Drug Interactions between Rifampicin and Ritonavir-Boosted Atazanavir Using PBPK Modelling. Clin Pharmacokinet (2021). https://doi.org/10.1007/s40262-021-01067-1.

Montanha, M.C., Cottura, N., Booth, M., Hodge, D., Bunglawala, F., PBPK modelling of dexamethasone in patients with COVID-19 and liver disease. Front Pharmacol. 2022 Jan 28;13:814134. doi: 10.3389/fphar.2022.814134

Communications

Bunglawala F, Kinvig H, Comotti M, Cottura N, Capparelli E, Mirochnick M, Siccardi M et al. Dose optimisation of long-acting injectables in neonates via PBPK modelling. Scientific Spotlight presentation at Conference on Retroviruses and Opportunistic Infections (CROI); 2021 March; Virtual Event.

Bunglawala F, Howarth A, Kinvig H, Comotti M, Cottura N, Siccardi M et al. Mechanistic modelling for the quantitative evaluation of ARV penetration in lymphatic tissues. Themed discussion at International Workshop on Clinical Pharmacology of HIV, Hepatitis, and Other Antiviral Drugs; 2020 September 21-23.

Bunglawala F, Rajoli RKR, Kinvig H, Cottura N, Owen A, Siccardi M. Identification of age-appropriate dosing strategies of bictegravir in neonates. Themed discussion at Conference on Retroviruses and Opportunistic Infections (CROI); 2020 March 9-12; Boston, MA.

Bunglawala F, Rajoli RKR, Owen A, Siccardi M. Prediction of dolutegravir pharmacokinetics and dose optimization in neonates via physiologically based pharmacokinetic (PBPK) modelling. Poster presented at Conference on Retroviruses and Opportunistic Infections (CROI); 2019 March 4-7; Seattle, WA.

Abstract

Human immunodeficiency virus (HIV-1) infection continues to be a significant public health concern, with 36.3 million lives being claimed by the infection thus far. Currently there is no cure for HIV. Antiretroviral (ARV) therapy has considerably increased life expectancy in people living with HIV (PLWH), however, several challenges remain. This thesis investigates the various ways in which physiologically based pharmacokinetic (PBPK) modelling can be developed and applied with the aim of optimising treatment for human immunodeficiency virus (HIV-1) infection.

Neonatal patients are considered a vulnerable population as limited clinical studies are conducted in this population. Newborns born to mothers with HIV are at risk of receiving HIV. Lack of pharmacokinetic (PK) data means fewer treatment options are available. Chapters 2 & 3 focus on developing and applying a neonatal PBPK model to investigate the PK of integrase inhibitors, dolutegravir and bictegravir in neonates. Chapter 4 goes on to describe how modelling can be used to predict the PK of novel formulations by simulating long-acting, intramuscular, cabotegravir in neonates.

Polypharmacy is routinely observed in PLWH, and drug-drug interactions (DDIs) prove an obstacle in HIV treatment, Chapter 5 involved developing an adult PBPK model to evaluate the magnitude of moderate inducers on novel ARVs. Residual levels of viraemia hinder the ability to develop a cure, Chapter 6 investigated the penetration of ARV drugs in lymphoid tissues using a mechanistic lymphatic PBPK model. Understanding the penetration of drugs in target tissues can help optimise ARV therapy.

Collectively, this thesis evaluates the possible ways HIV treatment can be improved and optimised by investigating the potential of treatments in special populations, novel formulations of ARV drugs, management of drug-drug interactions and the penetration of therapy in target tissues.

CHAPTER 1

General Introduction

Contents

1.1 Pharmacokinetics

Pharmacokinetics (PK) can be split into four key stages: absorption, distribution, metabolism, and elimination (ADME) and involves the study of the rate and magnitude of drug movement through, into and out of the body. The PK behaviour of a drug dictates its efficacy [1, 2].

There are multiple routes of drug administration, the most common include, per oral (PO), subcutaneous (SC), intravenous (IV) and intramuscular (IM) injections, with other routes such as transdermal, rectal, sublingual etc. less frequently used [1, 2].

1.1.1 Absorption

Absorption is the process in which a drug moves from its site of administration into the bloodstream. Several factors determine the rate of drug absorption including the route of administration, formulation, physiology, and the drug's physicochemical properties. With exception of IV administration, drugs must cross numerous biological membranes and barriers before they reach the systemic circulation. An orally administered drug moves across the enterocytes located in the gastrointestinal tract (GIT) into the gut wall to the venous blood. For drugs that are administered IM or SC, factors such as tissue density, composition and vascularity influence the rate of absorption. [1, 2]

1.1.2 Distribution

Distribution of a drug refers to the movement of drug through the blood and tissues in the body. Distribution is also influenced by physicochemical and physiological properties, with blood flow to organs and tissues, protein binding and blood-to-plasma ratio playing a major role in drug distribution.

Blood-to-plasma ratio determines the concentration of drug in blood relative to plasma and gives an indication on drug binding to erythrocytes. Plasma protein binding is the phenomenon where drugs bind reversibly to proteins present in plasma depending on ionisability and lipophilicity of the compound and an equilibrium is established shortly after. Albumin is found in abundance in plasma, followed by lower concentrations of α-acid glycoprotein (AGP) and other proteins such as globulins. Only the unbound fraction of drug can go on to exert a pharmacological effect at the site of action. The extent of binding is dictated by the drug's affinity for the protein which is dependent on its structure and physicochemical properties in addition to protein and drug concentrations. Protein concentration can fluctuate between individuals based on several physiological characteristics. Highly bound drugs can be characterised by limited distribution in organs and tissues.

1.1.3 Metabolism

The liver plays a crucial role in the metabolism of compounds. Metabolism can be split into two stages: phase 1 and phase 2. Phase 1 metabolism involves reduction, oxidation, and hydrolysis reactions that lead to the formation of new or modified functional groups; these reactions are predominantly facilitated by cytochrome (CYP) P450 enzymes. Conjugation reactions are carried out in phase II metabolism by uridine 5'-diphospho (UDP)-glucuronosyltransferase (UGT) enzymes. Phase II reactions usually involve the addition of an endogenous moiety (e.g., sulphate or glucuronic acid) to the drug to increase the hydrophilicity of the compound, easing excretion from the body. Compounds can be metabolised by one or several enzymes. For certain drugs, metabolism can lead to the production of pharmacologically active metabolites.

Metabolism can also occur in the intestine, where CYP3A4 is present in the mucosa. Intestinal metabolism, as well as first –pass metabolism by the liver, can reduce the systemic exposure of certain orally administered drugs. Once absorbed in the GIT, drug moves to the liver via the portal vein from where it is either passively or actively transported across membranes after which it is subjected to metabolism and biliary excretion, this process is dubbed first-pass metabolism and can profoundly influence bioavailability of oral drugs. Bioavailability (F) can be defined as the proportion of drug that reaches the systemic circulation and is often expressed as a percentage. In a low number of cases metabolism can also occur in other tissues such as the lungs and the kidney

1.1.4 Elimination

Drug elimination is the process in which drug is removed from the body irreversibly, in its metabolite form or unaltered, by the kidneys and/or the liver. Renal elimination can be summarised into three processes: tubular secretion, glomerular filtration, and passive reabsorption. Drugs can also be removed in the bile or excreted in faeces.

1.1.5 Quantitative Pharmacokinetic Parameters

The PK properties of a drug are deduced by studying concentration-time profiles following administration, a typical PK profile for an orally administered drug has been highlighted in Figure 1.1. Routinely used parameters to quantify PK include the maximum plasma concentration (C_{max}), minimum plasma concentration (C_{min}), area under the curve (AUC), the time taken to reach C_{max} (T_{max}) and clearance (CL). Clearance, defined as the volume of blood/plasma cleared of a drug over a given time period, can be expressed in multiple forms including, systemic clearance

(CLsys) or apparent clearance (CL/F) which is customarily used for oral drugs and takes into account bioavailability. [2]

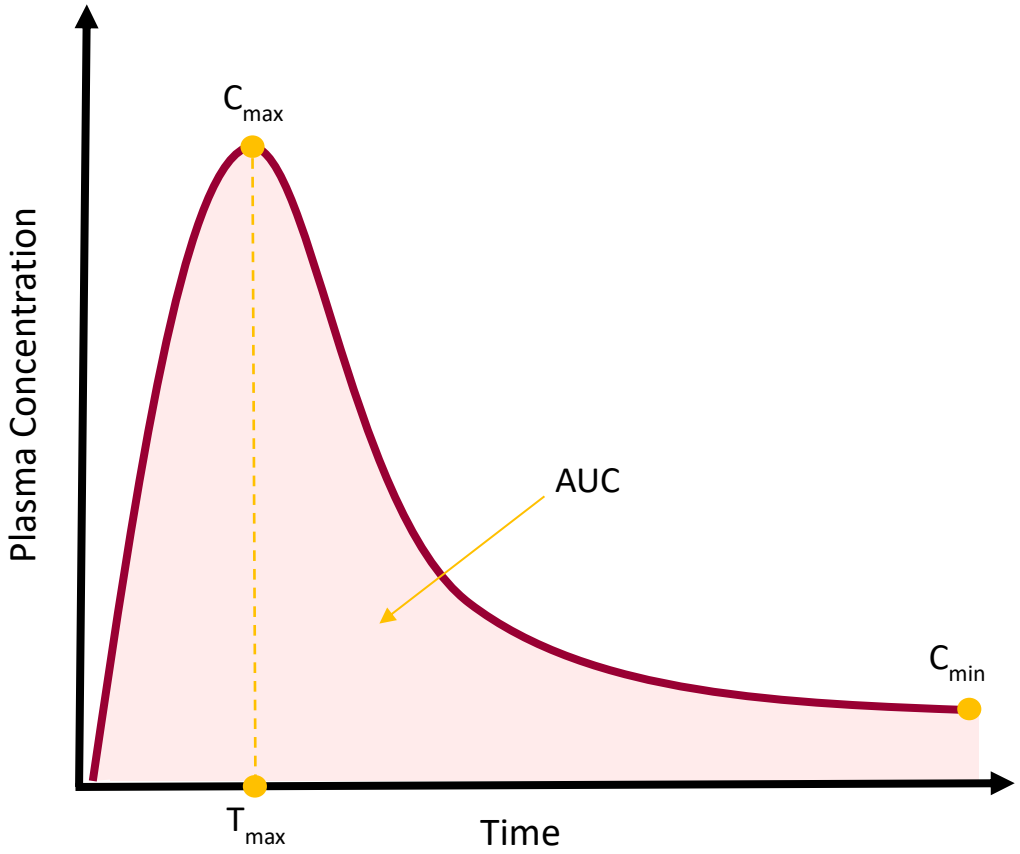

Figure 1.1 Concentration-time plot example following oral administration of a drug. Plasma concentration is plotted on the y-axis and time is plotted on the x-axis. Key PK parameters maximum concentration (C_{max}), minimum concentration (C_{min}), time taken to reach C_{max} (T_{max}) and area under the curve (AUC) have been highlighted within the figure

1.2 Physiologically Based Pharmacokinetic Modelling

Over the past two decades, physiologically based pharmacokinetic (PBPK) modelling has received widespread attention. Failures in the late stages of drug development can be costly so the ability to evaluate potential risks ahead of time is greatly favoured. Industries and regulatory bodies are becoming increasingly

interested in using PBPK modelling techniques in early drug discovery stages to facilitate drug development [1].

1.2.1 General Structure

PBPK modelling can be classed as a bottom-up approach that employs observed clinical data and *in vitro* data. PBPK modelling involves simulating important drug processes by integrating previous knowledge on organism and drug specific characteristics [3]. This modelling technique mimics the structure of the biological system being studied e.g., rat, monkey, human etc. and comprises distinct compartments that correspond the physiology of tissues and organs which are connected via the circulating blood system [3, 4]. Blood circulation is subdivided into a venous and arterial pool. The choice of compartments represented in a model often reflect the data that is available on the anatomical and physiological characteristics of the biological system and is also dependent upon the overall application/purpose of the model. Typically, each compartment is defined by a blood flow rate and tissue volume; a tissue is described as either permeability rate limited, or perfusion rate limited [3, 4]. Most PBPK models assume perfusion rate limited kinetics (rate at which blood is delivered to tissue) which is generally justified for small, lipophilic compounds. For larger, more polar compounds permeability across the cell membrane becomes the limiting step, in this instance, permeability rate limited kinetics is justified. It is also assumed that compartments are well-stirred and drug distribution is instantaneous [3-6]. Figure 1.2 below illustrates a typical schematic of a whole-body PBPK model.

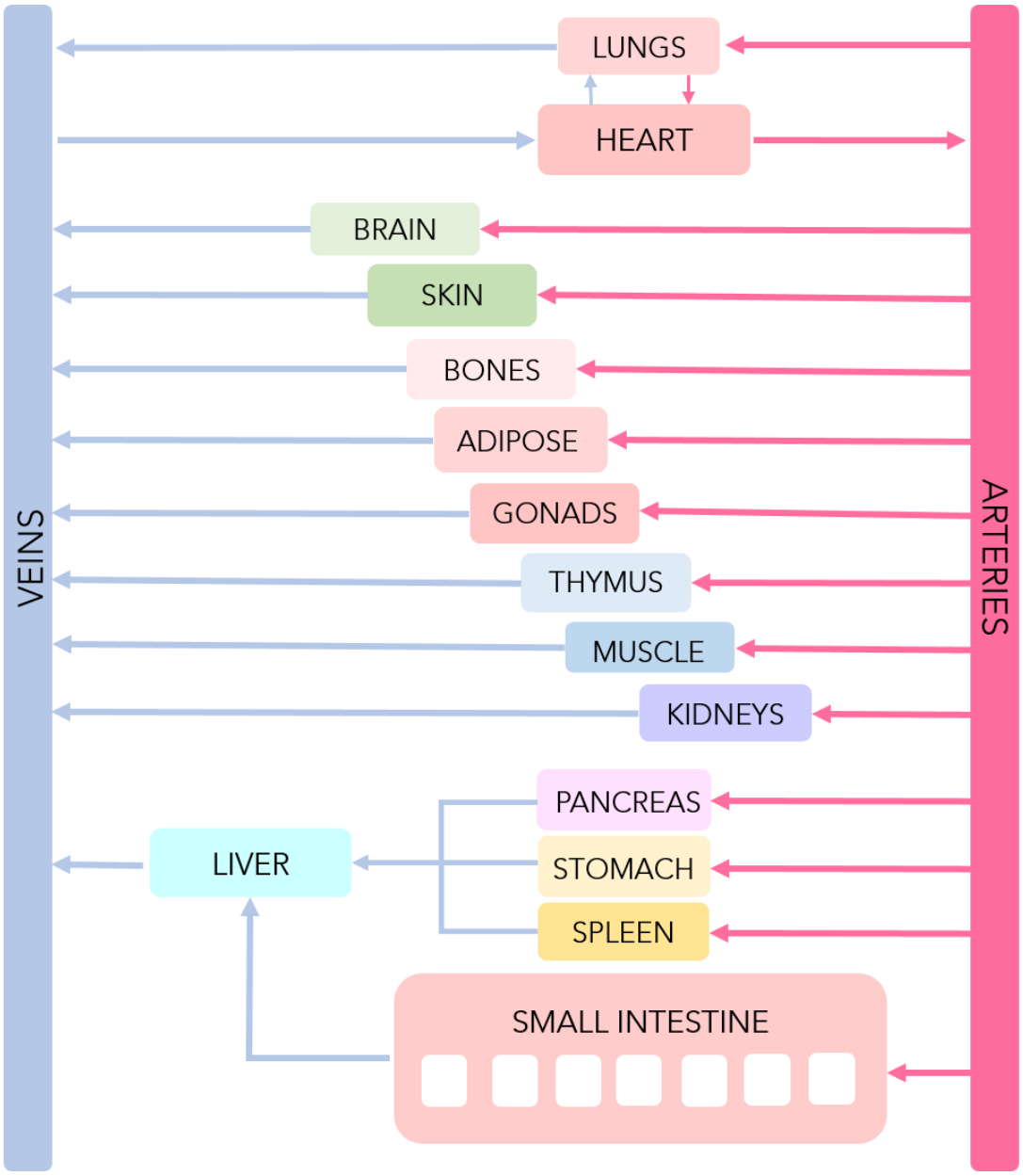

Figure 1.2 Whole-body PBPK model comprising tissues and organs as compartments. The small intestine is further divided into seven sub-compartments for absorption modelling. Arrows represent direction of blood flow.

1.2.2 Mathematical equations to represent drug distribution

The equations used in a PBPK model are fundamentally mass balance equations derived from the law of mass action; they are used to describe the rate of change of the amount of drug within compartments [3]. Four different types of mathematical

equations have been used in models thus far: 1) linear ordinary differential, these are routinely used to describe the dynamic pharmacokinetic processes, 2) non-linear differential, these equations are used when non-linear processes are present within particular tissues (e.g. binding and/or concentration-dependent elimination), 3) partial differential, when dispersion models are assumed, partial differential equations are implemented, 4) algebraic, these equations are used when processes are assumed to be static. [3, 4]

1.2.3 Drug and patient specific input data

Once equations have been distinguished, the model requires input parameters, these can be split into two main categories: physiological and drug-specific parameters. The physiological input parameters are needed to characterise the physiological processes and anatomical structure of the species being studied (e.g., body weight, height, blood flows, organ weights and volumes, enzyme ontogenies etc.) [1, 3, 4]. These parameters are usually informed by pre-existing literature data. Drug-specific parameters such as: solubility, partitioning (e.g., tissue: plasma coefficients and blood: plasma ratios) protein binding, logP, clearance etc. are used to characterise ADME related processes. Tissue: plasma partition coefficients represent an important input parameter for models as they describe and quantify the partitioning of drugs between plasma and tissues at steady-state. Drugs-specific parameters like these can be derived from *in silico* predictive models based on the structure of the compound, *in vivo* methods, or *in vitro* experiments [2].

A significant part of PBPK modelling is its reliance on extrapolation from experimental data, also known as *in vitro in vivo* extrapolation (IVIVE). The scaling up of clearance is an important example of this method, where the intrinsic clearance of a compound is determined using *in vitro* systems e.g., hepatocytes (uL/min/million cells) and microsomes (uL/min/mg) and scaled up using parameters

including: MPPGL, the microsomal protein per gram of liver or the number of cells per gram of liver and the weight of the liver [3, 6, 7].

1.2.4 Qualification

Since its introduction, PBPK modelling has rapidly evolved from informing first-in-human (FIH) doses to early testing of lead compounds during drug development. Its approval from regulatory bodies has led to the development of guidelines assessing model performance by the EMA for PBPK modelling and simulations developed for submission [8].

Generally, the aim of the PBPK model should be clearly defined including key information on the target population(s), investigational drug(s) and dose(s) etc. Once anatomical and physiological equations have been defined for the biological system being studied, it is important to run initial simulations to ensure the population is appropriately represented within the model. For more complex physiological parameters such as enzyme ontogenies a more thorough approach is applied, where a probe drug metabolised solely by the enzyme of interest is used to characterise its activity. In general, to qualify a model, drugs with similar ADME properties to the compound of interest with observed clinical data available in the target population should be used. For each drug used in the qualification and prediction process, the physicochemical, *in vitro*, *in vivo* data should be supplied. Where possible, multiple data sets should be used to qualify the model to cover a range of PK characteristics that could potentially influence the output. [8-10]

To assess the quality of predictions the absolute average fold error (AAFE) (Equation 1) is commonly calculated with a generic acceptance criterion of 2-fold (± 100% of observed value). If predictions fall within 2-fold the model is assumed qualified [10].

$$AAFE = 10^{\left|\frac{\Sigma \log \frac{Predicted}{Actual}}{N}\right|} \quad (1)$$

As model development is an iterative process, qualification of models can be an iterative process too. As more data becomes available or a better understanding of mechanisms is gained, models are constantly refined and validated.

It is important to ensure appropriate representation of physiological processes using mathematical descriptions. When appropriately qualified, models can increase confidence in predictions and extrapolations made outside of the studied scenarios.

1.2.5 Tools and Application

All models detailed in this thesis were built and developed in SimBiology®. This software provides tools for modelling, simulating, and analysing dynamic systems, centring on not only physiologically-based pharmacokinetic modelling but quantitative systems pharmacology (QSP) and pharmacokinetic/pharmacodynamic (PK/PD) applications. There is flexibility in model development and models can be built using the block diagram editor or by code using the MATLAB® language. This modelling software provides a range of techniques to analyse ordinary differential equation (ODE)-based models and simulations can be run to predict PK, test different frequencies of dosing, identify optimal dosing regimens etc. It is worth mentioning that several other commercial software's are available for PBPK modelling including GastroPlus, SimCYP, PK-Sim, PK Quest etc. However, due to cost restraints, scope, and application, SimBiology® was deemed the best fit for model development.

The recognition of PBPK modelling as a valuable pharmacological tool has led to several applications of this technique, some of which will be discussed herein. PBPK

modelling has proved itself a versatile tool in exploring multiple scenarios expanding quantitative drug PK studies.

1.2.4.1 Special/Complex Populations

Clinical trials are generally conducted in healthy adults between the ages of 18-30 years and typically exclude those that do not fit these criteria. Several patient specific characteristics such as age, weight, pregnancy, hepatic/renal impairment etc. can cause significant changes in drug absorption, distribution, metabolism, and elimination [11] however clinicians and researchers face multiple challenges which impede the ability of investigating drugs directly in such vulnerable populations. Variability from the standard testing population can mean alterations in dose, administration routes and frequency of dosing may be necessary. Limited knowledge on how these individual parameters affect the PK of drugs mean fewer therapeutics options are available and as a result lead to off-label use [11, 12].

Neonates, more specifically, represent a unique population; the rapid developmental changes observed during this period are complex and require drugs to be investigated directly in order to use them safely [11, 13-16]. PBPK models have been extensively developed to cover special populations by integrating knowledge on the physiological and anatomical changes that occur and can provide information on individualised drug therapies to deduce optimal dosing regimens [7]. For most special population PBPK models, the structure is adapted from an already validated adult PBPK model as described earlier. Appropriate changes in anatomy and physiology are considered using mathematical equations and/or additional compartments. To provide more confidence and support clinical trial design PBPK methods are more routinely being employed to predict dosing in paediatrics and neonates prior to conducting clinical trials [17]. An in-depth review

of existing PBPK models and challenges faced in the modelling of term and preterm neonates has been previously outlined [17].

Recently the exposure of efavirenz (EFV) in pregnancy was predicted via PBPK modelling [18]; Chetty et al evaluated a lower dose of EFV (400 mg) in pregnant women to determine whether this dose would not be therapeutically inferior to a 600 mg dose in pregnancy as had been clinically observed in the non-pregnant population. The model was validated using available clinical PK on a 600 mg dose of EFV in pregnancy [18]. Interestingly their results suggested a 2-fold increase in clearance in the third trimester of pregnancy in comparison to clearance before pregnancy [18]. Significant changes are observed in the maternal body including enzyme activity [19], which can lead to greater inter-individual variability in the PK of certain drugs, highlighted in the aforementioned study. The advancement of model-informed doses can help fill these knowledge gaps by incorporating population-specific data [19].

Extremities in age often pose ethical and logistical challenges in clinical trials, with elderly and paediatric patients undergoing significant developmental changes [11, 19, 20]. In elderly patients' changes are observed in, gastrointestinal motility, gastric pH, tissue volumes, glomerular filtration rates (GFR), total body water etc. these changes can affect the overall disposition of numerous drugs [20]. A comprehensive PBPK model for the elderly was developed with the aim of understanding which parameters most influenced the disposition of several drugs (midazolam, metoprolol, lisinopril, amlodipine, rivaroxaban, repaglinide, atorvastatin, rosuvastatin, clarithromycin and rifampicin) in this population [21]. The study investigated age-dependent correlations for each PK parameter e.g., AUC, C_{max}, clearance etc. and concluded changes in exposure were attributed to a progressive decrease in renal and hepatic blood flows as well as GFR and were more likely due

to altered clearance than absorption or distribution [21]. Such models provide insights into the important biological processes that are affected in special populations, thus being beneficial in the development of treatment regimens and informing clinical trial design.

1.2.3.2 Co-morbidities

An advantage of PBPK modelling is its ability to incorporate the biological and pathophysiological changes observed in organ impairment and predict its resulting effect on drug PK, allowing the study of otherwise complex clinical scenarios. Co-morbidities such as liver or renal impairment can significantly affect the PK of certain drugs through different mechanisms and in the most severe cases a dose adjustment may be necessary for efficacy and safety reasons. Reduced tubular secretion and glomerular filtration, hypoalbuminemia (low levels of albumin in the blood) and accumulation of uremic toxins are all characteristics of renal impairment [22]. These changes can lead to a reduced clearance of drugs that are majorly eliminated by renal and/or metabolic pathways. Liver impairment can be characterised by a decrease in hepatic blood flow, albumin, alpha-acid glycoprotein, hepatocytes, haematocrit and can be caused by numerous chronic disease conditions [23]. Several other changes are associated with liver cirrhosis including, changes in transporter and enzyme expression and activity; highlighting the importance to understand and evaluate the effect of such morbidities on the PK of therapeutics.

A model describing the PK of ceftazidime was developed with the aim of predicting the PK in renally impaired patients [24]. Ceftazidime is a commonly used antibacterial that is eliminated from the body through glomerular filtration. The severity of renal impairment was categorised in the model as healthy, mild,

moderate and severe. The model successfully predicted the PK of ceftazidime in all four renal impairment categories with simulations within 1.5-fold of observed data [24].

1.2.3.3 Novel Formulations

Novel formulations are continually being developed to effectively deliver drug to target sites and improve drug efficacy and safety. They can be used to enhance the ADME characteristics of drugs. Novel formulations include, delayed/sustained release, long-acting, targeted release, modified release and many others.

Sustained or delayed release drug delivery is where the drug/ active ingredient is released at a certain event, this type of formulation controls where and when drug is released. Orally administered therapeutics are subjected to different environments before entering the systemic circulation as discussed previously, of these, the stomach can prove an obstacle for certain drugs. The acidity of stomach fluids can cause drugs to breakdown before they have completed their therapeutic journey. An example of sustained/delayed release formulation includes a drug releasing only when it reaches an alkaline environment like the small intestine, avoiding breakdown in the stomach. [25, 26]

Long-acting (LA) formulations are another example of novel formulations. The main advantage of LA therapeutics is a reduced pill burden. Patients with chronic illnesses on life-long therapy can experience pill fatigue from multiple, frequent medications and can benefit from a less regular drug administration, leading to better therapy outcomes. LA therapies are commonly used in psychotic disorders and also in contraception e.g., medroxyprogesterone acetate, a contraceptive that is administered as an intramuscular or subcutaneous injection [27-29].

PBPK modelling can effectively model novel formulations to provide valuable information on doses, frequency of dosing, routes of administration, distribution to tissues etc. [30]

1.2.3.4 DDI Prediction

Drug-drug interactions (DDIs) can negatively impact therapies and clinical management is faced with numerous challenges. Drug metabolism, dosing, administration routes, age, gender, weight, comorbidities etc. all play a role in the cause and extent of interactions. With a 20-40% prevalence, a reduction in clinical efficacy or adverse drug reactions are consequences of DDIs and can further complicate treatments.

PBPK can predict differences in drug exposure and DDI magnitude enabling the identification of dose optimisation strategies. Screening for potential DDIs can be evaluated more efficiently using this modelling technique, PBPK DDI studies can deduce whether dose adjustments are needed, to what extent, dose frequencies and whether a DDI can be overcome, all in different populations.

1.2.6 Limitations

Although PBPK modelling is an advantageous pharmacological tool, it isn't without limitations. The input information required for PBPK modelling can be complex and wide-ranging, data on the physiological and anatomical characteristics of the biological system to the physicochemical and biochemical processes involved in drug PK are necessary for simulations. Obtaining these data can be met with several challenges, complex mechanisms underpinning a drug's ADME properties such as the effect of transporters, expression of transporters, ontogeny of enzymes in different age groups/systems etc. are difficult to define using *in vitro* methods and further complicated by IVIVE. Data is routinely collated from multiple sources and

can be conflicted while other parameters are poorly characterised causing knowledge gaps in certain areas. These knowledge gaps can hinder the ability of models to capture important processes and in turn generate poor simulations. The quality of models often mirrors the availability of current scientific knowledge regarding the topic of interest.

There is also a heavy reliance on preclinical data and extrapolation between different species can be a challenge. The use of correction factors is commonly practiced in modelling and come as a consequence to the above-mentioned limitations. Where poor predictions of drug properties such as distribution or absorption lead to the use of adjustments based on observed data when possible. Predictive models for processes like distribution are limited in their ability to characterise therapeutics that fall outside of the defined properties that determine distribution due to unique mechanisms that have not been elucidated. Therefore, a detailed understanding on the ADME, physicochemical and biological determinants of a compound are pivotal for successful modelling.

Qualification of models with observed clinical data can also represent a challenge. For special population PBPK modelling, the modeller can frequently find themselves struggling to acquire good quality clinical PK data for the qualification of a model. To evaluate a model's performance, comparison against observed data is essential. Good quality clinical data include a large sample population (to encompass variability), several dose scenarios (single/multiple dosing and varying amounts) and, ideally, should closely match the clinical scenario to be simulated where possible. Unfortunately, in special population modelling obtaining such data can be incredibly challenging due to the lack of data available. Clinical studies are routinely carried out in healthy 18–35-year-olds and data in vulnerable populations is

relatively sparse in comparison, further complicating qualification stages. When this is the case, observed data that closely match the simulated scenarios are used.

Overall, PBPK modelling is a fairly comprehensive approach that requires time, significant experience and numerous resources, however, its potential in drug discovery and development is vast.

1.3 Human Immunodeficiency Virus

The human immunodeficiency virus (HIV) has been suggested to be first introduced in humans around 1920 to 1940 but was discovered in 1983. Since the start of the epidemic, 79.3 million people have become infected with HIV and 36.3 million people have died. Globally, 37.7 [30.2 million–45.1 million] million people were living with HIV (PLWH) in 2020 (UNAIDS) though the number of new infections have been reduced by 52% relative to the peak in 1997, where 3 million new infections were recorded. [31]

1.3.1 HIV Structure

The virus is of the genus Lentivirus and belongs to the family of Retroviridae. With a diameter of ~100-200 nm, the virion has a spherical shape [31]. The outer most layer of HIV is known as the viral envelope and is composed of a lipid membrane derived from the host cell. Along the surface of the membrane exist trimers of glycoprotein (gp), gp120 is essential for viral attachment and gp41 mediates viral fusion [32-34], both are imperative for the virus to gain entry. Inside the virus is a layer known as the matrix, comprising gag proteins [35]. Within the virus is a cone-shaped structure called the capsid, inside which important enzymes such as reverse transcriptase, integrase, and two copies of ribonucleic acid (RNA) are present.

1.3.2 HIV Replication Cycle

The first stages of producing new viruses involves attachment and fusion [34]. The main target for HIV is immune cells with CD4+receptors i.e., T-lymphocytes (t-cells), macrophages, dendritic cells, and monocytes. Upon contact with a CD4+ cell, HIV binds to the host cell membrane receptors, with help from gp120 [32-34]. The HIV envelope is then fused to the cell wall using gp41, releasing the capsid into the host cell cytoplasm [34]. HIV RNA enters the cell and is reverse transcribed into deoxyribonucleic acid (DNA) using the enzyme reverse transcriptase [36]. Once converted, the integrase enzyme attaches itself to the viral DNA prior to passing through the wall of the cell nucleus [37]. The viral DNA binds to the host DNA once inside the nucleus and with the help of the integrase enzyme it inserts itself into the host DNA [37]. HIV remains dormant within the cellular genome, this phase is known as latency with cells being referred to as 'latently infected'. [38]

If a signal is received to become active, HIV RNA will be produced by the cell. Host enzyme RNA polymerase is used to make messenger RNA (mRNA), which facilitate the production of viral proteins.

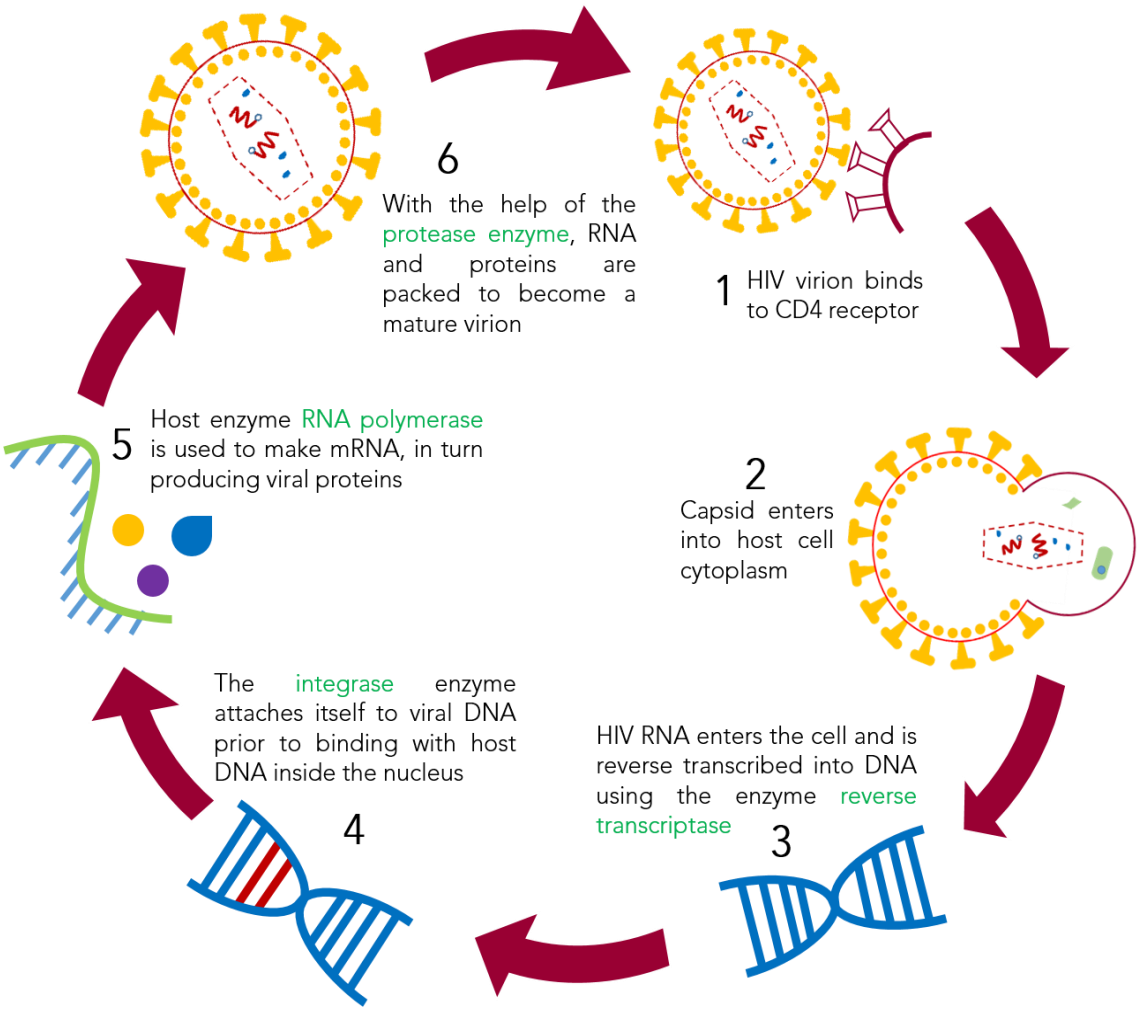

Figure 1.1 HIV replication cycle.

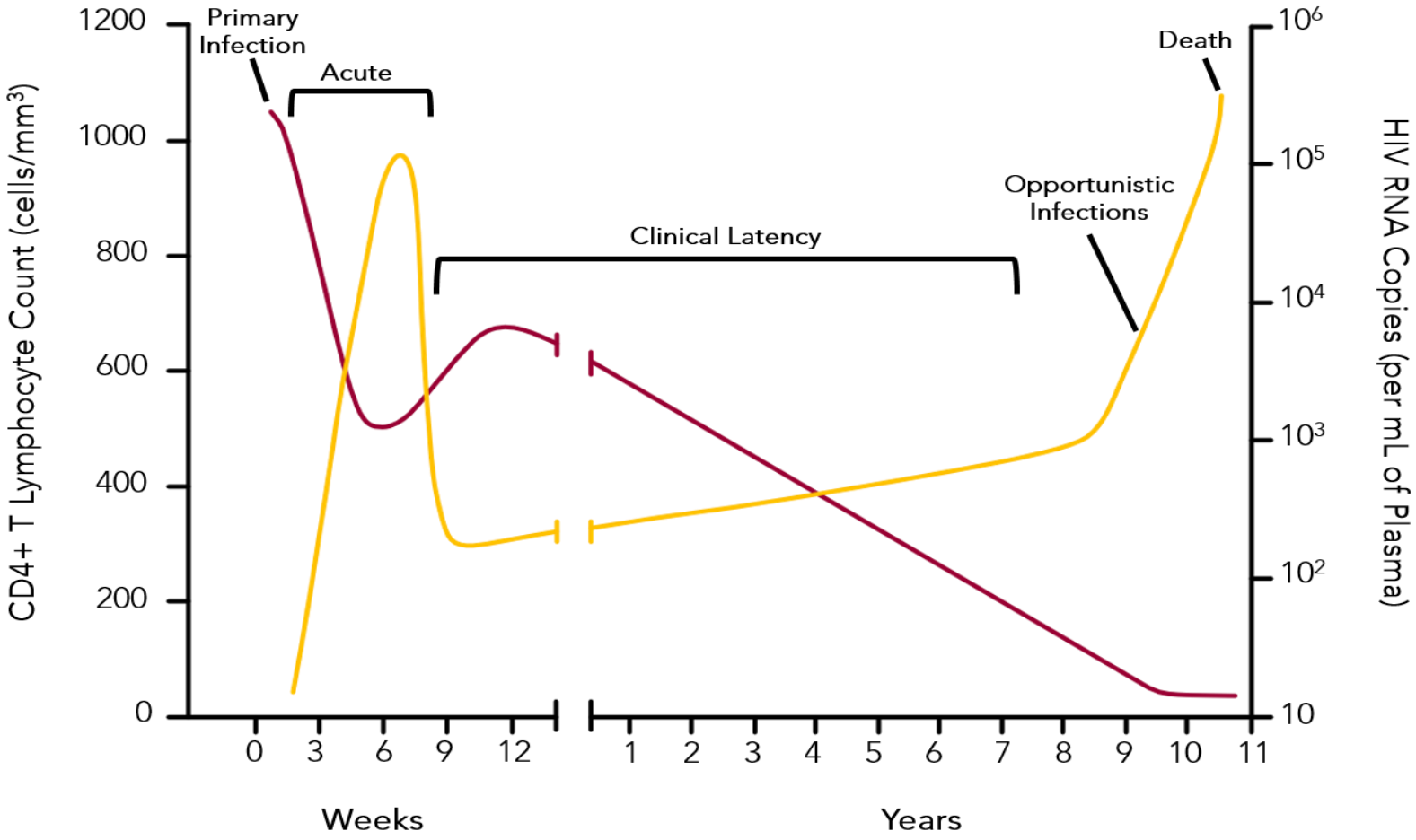

Figure 1.3 Untreated HIV disease progression. Orange line represents HIV RNA copies and burgundy line represents CD4+ T lymphocyte count. With stages of primary infection, acute, clinical latency, opportunistic infections, and death highlighted within the figure.

1.3.3 Antiretroviral Therapy

The high mortality and morbidity associated with HIV has substantially decreased since the introduction of highly active antiretroviral (ARV) therapy (HAART) in the late 90s [39]. HAART is a medication regimen used to treat and manage HIV-1. Traditionally consisting of a combination of at least three ARV drugs, of which two must belong to one of the classes of ARVs [40], recent guidelines now favour two-drug regimens and on occasion 3 NRTIs. Each class of drug is focused on inhibiting a specific stage of the viral replication cycle. A number of ARV guidelines recommend therapy should be initiated in all adults living with HIV at any CD4 cell count [40, 41]. Some of the most recently approved ARVs have been listed in Table 1.1.

Table 1.1 FDA's most recently approved antiretrovirals with brand names and approval dates.

Drug	Brand Name	FDA Approval Date
Maraviroc (MVC)	Selzentry	6th August 2007
Raltegravir (RAL)	Isentress	12th October 2007
Etravirine (ETR)	Intelence	18th January 2008
Rilpivirine (RPV)	Edurant	20th May 2011
Dolutegravir (DTG)	Tivicay	13th August 2013

Cobicistat (COBI)	Tybost	24th September 2014
Tenofovir Alafenamide Fumarate (TAF)	Genvoya, Odefsey, Descovy, Biktarvy, Symtuza	2015-2018
Ibalizumab-uiyk (IBA)	Trogarzo	6th March 2018
Doravirine (DOR)	Pifeltro	30th August 2018
Fostemsavir (FTR)	Rukobia	2nd July 2020
Cabotegravir (CAB)	Vocabria	22nd January 2021
Adapted from HIVinfo.NIH.gov and FDA.gov.		

1.3.3.1 Nucleoside reverse transcriptase inhibitors (NRTIs)

NRTIs target viral reverse transcriptase (RT) via competitive inhibition to prevent the synthesis of viral DNA. Cellular kinases facilitate the catalytic conversion of NRTIs to its active triphosphate form which exerts antiviral activity [42].

Zidovudine was the first NRTI to be approved by the FDA used in the treatment of HIV infection and was initially given to patients as monotherapy. Shortly after, dual therapy was introduced as more NRTIs were approved for use, including, didanosine, stavudine and lamivudine.

1.3.2.2 Non-nucleoside reverse transcriptase inhibitors (NNRTIs)

NNRTIs also target viral RT but act through a non-competitive binding mechanism. NNRTIs require no conversion and block the enzyme substrate, preventing viral RT from converting viral RNA into DNA. Examples of NNRTIs include nevirapine (NVP)

and efavirenz (EFV) which are also known as first generation NNRTIs and second-generation NNRTIs include etravirine, doravirine and rilpivirine.

1.3.2.3 Protease Inhibitors (PIs)

The mechanism of action of PIs is to prevent the cleavage of gag proteins facilitated by protease enzymes, subsequently inhibiting the maturation of virions. First generation PIs include, nelfinavir, lopinavir, ritonavir, indinavir, amprenavir, saquinavir etc. Second generation PIs include atazanavir and darunavir, which have an improved potency against HIV.

1.3.2.4 Integrase Inhibitors (INSTIs)

HIV-1 integrase enzyme is responsible for the insertion of the viral DNA into the genome of the host cell. Integrase inhibitors work by blocking this process and hindering the HIV-1 replication cycle [43, 44]. Targeting the integrase enzyme has proven advantageous as the human body has no homologue. [43, 44]

Raltegravir, dolutegravir, bictegravir, elvitegravir and cabotegravir are examples of INSTIs approved for use by the FDA.

1.3.2.5 Entry Inhibitors

Entry inhibitors block HIV from binding to CD4 cells, preventing them gaining access to the host cell [45]. They work by binding to a specific domain on the surface of CD4 cells or HIV. [46]

Enfuvirtide was the first entry inhibitor to be approved for use. It is a synthetic peptide that targets gp41 – the protein essential for viral fusion. Maraviroc, another entry inhibitor was later introduced, targeting the CCR5 receptor and consequently interrupting the HIV replication cycle.

1.3.3 Lymphatics

The lymphatic system is central to HIV pathology; the majority of HIV-targeted CD4+ T-cells reside in lymph nodes. The lymphatic system plays an important role in several processes in the body, including, immune surveillance, absorption of fats and nutrients and maintaining tissue fluid. It comprises lymphatic vessels, capillaries, ducts, lymph nodes, lymph (fluid contained within system) etc. [47] Lymphatic tissues can be categorised into two; bone marrow and thymus are primary lymphoid tissues whereas lymph nodes, spleen and tonsils represent secondary lymphoid tissues [47].

Previous studies have shown low concentrations of drug present within these tissue [48]. Low levels of ARV drugs can be a concern in HIV as this can allow for resistance and viral rebound. The lymph nodes represent a reservoir of inducible virus and are a well-known sanctuary site (anatomical site where HIV can replicate due to suboptimal concentrations of ARVs). Once an individual is infected, HIV spreads to lymph nodes within 6 days [49]. The reservoir has previously been thought to be established within the first 2 weeks of infection [50]. Understanding the degree in which ARV's penetrate lymphoid tissues could be pivotal in treatment optimisation.

1.4 Aims

The general aim of this thesis was to explore the different applications of PBPK modelling, by developing and applying several mechanistic models to optimise the treatment of HIV.

Before a potential treatment reaches the stages of a clinical trial it must undergo numerous approval stages during which it is subjected to various research studies and the process can take between 3-6 years. Once a certain level of safety, efficacy and toxicity has been established the treatment is put forward for animal studies before studying in humans, should the outcome be positive. However, this entire process is met with several limitations, from the length of approval to the type of populations being investigated. Routinely, clinical trials are conducted in healthy patients aged between 18-35 years old, with a poor representation of special populations like, paediatrics, elderly, pregnancy etc. PBPK modelling can effectively evaluate hard-to-study clinical scenarios prior to clinical studies and provide valuable insight which cannot be easily gained. The objective of Chapter 2 was to construct and validate a whole-body PBPK model to describe the neonatal population by incorporating mathematical descriptions of anatomical and physiological characteristics.

Chapter 3 focuses on how PBPK models can be used to inform appropriate doses in special populations, more specifically, it evaluates the potential treatment and prophylaxis of HIV in neonates with integrase inhibitors dolutegravir and bictegravir. PBPK models can also be used to simulate the PK of novel formulations, and this has been exemplified in Chapter 4, where long-acting cabotegravir was simulated in the validated neonatal PBPK model and optimal doses for treatment and prophylaxis were derived.

Polypharmacy is routinely observed in PLWH and DDIs prove an obstacle in HIV treatment, Chapter 5 involved developing an adult PBPK model to evaluate the magnitude of moderate inducers on novel antiretrovirals. Chapter 6 investigated the penetration of ARV drugs in lymphoid tissues using a mechanistic lymphatic PBPK model.

Collectively, this thesis evaluates the possible ways HIV treatment can be improved and optimised by investigating the potential of treatments in special populations, novel formulations of ARV drugs, management of drug-drug interactions and the penetration of therapy in target tissues.

CHAPTER 2

Neonatal PBPK model development and validation

Contents

2.1 Introduction

Neonates, defined as infants from birth up to 28 days of age, are generally neglected as a population in pharmacological research. As a result, data describing the pharmacokinetics (PK) and pharmacodynamics in this vulnerable population of most licensed drugs, are lacking [51]. Efforts have been made to elucidate the significant changes that are observed in the absorption, distribution, metabolism, and elimination of drugs from birth to adulthood, yet a great deal remains unanswered.

Neonatal dosing regimens were derived from adult doses using allometric scaling based on characteristics such as body surface area or body weight [52-54]. Extrapolation of PK data from older patients using this scaling approach is generally unsuccessful due to the complex physiological, anatomical and molecular changes that occur in neonates [54]. Maturity of the organ system plays a key role in the differences observed between these populations. Apparent differences in organ weights and blood flows are likely to impact the PK of drugs. Drug absorption in neonates can be altered due to multiple factors such as, delayed gastric emptying time, increased gastric pH, and decreased motility. Changes in extracellular fluid together with changes in protein concentrations can lead to a varied distribution of drugs. Other key factors including non-linear maturation of transporter and metabolic pathways play a major role in neonatal PK.

To understand the degree of effect the aforementioned characteristics have on ADME processes, it is important to investigate drugs directly to use them safely and effectively. However, clinical trials in paediatric patients are impeded by the difficulties and clinical constraints researchers are faced with, and this is particularly true for neonates. [55]

Physiologically based pharmacokinetic (PBPK) modelling can be employed to rationalise the design of clinical trials in neonates, increasing trial efficacy and safety. PBPK modelling simulates important drug processes by integrating existing knowledge on patient-specific characteristics and drug-related data to provide more accurate predictions in the patient-population being investigated [3, 56] [57]. PBPK modelling is gaining popularity as the preferred methodology to appropriately predict the PK of investigational drugs in the neonatal population. Regulatory bodies have become increasingly interested in the use of these models to support and rationalise the design of future clinical studies in multiple populations [6].

The aim of this chapter was to validate the anatomical and physiological characteristics of the neonatal model. To validate the enzyme ontogenies of cytochrome P450 A (CYP3A4) and UDP-glucuronosyltransferase 1A1 (UGT1A1) which represent some of the key metabolic pathways involved in the metabolism of antiretrovirals; probe substrates that had available neonatal clinical data were used for comparison against simulated data.

2.2 Methodology

The PBPK model was designed in SimBiology version 5.8, a product of MATLAB R2018a (MathWorks, Natick, MA, USA 2018) [58]. Virtual, full-term, healthy neonates between 0 – 28 days were simulated. Neonatal maturation characteristics and a description of physiological and anatomical growth data were incorporated where appropriate. The model was based on the following assumptions: (1) well-stirred compartments with instant distribution of the drug; (2) no absorption of the drug from the colon; and (3) the model is blood flow limited. Simulated data were compared to observed neonatal PK data for raltegravir and midazolam.

2.2.1 Anatomy

World Health Organization (WHO) reference growth charts relating age to body weight and height were used for male and female neonates [59] (shown in Table 2.1). The charts were digitalised using Plot Digitizer Tool (plotdigitizer.sourceforge.net); a linear relationship was derived for both parameters using Microsoft Excel.

2.2.2 Tissue and organ weights

The organ weights were collated from multiple sources and detailed in Table 2.3 [52, 60], these values along with organ density data were used to calculate organ volumes [56]. The organ weights and volumes were validated against available published data on neonates. In the absence of literature data the small intestine fluid capacities from the published paediatric model [58] were allometrically scaled and applied to the neonatal model.

2.2.3 Blood flow

Neonatal blood flow data previously described by Bjorkman [52] and integrated into the model. Blood flow to the portal vein was defined as the sum of the blood flow to the gut, stomach, pancreas, and spleen (Table 2.2).

2.2.4 Intestinal Absorption

2.2.4.1 Modelling absorption

For orally administered drugs, a previously defined compartmental absorption and transit (CAT) model was implemented in the model [61]. The gastrointestinal tract was split into three major compartments: the stomach, small intestine, and colon (Figure 2.1). The small intestine was further sub-divided into seven compartments to describe the transit flow, where drug transfer from one compartment to the next was assumed to follow first order kinetics. The CAT model assumes the following: 1) Absorption from the stomach and colon is minimal in comparison to the small intestine; 2) passive transport across the small intestine membrane; 3) instant dissolution of drug.

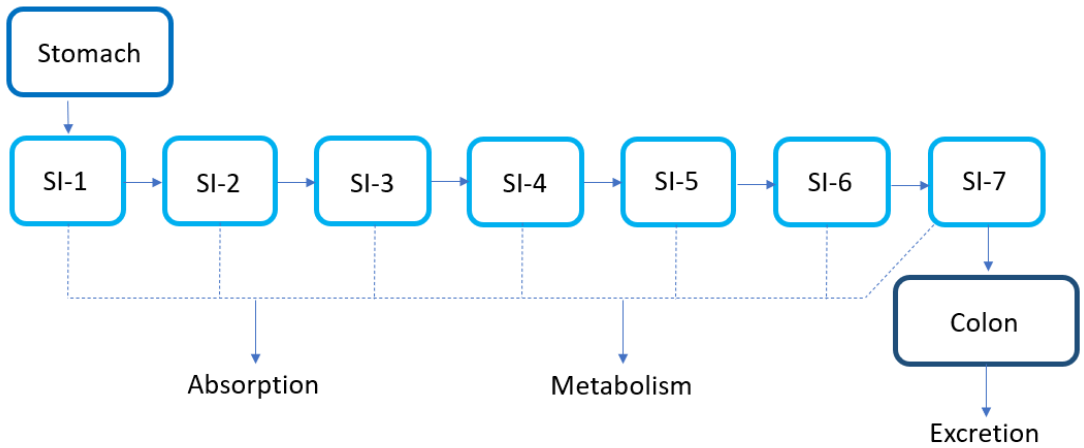

Figure 2.1 Schematic representation of ACAT model comprising stomach, small intestine split into 7 compartments and colon. SI, Small intestine.

Small intestine capacities in neonates were allometrically scaled from adult values due to the paucity of data. Literature indicated neonatal transit times were similar to adult transit times, therefore adult values were implemented in the neonatal model [62].

Absorption rates were calculated using equations 1-3 [61, 63, 64], involving the apparent permeability derived from caco-2 cells [64] or the polar surface area (PSA) and hydrogen bond donor (HBD) values [63]. A correlation between the *in vivo/in vitro* permeability was established using 24 drugs at pH 7.4 with data on human jejunum permeability and caco-2 permeability.

$$\mathrm{Log\ P_{eff}} = -2.546 - 0.011\mathrm{PSA} - 0.278\mathrm{HBD} \quad (1)$$

$$\mathrm{Log\ P_{eff}} = (0.6836 \times \mathrm{P_{app}}) - 0.5579 \quad (2)$$

$$\mathrm{K_a} = \frac{2 \times \mathrm{P_{eff}}}{\mathrm{R}} \quad (3)$$

2.2.4.2 Solubility

The solubility of drugs was considered in the model using equation 4, where the amount of drug available for absorption in each small intestine compartment was confined by the overall solubility of the drug (D_{sol}).

$$\mathrm{Conc_{soluble}} = \max(0, \min(\mathrm{D_{sol}}, \mathrm{C_{SI}})) \quad (4)$$

Where $Conc_{soluble}$ is the concentration of soluble drug available for absorption and C_{SI} is the concentration of dissolved drug in the small intestine compartment.

2.2.5 Plasma protein binding

The pharmacokinetics of a drug is influenced by the extent to which it is bound to plasma proteins. Plasma protein binding of drugs in neonates was calculated using a previously combined database on age-related changes in plasma albumin and α_1-acid glycoprotein, to factor in the importance of developmental pharmacology on protein binding [65]. The unbound fraction (*fu*) of drug was estimated using equation 5 [66].

$$\mathrm{fu_{Paediatric}} = \frac{1}{1 + \frac{(1 - \mathrm{fu_{Adult}}) \times [\mathrm{P}]_{\mathrm{Paediatric}}}{[\mathrm{P}]_{\mathrm{Adult}} \times \mathrm{fu_{Adult}}}} \quad (5)$$

Where $[P]_{Adult}$ is the adult plasma protein concentration, $[P]_{Paediatric}$ is the paediatric plasma concentration, fu_{Adult} is the fraction unbound in adults and $fu_{Paediatric}$ is the fraction unbound in paediatric patients.

2.2.6 Metabolism

2.2.6.1 Intestinal metabolism

The abundance of metabolic enzymes differs in neonates compared to adults, these changes can affect the overall clearance and pharmacokinetics of a drug making it essential to characterise the differences. The expression of CYP3A4 in the gut was estimated using an equation describing the fraction of CYP3A4 present in the neonatal gut in relation to the adult abundance. Clearance of drugs in the gut (CLgut) was evaluated using the *in vitro* intrinsic clearance (CLint) and the neonatal abundance of CYP3A4 and has been outlined in equation 6 [58, 65].

$$\text{CLgut (L/h)} = \frac{\text{CL}_{\text{int}} \text{ x } \text{Ab}_{\text{CYP3A4}} \text{ x } 1000 \text{ x } 60}{1000000} \quad (6)$$

2.2.6.2 Ontogeny of CYP3A4 and UGT1A1

Equations for CYP3A4 expression in neonates was calculated as a fraction of adult expression (Table 2.4) [65]. A UGT1A1 ontogeny profile detailing the age-related changes in enzyme maturation elucidated by Miyagi et al [67] was digitalised using Plot Digitizer. From this, a polynomial equation describing the fraction of UGT1A1 present in neonates in relation to adult abundance was derived, where age is expressed in days. The profile was adjusted during the qualification of raltegravir to better characterise UGT1A1 expression in neonates which yielded the following equation (equation 7).

$$\text{UGT1A1} = \left(-5 \text{ x } 10^{-10} \text{x Age}^4\right) + \left(-5 \text{ x } 10^{-7} \text{x Age}^3\right) - \left(-0.0002 \text{ x Age}^2\right) + (0.0203 \text{ x Age}) + 0.0305 \quad (7)$$

2.2.6.3 Prediction of Hepatic Clearance from in vitro data

Assuming the well-stirred model, hepatic clearance was estimated using equations 8-10 [63, 68, 69].

$$\text{CLint}_{\text{total}} = (\text{Clint}_{\text{E}} \text{x Abundance x MPPGL x WLiver}) \quad (8)$$

$$\text{MPPGL} \left(\frac{\text{mg}}{\text{g}}\right) = 10^{1.407+0.0158 \text{ x Age}-0.00038 \text{ x Age2}+0.0000024 \text{ x Age}^3} \quad (9)$$

$$\text{Total Hepatic Clearance} = \frac{(\text{Qhv x fu x CLint}_{\text{h}})}{(\text{Qhv} + \text{CLint}_{\text{h}} \text{ x fu}))} \quad (10)$$

Where $CLint_{total,}$ $Clint_{E,}$ Abundance, MPPGL, $Q_{hv,}$ f_u and $CLint_h$ is the total intrinsic clearance of the enzyme(s) involved in metabolism of the drug, *in vitro* clearance of said enzyme(s), abundance of enzyme(s) in neonates, microsomal protein content per gram of liver, hepatic blood flow, fraction unbound of drug and the sum of all $CLint_{total}$ values, respectively.

2.2.7 Distribution

The volume of distribution (V_{ss}) was calculated using previously published *in silico* models [70] described in equations 11-16. The model considers the composition of plasma and tissue to comprise water, phospholipids, and lipids. Drug lipophilicity determines where in the body the drug will distribute. Equation 11 calculates the erythrocyte: plasma (E:P) ratio; equations 12 & 13 describes partitioning of ionised and non-ionised species in olive oil:buffer at pH 7.4.

$$\mathrm{E{:}P} = (\mathrm{B{:}P} - (1 - 0.45))/0.45 \tag{11}$$

$$\mathrm{logD_{vo:w}} = 1.115 \times \mathrm{logP_{vo:w}} - 1.35 \tag{12}$$

$$\text{Monoprotic Acid: } \mathrm{LogD^{*}_{vo:w}} = \mathrm{LogD_{vo:w}} - \mathrm{Log}(1 + 10^{\mathrm{pH - pKa}}) \tag{13}$$

$$V_{ss} = (\Sigma V_t \times P_{t:p}) + (V_e \times \mathrm{E{:}P}) + V_p \tag{14}$$

$$P_{t:p,adipose} = \frac{(D^{*}_{vo:w} \times (V_{nlt} + 0.3 \times V_{pht})) + (1 \times (V_{wt} + 0.7 \times V_{pht}))}{(D^{*}_{vo:w} \times (V_{nlp} + 0.3 \times V_{php})) + (1 \times (V_{wp} + 0.7 \times V_{php}))} \times \frac{f_{u,p}}{1} \tag{15}$$

$$P_{t:p,non\text{-}adipose} = \frac{(P_{vo:w} \times (V_{nlt} + 0.3 \times V_{pht})) + (1 \times (V_{wt} + 0.7 \times V_{pht}))}{(P_{vo:w} \times (V_{nlp} + 0.3 \times V_{php})) + (1 \times (V_{wp} + 0.7 \times V_{php}))} \times \frac{f_{u,p}}{f_{u,t}} \quad (16)$$

Equation 15 and 16 calculate the partitioning of drug in tissue and plasma and assume the following i) the neutral lipids in tissues have the same lipophilicity as vegetable oil (vo), ii) the water in tissues has the same characteristics as pure water, and iii) the phospholipids in tissues have a lipo-hydrophilicity similar to a mixture of 70% water and 30% neutral lipids [70].

Table 2.1 Equations describing neonatal weight and height.

Weight (male and female)	Weight_initial: 3.0495 x female + 3.1572 x (1-female) Weight_maturation: ((0.014 x Age +1) x female) + ((0.018 x Age+ 1) x (1-female)) Weight: Weight_initial x Weight_maturation
Height (male and female)	Height = (0.0836 x Age + 49.802))/100) x female +((0.0954 x Age + 50.981)/100) x (1-female)
Age expressed in days, weight expressed in Kg, height expressed in m.	

Table 2.2 Equations describing blood flow rate to organs in neonates. **[52, 60]**

Cardiac Output	Qco = Qad + Qbr + Qgut + Qha + Qki + Qlu + Qmu + Qpa + Qre + Qsk + Qsp + Qst
Adipose tissue	Qad = (1.56 x WAdipose) x female + (1.44 x WAdipose) x (1-female)
Brain	Qbr = 30 x WBrain

Gut	Qgut = (123 x WIntestines) x female + (126.6 x WIntestines) x (1-female)
Hepatic artery	Qha = (34.2 x WLiver) x female+ (35.4 x WLiver) x (1-female)
Hepatic vein	Qhv = Qha+Qpv
Kidneys	Qki = (64.8 x WKidneys) x female + (80.4 x WKidneys) x (1-female)
Lungs	Qlu = 9.6 x WLungs
Muscle	Qmu = 2.34 x WMuscle
Pancreas	Qpa = (63.3 x WPancreas) x female + (65.4 x WPancreas) x (1-female)
Portal vein	Qpv = Qst+Qgut+Qpa+Qsp
Remaining tissues	Qre = (5.4 x WRemaining) x female + (5.04 x WRemaining) x (1-female)
Skin	Qsk = 9.6 x WSkin
Spleen	Qsp = (63.3 x WSpleen) x female + (65.4 x WSpleen) x (1-female)
Stomach	Qst = (67.8 x WStomach) x female + (75 x WStomach) x (1-female)
Blood flows described in L/h in the model.	

Table 2.3 Equations describing weight of organs in neonates. **[52, 60]**

Adipose	WAdipose = Weight x 0.245
Blood	WBlood = (Weight x 0.041) x female + (Weight x 0.044) x (1-female)
Bones	WBones = Weight x 0.047

Brain	WBrain = Weight x 0.10876
Heart	WHeart = Weight x 0.00619
Intestines	WIntestines = Weight x 0.014
Kidneys	WKidneys = Weight x 0.00744
Liver	WLiver = Weight x 0.03862
Lungs	WLungs = Weight x 0.01492
Muscle	WMuscle = Weight x 0.220
Pancreas	WPancreas = Weight x 0.00111
Remaining	WRemaining = (Weight x 0.102) x female + (Weight x 0.154) x (1-female)
Skin	WSkin = (Weight x 0.044) x female +(Weight x 0.047) x (1-female)
Spleen	WSpleen = Weight x 0.00295
Stomach	WStomach = Weight x 0.003
Thymus	WThymus = Weight x 0.00274
Adrenals	WAdrenals = Weight x 0.00222
Gut	WGut = Weight x 0.039

Total Weight	WTotal_weight= WLungs + WHeart + WBones + WKidneys + WStomach + WIntestines + WSpleen + WPancreas + WLiver + WRemaining + WBrain + WSkin + WBlood + WAdipose + WThymus + WMuscle + WGut + WAdrenals
Organ weights in kg	

Table 2.4 Equations describing enzyme ontogenies in neonates as a fraction of adult abundance. [65, 67, 71, 72]

Fraction: CYP2B6	Fraction_CYP2B6 = (1.07 x (Age/365)) / (1.31 + (Age/365))
Fraction: CYP2C8	Fraction_CYP2C8 = (0.716 x (Age/365))/(0.02+ (Age/365)) +0.3
Fraction: CYP2C9	Fraction_CYP2C9 = (0.821 x (Age/365))/(0.01 + (Age/365))+0.21
Fraction: CYP2C18	Fraction_CYP2C18 = (0.857 x (Age/365)) /(0.99+(Age/365)) +0.23
Fraction: CYP2C19	Fraction_CYP2C19 = ((0.857 x (Age/365)) / (0.99+(Age/365)) +0.23)
Fraction: CYP2D6	Fraction_CYP2D6 = ((1.01 x (Age/365))/(0.101 + (Age/365)))+0.036
Fraction: CYP2E1	Fraction_CYP2E1 = (4.22 x Age/365^0.27) / (7.66+(Age/365))
Fraction: CYP3A4	Fraction_CYP3A4 = (1 x (Age/365)^0.83)/(0.31+((Age/365)^0.83)) + 0.08
Fraction: CYP3A4 in neonatal gut	Fraction_Gut = ((0.639 x (Age/365))/(2.36+(Age/365)))+0.42
UGT1A1 Maturation	UGT1A1 = ($-5x10^{-10}$ x Age^4) + ($5x10^{-7}$ x Age^3) – (0.0002 x Age^2) + (0.0203 x Age) + 0.0305
Age expressed in days.	

Table 2.5 Physicochemical characteristics of raltegravir and midazolam.

Property	Raltegravir [73]	Midazolam [65]
Molecular weight, g/mol	445.2	325.8
Log $P_{o:w}$	0.58	3.89
f_u	0.17	0.034
pK_a	6.67	6.57
R	0.60	0.55
Polar surface area, $Å^2$	150	30.2
Hydrogen bond donors	3	0
Caco-2 permeability, 10^{-6} cm/sec	6.6	32.4 [63]
Clearance	NA	NA
CL_{int} CYP3A4	NA	3.75
CL_{int} UGT1A1	12.4	NA
Solubility, mg/L	70000 [74]	0.134 [63]

Abbreviations: A, L/h; CLint, intrinsic clearance; CYP, cytochrome P450 (µL/minute/pmol); log Po:w, partition coefficient between octanol and water; NA, not applicable; pKa, logarithmic value of the dissociation constant; R, blood-to-plasma drug ratio; UGT, uridine diphosphate glucuronosyltransferase (µL/minute/10^6).

2.2.6 Model Qualifications and Simulations

2.2.6.1 Clinical PK data in neonates

Clinical PK data for midazolam were available in critically ill neonates with respiratory distress syndrome or neonatal infection [75]. The study involved administration of a 0.2 $mg.kg^{-1}$ intravenous bolus of midazolam in neonates with a mean gestational age of 37 weeks. The effect of the illness on the overall disposition of the drug could not be determined, however due to the lack of data available, it was used for the qualification of CYP3A4. Two cohorts of clinical data were available [76] for the qualification of UGT1A1 activity with raltegravir.

2.2.6.2 Simulations

Physicochemical parameters describing both raltegravir and midazolam were used as input data for the model and have been described in Table 2.5. Simulations were initially carried out for raltegravir and midazolam, in 100 virtual neonates. For raltegravir, the mean maximum plasma concentration (C_{max}) and AUC were recorded for comparison against clinical data. For midazolam, the mean AUC, C_{max}, trough plasma concentration (C_{trough}) and CL values were recorded for comparison.

2.2.6.3 Statistical evaluation of the model

The PBPK model was qualified by calculating the absolute average fold error (AAFE) and root mean squared error (RMSE) where appropriate. AAFE is a useful parameter to assess over or under-prediction of the model, values closer to 1 indicate a closer similarity with observed values. The RMSE calculates the error between the predicted value and the observed value. The model was assumed to be qualified if the predicted values fell within the following criteria: with AAFE < 2 and RMSE < 1 as per convention for the approach [10].

2.3 Results

2.3.1 Anatomical Qualification

For the qualification of neonatal anatomy, the mean simulated values were recorded for comparison against literature data. The simulated values for weight and height agreed with observed values. Equations describing the tissue and organ weights were sufficient in reflecting observed literature data (Table 2.6). Other neonatal anatomical characteristics such as organ volumes and blood flows (Table 2.7) described in the PBPK model were well within the 2-fold acceptance criteria for model validation.

2.3.2 Raltegravir Qualification

Comparison between observed and simulated PK data of oral raltegravir has been outlined in Table 2.8 and Table 2.9. In Cohort 1, the predicted mean AUC_{12} and C_{max} values are within 1.6-fold of observed data. The predicted mean AUC and C_{max} values in Cohort 2 were on average within 1.25-fold of the observed data, and C_{trough} values were within 1.8-fold of observed data with the simulated concentration-time profile yielding a RMSE value below 1 (Table 2.10 & Figure 2.2).

2.3.3 Midazolam Qualification

Comparison of intravenous midazolam PK parameters have been detailed (Table 2.11), with mean simulated values of AUC, C_{max}, C_{trough} and CL, all within 1.4-fold of observed data. As both drugs were in sensible agreement with literature values, the model was considered qualified.

Table 2.6 Model qualification of neonatal organ weights; observed vs simulated data (data represented as Male/Female where a distinction in organ weights were observed).

Organ Weight	Reference (kg)	Simulated (kg)
Brain	0.395	0.399
Lungs	0.054	0.055
Heart	0.022	0.023
Kidneys	0.027	0.027
Liver	0.140	0.142
Spleen	0.011	0.011
Thymus	0.010	0.010
Pancreas	0.004	0.004
Adrenals	0.008	0.008
Gut Contents	0.140	0.143
Bones	0.170	0.172
Adipose	0.890	0.896
Intestines	0.050	0.051
Muscle	0.800	0.807
Stomach	0.010	0.011
Remaining	0.56/0.37	0.618/0.374
Blood	0.16/0.15	0.176/0.157
Skin	0.17/0.16	0.189/0.161
Age range evaluated in model is 0-28 days.		

Table 2.7 Model qualification of neonatal organ blood flows, comparison of observed vs simulated data (data represented as Male/Female data represented as Male/Female where a distinction in blood flows were observed).

Organ Blood Flow	Reference (L/h)	Simulated (L/h)
Stomach	0.75/0.68	0.88/0.74
Skin	01.63/1.54	1.77/1.53
Kidneys	2.17/1.75	2.35/1.75
Liver- Hepatic Artery	4.96/4.79	5.37/4.77
Heart – Cardiac Output	34.80/33.0	37.66/33.18
Brain	11.84	12.81/11.82
Lungs	0.52	0.52
Adipose	1.28/1.39	1.38/1.39
Spleen	0.70/0.68	0.78/0.68
Pancreas	0.26/0.25	0.28/0.25
Hepatic vein	13.2/12.6	13.93/12.47
Portal Vein	8.04/7.76	8.88/7.91
Remaining	2.82/2.00	3.05/2.00
Muscle	1.87	2.02/1.87
Gut	6.33/6.15	6.96/6.24
Age range evaluated in model is 0-28 days.		

Table 2.8 Comparison between predicted and observed pharmacokinetics of raltegravir in cohort 1 [76, 77].

Raltegravir Cohort 1						
	2 mg/kg single dose			3 mg/kg single dose		
	Clinical†	Simulated*	AAFE	Clinical†	Simulated*	AAFE
AUC_{12} (mg.h/L)	28.13 (17.42-44.0)	27.71 ± 3.57	1.02	29.47 (18.89-46.26)	43.11 ± 5.14	1.46
C_{max} (mg/L)	3.40 (2.23-4.32)	3.41 ± 0.40	1.00	3.36 (2.00-5.32)	5.27 ± 0.58	1.57
Abbreviations: †Values shown as geometric mean (range); AUC_{12}, *Simulated values shown as mean ± standard deviation; area under curve over 12 hours, Cmax, maximum plasma concentration; Cmax, maximum plasma concentration.						

Table 2.9 Comparison between predicted and observed pharmacokinetics of raltegravir in cohort 2 [76, 77].

Raltegravir Cohort 2						
	1.5 mg/kg, Q24h; days 1-7			3 mg/kg twice daily; days 8-28		
	Clinical †	Simulated*	AAFE	Clinical †	Simulated*	AAFE
AUC (mg.h/L)	38.2 (38.4)	32.09 ± 5.40	1.19	14.3 (43.3)	15.29 ± 3.56	1.07
C_{max} (mg/L)	2.35 (35.0)	2.64 ± 0.29	1.12	2.85 (41.9)	2.34 ± 0.45	1.22
C_{trough} (mg/L)	0.948 (64.2)	0.564 ± 0.22	1.68	0.176 (93.8)	0.316 ± 0.13	1.80

Abbreviations: Cmax, maximum plasma concentration; *Values shown as simulated mean ± standard deviation; †Values shown as geometric mean (CV%); Q24h, once daily; AUC, area under curve over 24 hours, Cmax, maximum plasma concentration, Ctrough, minimum plasma concentration.

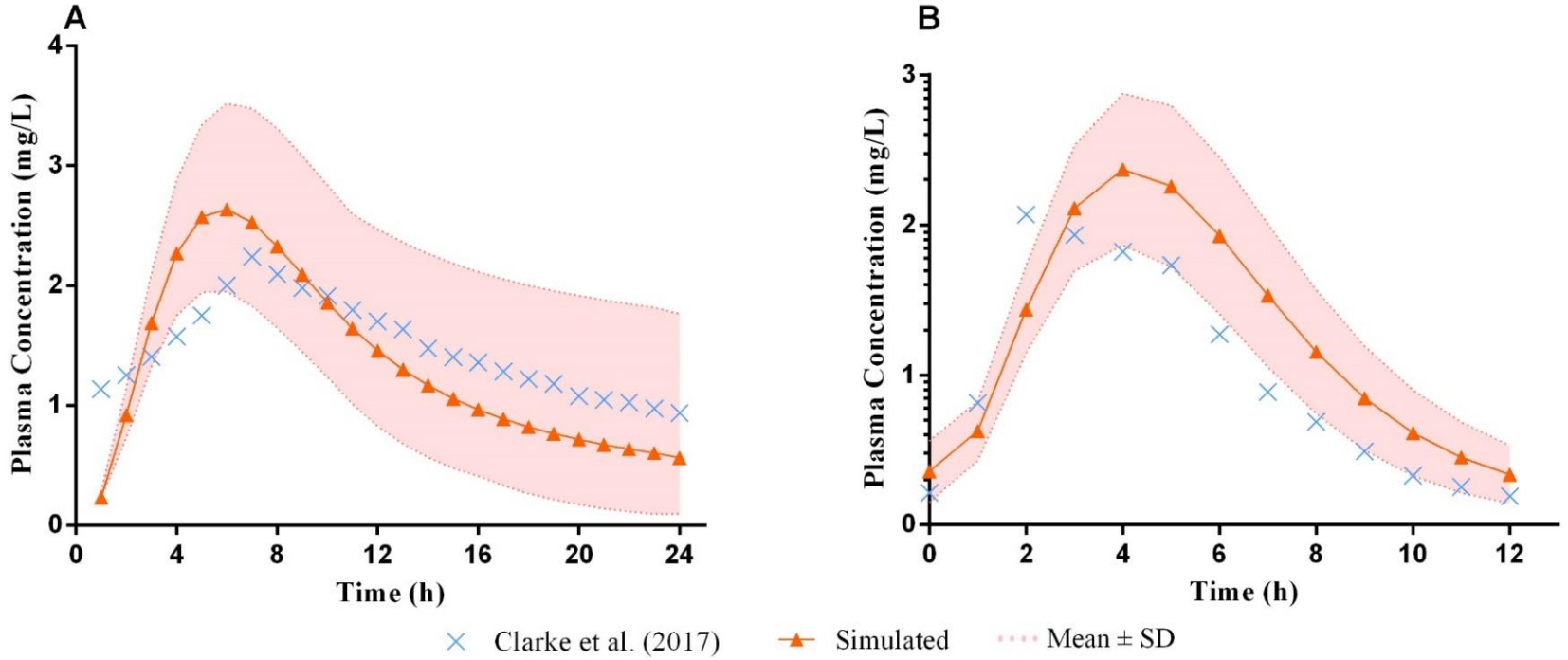

Figure 2.2 Simulated and experimental concentration-time profiles of orally administered raltegravir. A (Cohort 1): 1.5 mg/kg once daily, B (Cohort 2): 3 mg/kg twice daily [76]. Cohort 1; a 'dose finding' study where single doses of raltegravir were orally administered (PO) to neonates. Cohort 2 involved a multiple dosing regimen of 1.5 mg/kg PO raltegravir once daily in the first week of life and increasing the dose to 3.0 mg/kg twice daily on day 8 to day 28.

Table 2.10 Comparison between observed and simulated PK profile of raltegravir in neonates (Cohort 2) [76].

	Raltegravir 1.5 mg/kg Q24h; Days 1-7	Raltegravir 3 mg/kg Twice Daily; Days 8-28
AAFE	1.247	1.392
RMSE	0.432	0.430
Abbreviations: AAFE, absolute average fold error; RMSE, root mean squared error; Q24h, once daily. Comparison between simulated and observed PK profiles of Raltegravir in Cohort 2, clinical data extrapolated using Plotdigitiliser.		

Table 2.11 Comparison between observed and simulated PK of midazolam 0.2 mg/kg IV bolus in neonates [75].

	Clinical	Simulated	AAFE
AUC (mg.h/L)	2.20	2.89	1.31
C_{max} (mg/L)	0.41	0.42	1.02
C_{trough} (mg/L)	0.11	0.11	1.02
CL (L/h)	0.41	0.38	1.06
Abbreviations: AUC, extrapolated to infinity, Cmax, maximum plasma concentration, Ctrough, minimum plasma concentration, CL, clearance.			

2.4 Discussion

The PBPK model was built incorporating neonatal anatomical and physiological maturation characteristics. Equations relating growth to age were derived from existing literature [52, 59, 65]. For a PBPK model to be reliable it is important that equations describing the basic anatomy and physiology of the target population are represented appropriately and equations are sufficient in their characterisation of such parameters. The PBPK model was qualified for the duration of the neonatal period (0-28 days); 100 virtual patients were simulated to estimate population variability and the mean value for each parameter was recorded for comparison against observed data. All blood flows, organ and tissue weights were within the acceptance criteria (<50% of clinical data) and successfully passed model qualification. Pre-term neonates are routinely delivered to HIV positive mothers, the models described in this chapter are based on full-term neonates. There are several physiological and anatomical differences between full-term and preterm neonates, availability on these types of data is sparse in full-term neonates and increasingly so in pre-term cases. The choice to build a PBPK model for full-term neonates were based on these limitations. However, for additional and further application, it may be worth looking into quantifying these changes.

To validate the ontogeny of key enzyme CYP3A4, observed neonatal clinical data on probe substrate midazolam was utilised. The maturation profile of CYP3A4 was derived from Johnson et al [65] and expressed as the fraction of CYP3A4 present in a neonatal liver in relation to adult content. Clinical PK data for midazolam was available in critically ill neonates with respiratory distress syndrome or neonatal infection [75]. The study involved an administration of a 0.2 $mg.kg^{-1}$ intravenous (IV) bolus of midazolam in neonates. The effect of the illness on the overall disposition

of the drug could not be concluded, however due to the lack of data available, it was used for the qualification of CYP3A4. The model was successful in predicting the PK characteristics of IV midazolam, with concentration-time profiles generating AAFE values < 2-fold. C_{max}, C_{min} and CL values produced an average percentage difference of 3.9%, with AUC yielding a 31% difference from observed data.

The ontogeny profile of UGT1A1 in neonates was derived from literature [67] and expressed as the fraction of enzyme present in neonates compared to the adult expression. Two cohorts of clinical data on raltegravir, a UGT1A1 substrate, were available [76] for the qualification of UGT1A1 activity in neonates. The first cohort involved a dose-finding study which entailed administering a single oral dose, either 2 or 3 mg/kg of raltegravir once daily to infants. The second cohort involved administering a daily dose of 1.5 mg/kg to neonates aged 1-7 days, with a dose escalation of 3 mg/kg twice daily on day 8 through to 28. These conditions were replicated *in silico* for evaluation of model performance. The clinical PK from these studies was used to calibrate the UGT1A1 expression. The equation extrapolated from Miyagi et al [67] had a tendency to over-predict UGT1A1 expression in the first two weeks of the neonatal period and under-predict expression in the latter two weeks of the neonatal period. The ontogeny profile was adjusted accordingly to better replicate the observed data represented in Figure 2.2.

Underrepresentation of clinical PK data in the neonatal population proves a challenge when qualifying PBPK models. The *in vivo* clinical data that was used for the comparison between predicted and observed values in this chapter were carried out in only a handful of neonates [75, 76]. The few clinical studies that have been conducted in neonates have, often by necessity, numerous limitations from small sample sizes to restricted clinical and demographic detail due to ethical and logical

restrictions. Although there are data available on the ontogeny of hepatic enzymes, a significant portion of these studies are routinely carried out on small samples with large gaps in different age groups. In some cases, there are only one or two samples in the neonatal age bracket, making it problematic to accurately characterise expression. For this reason, the UGT1A1 maturation profile was adjusted during the model qualification stage to adequately predict the PK of raltegravir; a probe substrate that allowed the fine-tuning of equations describing age-related maturation.

Many parameters remain underexplored in neonates, hindering the ability to mathematically represent their changes with growth and development. In the absence of such data, parameters from a previously published paediatric model [58] were utilised and assumed to be similar, including solubility, body composition, gastric and intestinal pH. For other parameters like small intestinal transit time, literature suggested there were no significant growth-related changes, thus adult values were implemented [62]. The lack of data on developmental changes in transporter expression make it inherently difficult to replicate this parameter *in silico* and so data on transporters was not included in the model. Previously developed neonatal PBPK models faced with this limitation have taken similar approaches [52, 65], where data in neonates is lacking adults, values were implemented and on occasion allometrically scaled. Models were compared against observed data for overall evaluation of model performance. Johnson et al employed PBPK models to predict the clearance of eleven drugs in neonates and infants [65]. Due to the paucity of quantifiable data in neonates, similar assumptions were made in their models, nevertheless 70% of their predictions in neonates were within 2-fold of observed values [65].

Changes in composition of plasma proteins such as alpha 1-acid glycoprotein and albumin can change and influence the distribution of drugs. At birth, newborns have lower concentrations of albumin and alpha 1-acid glycoprotein present in plasma, reaching adult levels when they are 1 year of age. This reduced concentration could translate into a greater fraction of unbound drug being available; the unbound drug moves across membranes to elicit a biological response before being eliminated from the body. To account for these changes a previously established database quantifying these changes was used and implemented in the PBPK model [66].

Despite the gaps in knowledge, PBPK models are extremely valuable and can provide important information on the PK of drugs in vulnerable populations. In this chapter intravenous and oral administration routes were developed and modelled however modelling different routes of administration and formulations are also feasible using this technique. PBPK modelling has numerous applications from assisting in candidate selection in early drug discovery to predicting drug-drug interaction potentials. PBPK models can be constantly refined in an iterative manner as more information from pre-clinical and clinical studies become available, helping to improve overall model performance making them an advantageous pharmacological tool.

CHAPTER 3

Dose optimisation of Dolutegravir & Bictegravir in neonates

Contents

3.1 Introduction

In 2019, 150,000 new cases of HIV were reported in children under 15 years of age and 1.8 million children were living with HIV [78]. The majority of paediatric HIV infections are caused by perinatal transmission, in utero, during birth or afterwards through breastfeeding [79]. Of the measures taken to prevent mother to child transmission (PMTCT), initiating or maintaining effective antiretroviral (ARV) therapy in pregnant and breastfeeding women is the most successful. In addition, all neonates with perinatal HIV exposure should receive ARVs as part of PMTCT. Those infants who are infected with HIV despite these efforts at prophylaxis can be detected with successful early diagnosis techniques and early initiation of ART can maintain an undetectable viral load and improve clinical outcomes in these infants [79, 80].

Current guidelines for ARV use in neonates recommend either a 1 or 2-drug prophylaxis regimen or 'empiric therapy', using a 3-drug regimen, including 2 NRTI and a NNRTI or integrase inhibitor (II), in high risk or infected infants [81]. Zidovudine, an NRTI, and/or nevirapine, an NNRTI are currently recommended for prophylaxis of neonates born to women living with HIV. Few ARVs have been studied in newborn infants, and only zidovudine, nevirapine, lamivudine and raltegravir have sufficient neonatal safety and PK data to be recommended for use from birth and lopinavir/ritonavir from 2 weeks of age, resulting in limited options for neonatal 3-drug treatment regimens [81].

Dolutegravir and bictegravir are highly potent HIV-1 integrase inhibitors but are not currently approved for use in neonates. Integrase inhibitors are well known for their safety and high efficacy and are accordingly favoured for first-line treatment in both ARV-naïve and experienced adult patients. Bictegravir, branded under the name

Biktarvy®, is currently available as a once-daily, single-tablet regimen and is co-formulated with the NRTI's emtricitabine and tenofovir alafenamide for the treatment of HIV-1 in adults [82]. Bictegravir has recently been studied in children older than 6 years and adolescents and studies are currently ongoing in children older than 2 years [83]. Safety and PK of dolutegravir have previously been studied in paediatric patients and a recent study investigated the safety in infants older than 4 weeks of age [84]. Dolutegravir was generally well tolerated in all the cohorts with doses meeting the target concentrations [84].

The aim of this chapter was to model the exposure of dolutegravir and bictegravir in neonates, to identify optimal dosing regimens for evaluation in neonates.

3.2 Methodology

The PBPK model was designed in SimBiology version 5.8, a product of MATLAB R2018a (MathWorks, Natick, MA, USA 2018). [58] Virtual patients between 0 – 28 days were simulated. The model was based on the same assumptions described in Chapter 2. Model was developed in 2019.

3.2.1 Anatomy

Equations describing the basic anatomy and physiology of neonates have been previously described (Chapter 2) and were implemented in the neonatal PBPK model. The adult PBPK model was constructed using physiological and anatomical equations previously defined in the literature.

3.2.2 Simulation of ADME processes

3.2.2.1 Dolutegravir Clearance

The liver is the main site of dolutegravir metabolism [85]. A large portion of dolutegravir (51%) is estimated to be conjugated into an ether glucuronide by UGT1A1 and approximately 21% is hydroxylated by CYP3A4. UGT1A3 and UGT1A9 are minor routes of elimination, owing to 2.8% and 5.5% of hepatic metabolism, respectively [85]. The remainder of the clearance (19.7%) is suggested to be undertaken by extrahepatic metabolism [85]. Due to the difficulty of approximating dolutegravir clearance from *in vitro* experiments, clearance was estimated via retrograde modelling from adult *in vivo* systemic clearance using equations 17-24. The total systemic clearance was multiplied by 0.72, the fraction of hepatic clearance (UGT1A1 +CYP3A4) (Equation 17). The total intrinsic clearance was then calculated using equation 18.

The fractions metabolised by each enzyme were incorporated in the final calculation of dolutegravir clearance (Equation 19, 20 & 23). However, data on UGT1A3, UGT1A9 and extrahepatic enzyme expression were inadequate, hence the fraction metabolised by each were totalled and scaled allometrically (Equation 23).

$$\mathrm{CL_{DTG,hepatic}} = \mathrm{CL_{DTG,sys}} \times 0.72 \quad (17)$$

$$\mathrm{CL_{int,total}} = (\mathrm{CL_{DTG,hepatic}} \times \mathrm{Q_{HV}})/(\mathrm{fu/R}(\mathrm{Q_{HV}} - \mathrm{CL_{DTG,hepatic}})) \quad (18)$$

$$\mathrm{CL_{3A4}} = ((\mathrm{CL_{int,total}} \times 0.29)/\mathrm{W_{Liver}}/\mathrm{MPPGL}) \times \mathrm{W_{Liver,n}} \times \mathrm{MPPGL_n} \times \mathrm{CYP3A4_n} \quad (19)$$

$$\mathrm{CL_{1A1}} = ((\mathrm{CL_{int,total}} \times 0.71)/\mathrm{W_{Liver}}/\mathrm{MPPGL}) \times \mathrm{W_{Liver,n}} \times \mathrm{MPPGL_n} \times \mathrm{UGT1A1_n} \quad (20)$$

$$\mathrm{CL_{int,total,n}} = \mathrm{CL_{3A4}} + \mathrm{CL_{1A1}} \quad (21)$$

$$\mathrm{CL_{DTG,hepatic,n}} = (\mathrm{Q_{HV}} \times (\mathrm{fu/R}) \times \mathrm{CL_{int,total,n}})/(\mathrm{Q_{HV}} + \mathrm{CL_{int,total,n}} \times (\mathrm{fu/R})) \quad (22)$$

$$\mathrm{CL_{DTG,extrahepatic,n}} = ((\mathrm{CL_{DTG,sys}} \times 0.28)/70) \times \mathrm{Weight} \quad (23)$$

$$\mathrm{CL_{DTG,sys,n}} = \mathrm{CL_{DTG,hepatic,n}} + \mathrm{CL_{DTG,extrahepatic,n}} \quad (24)$$

Where $CL_{DTG,hepatic}$ is the hepatic clearance of dolutegravir in adults, $CL_{DTG,sys}$ is the systemic clearance of dolutegravir in adults, $CL_{int,total}$ is the total intrinsic clearance by

the liver in adults, CL_{3A4} is the clearance facilitated by CYP3A4 enzyme in neonates, CL_{1A1} is the clearance facilitated by UGT1A1 enzyme in neonates, $UGT1A1_n$ is the expression of UGT1A1 enzyme in neonates relative to the adult expression, $CYP3A4_n$ is the expression of CYP3A4 enzyme in the neonatal liver in relation to the adult abundance, MPPGL is the microsomal protein per gram of liver in adults, $MPPGL_n$ is the microsomal protein content per gram of liver in neonates, W_{Liver} is the weight of the liver in adults expressed in kg, $W_{Liver,n}$ is the neonatal liver weight in kg, and Weight is the neonatal total body weight expressed in kg.

3.2.2.2 Bictegravir Clearance

Clearance of bictegravir was estimated via retrograde modelling due to the difficulty in approximating clearance from in vitro experiments and have been detailed below (Equations 9-12). Bictegravir is estimated to be conjugated into an ether glucuronide by UGT1A1 (50%) and hydroxylated by CYP3A4 (50%) in equal amounts. The fractions metabolised by each enzyme were incorporated in the final calculation of bictegravir clearance (Equation 26- 28).

$$\mathrm{CL_{int,total}} = (\mathrm{CL_{BIC,hepatic}} \times \mathrm{Q_{HV}})/(\mathrm{fu}/\mathrm{R}(\mathrm{Q_{HV}} - \mathrm{CL_{BIC,hepatic}})) \quad (25)$$

$$\mathrm{CL_{3A4}} = ((\mathrm{CL_{int,total}} \times 0.5)/\mathrm{W_{Liver}}/\mathrm{MPPGL}) \times \mathrm{W_{Liver,n}} \times \mathrm{MPPGL_n} \times \mathrm{CYP3A4_n} \quad (26)$$

$$\mathrm{CL_{1A1}} = ((\mathrm{CL_{int,total}} \times 0.5)/\mathrm{W_{Liver}}/\mathrm{MPPGL}) \times \mathrm{W_{Liver,n}} \times \mathrm{MPPGL_n} \times \mathrm{UGT1A1_n} \quad (27)$$

$$\mathrm{CL_{BIC,n}} = \mathrm{CL_{1A1}} + \mathrm{CL_{3A4}} \quad (28)$$

Where $CL_{BIC,n}$ is the clearance of bictegravir in neonates and $CL_{BIC,adults}$ is the systemic clearance of bictegravir in adults, $CL_{int,total}$ is the total intrinsic clearance by the liver in

adults, CL_{3A4} is the clearance facilitated by CYP3A4 enzyme in neonates, CL_{1A1} is the clearance facilitated by UGT1A1 enzyme in neonates, $UGT1A1_n$ is the expression of UGT1A1 enzyme in neonates relative to the adult expression, $CYP3A4_n$ is the expression of CYP3A4 enzyme in the neonatal liver in relation to the adult abundance, MPPGL is the microsomal protein per gram of liver in adults, MPPGL is the microsomal protein content per gram of liver in neonates and $W_{Liver,n}$ is the neonatal liver weight in kg.

3.2.3 Model Validation

The physicochemical properties of dolutegravir and bictegravir used as input data in the model have been represented in Table 3.1. For qualification of the drug properties for both dolutegravir and bictegravir, simulations were performed in the adult PBPK model [72] and comparisons were made between clinical [84, 86] and predicted values. The simulations were conducted in 100 virtual adults for a 50 mg daily dose of dolutegravir and a 50 mg daily dose of bictegravir, in adults.

3.2.4 Simulations in neonates

Each multiple dose strategy (bictegravir and dolutegravir) was simulated in 100 healthy term neonates with the aim of achieving plasma exposure comparable to therapeutic levels observed in paediatric patients, for dolutegravir: C_{trough}: 0.99 mg/L and AUC_{24}: 50.1 mg.h/L [87]. For bictegravir, plasma exposures comparable to therapeutic levels observed in adults was set as the target, with a C_{trough} of 2.61 mg/L and an AUC_{24} of 102 mg.h/L [88]. Doses ranged from 2 - 5 mg for dolutegravir and 2.5 – 5 mg for bictegravir, with weight ranging from 3.0 – 4.5 kg, representing healthy, full-term neonates in the model.

As a qualified infant PBPK model was not available, infant dolutegravir PK was simulated by extrapolating from the neonatal PBPK model, for comparison against clinical values.

Table 3.1 Summary of physicochemical properties of dolutegravir and bictegravir.

Property	Dolutegravir [72, 89-93]	Bictegravir [94-96]
Molecular weight, g/mol	419.4	449.4
Log $P_{o:w}$	2.2	2.7
f_u	0.0171 (0.0103-0.024)†	0.01
pK_a	8.20	9.8
R	0.535	0.64
Polar surface area, $Å^2$	99.2	99.2
Hydrogen bond donors	2	2
Caco-2 permeability, 10^{-6} cm/sec	40.17	14.8
Clearance	0.901^A, 1.48^A	621.9^B
CL_{int} CYP3A4	NA	7.71×10^{-4}
CL_{int} UGT1A1	NA	NA
Solubility, mg/L	95	62.3

Abbreviations: †, Median (range); A, L/h; B, mL/h; CLint, intrinsic clearance; CYP, cytochrome P450 (µL/minute/pmol); log Po:w, partition coefficient between octanol and water; NA, not applicable; pKa, logarithmic value of the dissociation constant; R, blood-to-plasma drug ratio; UGT, uridine diphosphate glucuronosyltransferase (µL/minute/10^6).

3.3 Results

The PBPK model was initially validated in an adult model against clinical data for dolutegravir and bictegravir to ensure that the selected drug properties could appropriately characterise both drugs. The mean simulated values for pharmacokinetic parameters C_{max}, C_{trough} and AUC were recorded for comparison against available clinical data for oral formulations of both these drugs. To assess the accuracy of the simulations, the PBPK model was considered validated if the mean values were within 2-fold of observed data.

3.3.1 Model Qualification

The qualification of dolutegravir in adults and infants has been outlined in Tables 3.2 and 3.3, with AAFE values of mean simulated PK parameters falling within the 2-fold acceptance criteria [10].

3.3.2 Dolutegravir Predictions

The qualified model predicted the exposure of dolutegravir in neonates, with doses ranging from 2-5 mg (summarised in Table 3.4 and Figure 3.1). The predictions indicated that a 5 mg dose may be suitable for neonates. The mean predicted systemic clearance of DTG in neonates was 0.0274 (0.0142 - 0.0513) L/h. Regimen 6 comprising a 5 mg dose with prolonged intervals between dosing resulted in AUC_{av} and C_{trough} values of 37.6 mg.h/L and 1.9 mg/L, respectively. These values are comparable to the paediatric target (AUC_{24}: 50.1 mg.h/L and C_{trough}: 0.99 mg/L) [86, 87].

3.3.3 Bictegravir Predictions

Following successful validation in the adult model, bictegravir was simulated in neonates with doses ranging from 2.5- 5 mg, the mean PK parameters have been

outlined in Table 3.5. Simulations suggest regimens 4 and 5 were slightly above target exposures, with regimens 1-3 falling within the expected therapeutic concentrations (AUC: 102 mg.h/L); C_{trough} 2.61 mg/L) [88].

Table 3.2 Comparison between predicted and observed pharmacokinetics of dolutegravir and bictegravir in adults.

	Dolutegravir 50 mg dose			Bictegravir 50 mg dose		
	Clinical*	Simulated	AAFE	Clinical*	Simulated	AAFE
AUC (mg.h/L)	53.6 (27)	74.62 (32)	1.392	102 (26.9)	110 (26)	1.075
C_{max} (mg/L)	3.67 (20)	4.42 (24)	1.204	6.15 (22.9)	6.21 (19)	1.010
C_{trough} (mg/L)	1.11 (46)	1.90 (48)	1.712	2.61 (35)	3.05 (37)	1.167
CL (L/h)	0.776	0.754 (25)	1.029	0.541	0.610 (24)	1.129

Abbreviations: *Values shown as geometric mean (%CV); Cmax, maximum plasma concentration; Q24h, once daily; AUC, area under curve over 24 hours; Ctrough, minimum plasma concentration; CL, total systemic clearance; AAFE, absolute average fold error.

Table 3.3 Summary of simulated vs observed PK for dolutegravir in infants.

	Clinical	Simulated	AAFE
AUC (mg.h/L)	61.0 (44)	46.2 (32)	1.32
C_{trough} (mg/L)	1.21 (55)	1.79 (31)	1.49
Abbreviations: *Values shown as geometric mean (%CV); Cmax, maximum plasma concentration; AUC, area under curve over 24 hours, Ctrough, minimum plasma concentration; AAFE, absolute average fold error.			

Table 3.4 Predicted PK of dolutegravir dosing regimens in neonates.

Regimen	Total Dose	Dose* (mg/kg)	C_{max}[1] (mg/L)	AUC_{av} (mg.h/L)	C_{max}[2] (mg/L)	AUC (mg.h/L)	C_{trough} (mg/L)	$T_{1/2}$ (h)
1	5 mg Q24h	1.4 (1.7 - 1.1)	3.7 (27.5)	68.1 (34.6)	3.1 (27.8)	42.9 (15.9)	1.9 (23.6)	34.3
2	3 mg Q24h	0.85 (1 - 0.7)	2.2 (25.0)	40.0 (28.1)	1.7 (23.8)	28.2 (17.1)	1.4 (27.2)	33.6
3	2 mg Q24h	0.55 (0.7 - 0.4)	1.5 (18.8)	26.9 (28.1)	1.13 (22.5)	17.6 (14.7)	0.9 (18.9)	31.4
4	5 mg Q48h	1.4 (1.7 - 1.1)	2.0 (16.0)	33.9 (22.1)	1.4 (28.6)	26.1 (20.2)	1.0 (32.1)	33.1

5	Day 1-14 = 5 mg Q48h, Day 15-28 = 5 mg Q24h	1.4 (1.7 - 1.1)	2.9 (25.9)	46.3 (30.0)	2.8 (34.8)	42.6 (26.9)	2.4 (39.8)	36.4
6	Day 1-20 = 5 mg Q48h, Day 21-28 = 5 mg Q24h	1.4 (1.7 - 1.1)	2.3 (20.0)	37.6 (30.4)	2.1 (33.3)	38.1 (22.1)	1.9 (23.1)	37.2

*Median (Range), neonate weight range in the model is 3.0 - 4.5 kg. $Cmax^1$, Average maximum plasma concentration over 28-day simulations; $Cmax^2$, Maximum plasma concentration after final dose has been administered; AUC_{av}, Average area under curve over 28-day simulations; AUC, Area under curve after final dose; C_{trough}, Minimum plasma concentration after final dose; $T_{1/2}$, Half-life; Q24h, one daily; Q48h, once every 2 days (48 hours).

Table 3.5 PK summary of predicted bictegravir dosing regimens in neonates.

Regimen	Total Dose (mg)	C_{max}[1] (mg/L)	AUC_{av} (mg.h/L)	C_{max}[2] (mg/L)	AUC (mg.h/L)	C_{trough} (mg/L)	Above 5*PA-EC_{95} (Yes/No)
1	Day 1-28 2.5mg Q24h	4.97 (18.6)	92.26 (28.9)	4.35 (24.8)	81.92 (21.2)	3.96 (32.1)	Yes
2	Day 1-28 5mg Q24h	8.20 (16.7)	128.83 (29.1)	8.93 (32.3)	104.67 (20.2)	8.17 (31.1)	Yes
3	Day 1-28 5mg Q48h	5.32 (17.4)	95.63 (28.5)	4.61 (11.1)	77.50 (22.1)	3.76 (24.6)	Yes
4	Day 1-13 5mg Q48h; Day 14-28 5mg Q24h	8.35 (19.8)	130.23 (29.8)	8.20 (36.0)	134.24 (27.5)	7.56 (20.3)	Yes

5	Day 1-20 5mg Q48h; Day 21-28 5mg Q24h	6.77 (20.8)	107.01 (32.3)	6.8 (24.8)	108.30 (39.9)	6.24 (20.1)	Yes

C_{max}[1], Maximum plasma concentration over 28 day simulations; AUCav, Average area under curve over 28 day simulations; C_{max}[2], Maximum plasma concentration after final dose; AUC, Area under curve after final dose; Ctrough, Minimum plasma concentration over 28 day simulations; PA-EC_{95}, Protein binding-adjusted effective concentration (BIC PA-EC_{95}: 0.162 mg/L).

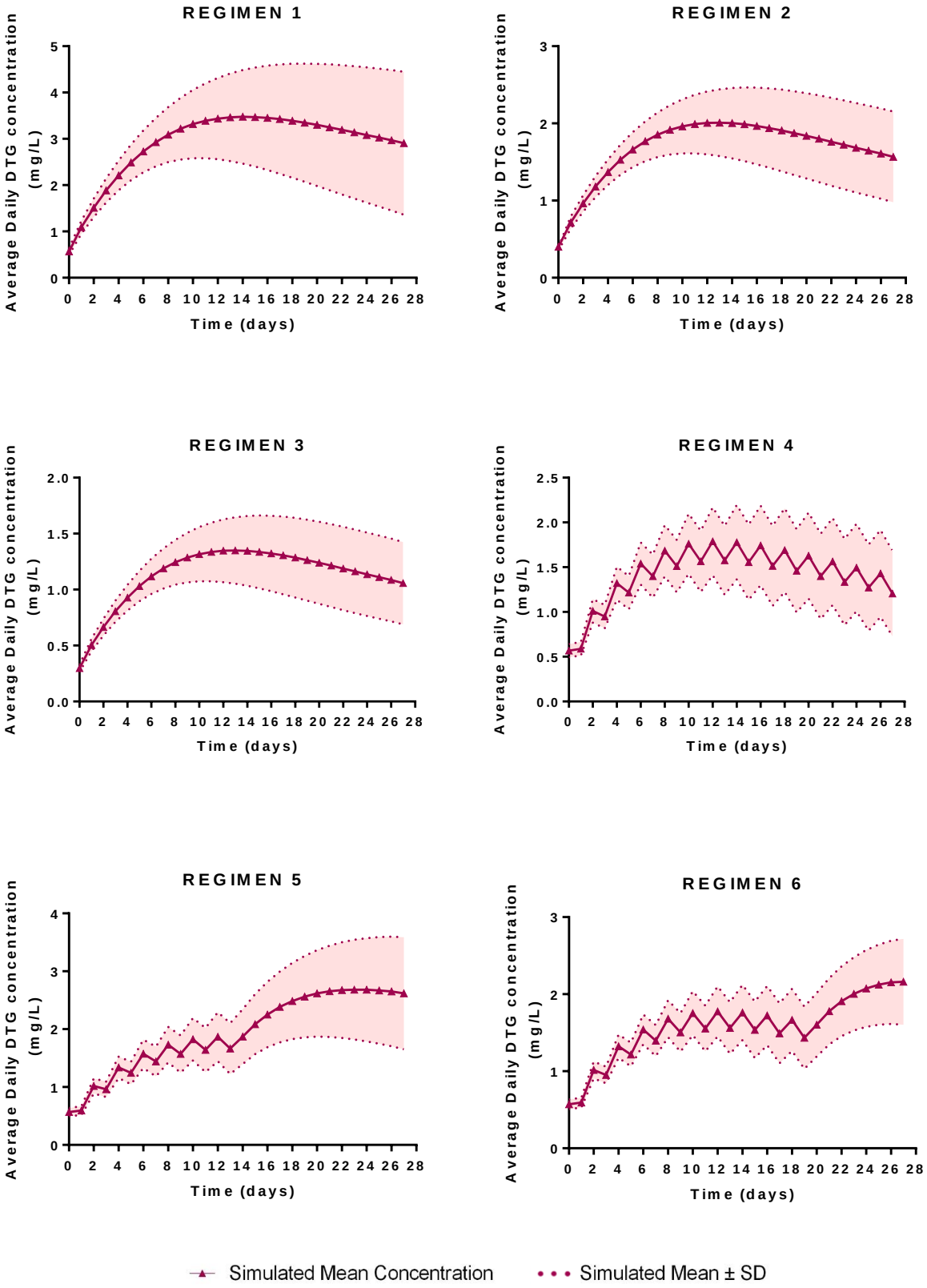

Figure 3.1 Average daily DTG concentration time profiles in neonates

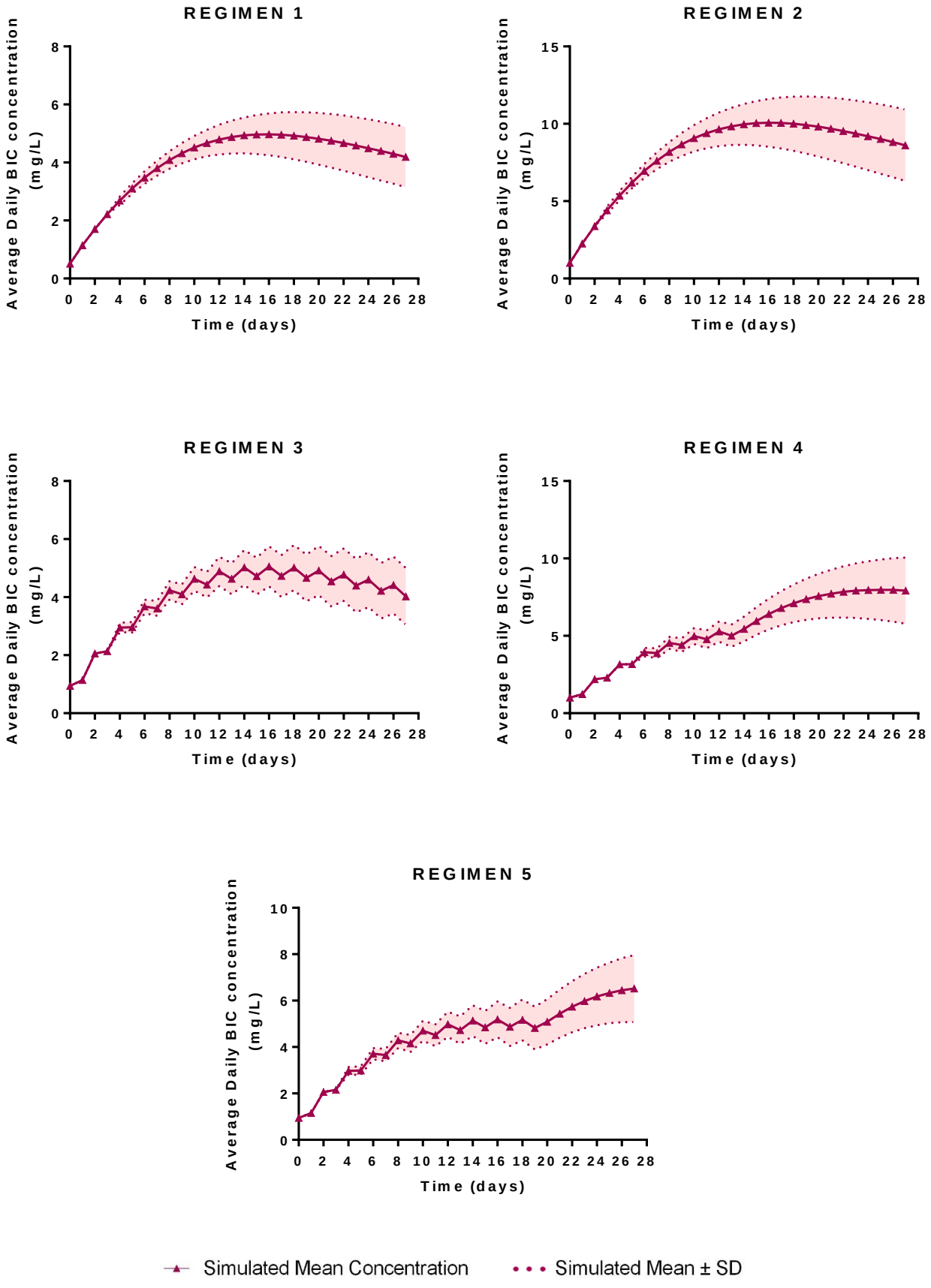

Figure 3.2 Neonatal average daily BIC concentration time plots

3.4 Discussion

The benefits of initiating ARV therapy shortly after birth may include prevention of infection in at-risk infants and early viral suppression in those infants who are infected [97]. Breastfeeding increases the risk of infection in newborns but has enormous benefits for health and is recommended by WHO for at least the first six months of life [98]. In low- and middle-income countries, breastfeeding is favoured to avoid infant mortality from other life-threatening infections and initiating prophylaxis in breastfed neonates is encouraged for PMTCT [99]. There are only 5 ARVs with adequate neonatal PK and safety data and a formulation suitable for use in neonates, the need for more potent alternatives is essential for effective early treatment and prophylaxis [100]. Dose optimisation in neonatal patients is complex and PBPK modelling may help inform knowledge gaps in the absence of empirical data. This is exemplified here with dose prediction for dolutegravir and bictegravir deployment in neonates.

UGT1A1 polymorphism is known to affect dolutegravir exposure [101], certain polymorphisms are responsible for reduced enzyme activity resulting in an increase in exposure [101]. A previous study in adults concluded that this reduction in activity did not have a clinically significant impact on the exposure of dolutegravir [101], however this would need exploring further in neonates. The expression of CYP3A7 in newborns is considerably high in comparison to CYP3A4. Although CYP3A7 and CYP3A4 have similarities in sequence identity and substrate range, the activity of CYP3A7 is known to be significantly less. The effect of CYP3A7 on dolutegravir and bictegravir has not yet been fully elucidated however CYPs play a minor role in the metabolism of dolutegravir hence was not included in the model [85]. Metabolic differences, like the ones highlighted in this paragraph, observed between adults

and infants can play a profound role in drug pharmacokinetics and remains a widely understudied area [102].

Though the presented model predicts the PK of dolutegravir it has some key limitations. Maternal transfer of drug through breast milk or placenta has not been considered by the model. Pregnant women with HIV infection are expected to start or already be receiving treatment which involves a combination of ARVs. A cause for concern in breastfed neonates is maternal transfer of these drugs. The dolutegravir transfer into breast milk in a mother-infant pair was previously estimated to be equal to a daily infant exposure of 0.015 mg/kg [103]. Dolutegravir also readily crosses the placenta, therefore mothers receiving this treatment will be exposing neonates to dolutegravir with or without breastfeeding [104]. Based on our findings, the neonate's first dose may be postponed until 24-48 hours after birth if the mother has received dolutegravir 2-24 hours prior to delivery. Data on bictegravir's ability to cross the placenta is not yet available and studies must be done to understand the impact on neonates.

Although exposure from breast milk was not considered in this study, the model does provide information on a range of parameters from absorption through to risk of concentration-dependent fetal toxicity. Several models have previously been published describing infant exposure via breast milk [105-108]. The most recent involved a model to estimate isoniazid exposure in infants, a drug used in the first-line treatment of tuberculosis [108]. Two multi-compartment models were coupled together, one adult and one infant; a separate compartment for breast milk was incorporated into the model. Predictions generated from the model suggested infant isoniazid exposure was relatively low and would not result in any clinically significant adverse effects. While progress has been made in the development of

these models, similar limitations arise from the lack of knowledge on specific neonatal characteristics. A recently published review on PBPK modelling in neonates [57] highlighted the importance of cross-talk between modellers and clinicians to bridge the understanding of age-related changes. Clinical observations and modelling can be combined in an attempt to explicate the developmental changes observed in the first month of life, utilising the knowledge that cannot solely be gained from existing *in vitro* and *in vivo* methods. The integration of molecular and clinical approaches represents an ideal interdisciplinary framework for the enhancement of modelling and its translation to various clinical scenarios [58, 69, 72, 105].

Despite limitations, PBPK models are considered validated if predicted mean values lie within 2-fold of observed data [10]. Clearly, in the absence of clinical data it was not possible to specifically qualify the presented neonatal dolutegravir/bictegravir model. However, the raltegravir and midazolam qualification described in chapter 2 does provide confidence that the ontogeny profiles of CYP3A4 and UGT1A1 appropriately described expression in neonates. Observed differences between simulated and clinical drug concentrations (e.g., C_{max} and T_{max}) can additionally be caused by the model limitations described above but will likely have limited clinical impact. A study evaluating the PK of dolutegravir in pregnant women and their infants reported the median elimination half-life in 21 infants as 38.2 hours, following in utero exposure [104]. Although infants did not directly receive dolutegravir, the half-life provides information on the elimination kinetics of dolutegravir in the first days of life. The simulations generated by the neonatal PBPK model are in keeping with this value with predictions of half-life within 20% of observed data (Table 3.4). The PK, efficacy and safety of dolutegravir in infants with HIV and children aged ≥ 4 weeks to < 6 years was previously investigated [84] and used for further qualification

of the neonatal model. Within this study, 10 subjects were aged between 4 weeks and 6 months receiving a once daily 5 mg dispersible tablet, the same dose was simulated *in silico*. In the absence of a PBPK model for infants, predictions were carried out by extrapolating from the existing neonatal model. To minimise the difference between subpopulations, extrapolations were taken between weeks 4-5. Though the simulated data of dolutegravir in infants were close to the clinical values (within 2-fold), there was a trend to overestimate clearance, resulting in lower mean AUC values (Table 3.3). The simulations for dolutegravir were carried out over a 28-day period for several multiple dose regimens outlined in table 3.4, with a maximum dose of 5 mg set by the adequate AUC and C_{trough} values achieved clinically in infants. From the fixed-dose (regimens 1-3) concentration-time profiles, a steady increase in plasma concentrations of dolutegravir is observed during the first week of life, reaching maximum concentrations on days 7-10 (Figure 3.1); this may partly be explained by the immaturity of enzymes. Based on this prediction, a greater initial dose may be needed if the goal is to reach therapeutic concentrations within the first hours of life.

It is also worth noting that the smallest dose formulation currently available for dolutegravir is a 5 mg dispersible tablet, however, administering 5 mg of dolutegravir daily (regimen 1) may lead to over-dosing. Regimens 4-6 propose alternative strategies to accommodate for the formulation restrictions that currently surround dolutegravir. Based on the simulated data, introducing a longer interval between dosing could pose a solution; regimen 6 involved 5 mg doses with a 48h interval from day 1-20 escalated to 5 mg once daily on week 4, yielding AUC and C_{trough} values of 37.6 mg.h/L and 1.9 mg/L, respectively (Table 3.4). These values fall within the target criteria and are comparable to the clinical paediatric exposure.

Simulations for bictegravir were similarly carried out for the duration of the neonatal period (0-28 days) and several dosing regimens have been outlined in Table 3.5. Due to the unavailability of clinical data a previously qualified adult PBPK model was employed to validate input parameters. The simulated values were in good agreement with literature data with AAFE values well within the 2-fold acceptance criteria. Although the model passed qualification stages, it was met with a number of limitations. Clearance in the model was calculated using the apparent systemic clearance obtained from literature as data on the intrinsic clearance of dolutegravir and bictegravir were lacking. This clearance value was adjusted to take into account bioavailability. Since information was limited, it was assumed bioavailability in humans was the same as observed in macaques for dolutegravir (87%). Once the clearance had been adjusted to represent total systemic clearance the model generated PK in accordance with clinical PK. These physicochemical properties were then used as input data for the neonatal PBPK model. The retrograde calculation of clearance also took into account differences in protein binding, microsomal content, weight of the neonatal liver etc., before it was applied in the neonatal model. For bictegravir in neonates, regimens 1 and 3 produced the most promising outcome in terms of PK, with AUC and C_{trough} values comparable to adult exposures (AUC: 102 mg.h/L); C_{trough} 2.61 mg/L) [88], with neonates receiving either a daily fixed dose of 2.5 mg (regimen 1) or a dose of 5 mg every 48 hours (regimen 3) throughout the neonatal period (28 days).

Transporters can represent a factor influencing pharmacokinetics and dolutegravir has been identified as a substrate for P-glycoprotein (Pgp) and breast cancer resistance protein (BCRP) [85], although the role of these transporters in the definition of dolutegravir has not been fully characterized. This modelling approach does not include a maturation function for transporter expression, and this could

represent a potential limitation of our approach. Data concerning transporter abundance in neonates is largely understudied. Future studies elucidating expression in good quality paediatric tissue could help resolve this issue, however, these experiments are complicated by factors such as small sample sizes.

With the previously stated formulation limitations, an advantage of PBPK modelling is its ability to simulate the PK of novel formulations [72]. Large dose adjustments are commonly observed between adult and paediatric patients, a more robust formulation approach would prove invaluable as drug approval in neonates and infants is often hindered by a lack of suitable formulations. PBPK modelling can be used to evaluate and help direct development of alternative formulations appropriate for use in paediatric patients.

CHAPTER 4

Simulation of Long-Acting, Intramuscular, Cabotegravir in Neonates

Contents

4.1 Introduction

As highlighted in Chapter 3, HIV receives widespread global attention for being one of the leading causes of death, with 150,000 new cases of HIV reported in children under 15 years of age in 2020 [78].

Cabotegravir (CAB) is a HIV-1 integrase inhibitor that stimulates a potent virological response [109] and has potential for treatment and prophylaxis within neonatal populations [110]. High efficacy and safety make integrase inhibitors the preferred first-line treatment of HIV in adult patients. In addition, CAB's unique physicochemical and DMPK characteristics are compatible with different drug delivery strategies and has been identified as an excellent candidate for its use as a long-acting formulation [109, 111]. As we move towards the use of LA injectables for HIV treatment and prevention, there is great interest in the potential of these formulations for neonates and children. Administration of oral medications in neonates has posed significant challenges, with a number of factors including, formulation, palatability and caregiver burden negatively impacting treatment outcomes [112]. Long-acting formulations reduce the frequency of dosing and in regard to neonates, hold the potential of a single administration for the duration of the neonatal period, alleviating many of the aforementioned difficulties.

The use of long-acting formulations in paediatric patients has been proposed in several disease areas. The treatment of schizophrenia, autism spectrum disorder, bipolar disorder and other mental disorders involves the use of LA/extended release antipsychotics, namely, paliperidone palmitate, aripiprazole, and risperidone [113]. Lack of compliance with maintenance treatment in patients with such disorders is associated with higher rates of relapse [113, 114]. LA injectable antipsychotics (LAIA) have been developed to maintain stable serum levels of the drug and to improve

adherence in adults. While these formulations have not been approved in adolescents and paediatric patients, the benefits of LAIA lead to the off-label use of these products in children and adolescents [115, 116] and have been suggested to be a safe treatment option during adolescence [115].

The safety and pharmacokinetics (PK) of CAB have previously been studied in healthy, HIV-infected, co-morbid adult patients. In early 2021, the U.S. Food and Drug Administration (FDA) approved the LA injectable antiretroviral regimen, CAB and rilpivirine (RPV), in adults with HIV [111, 117]. Prior to the initiation of the intramuscular (IM) injection it is recommended that patients receive oral formulations of both CAB and RPV to assess patient tolerance [111]. Currently no studies have been conducted in adolescents and paediatric patients aged <18 years for these drugs.

To date, few ARV's have been studied in neonates; lack of suitable formulations and treatment options limit the possibilities for neonatal antiretroviral therapy. The objective of this study was to simulate the pharmacokinetics of IM and oral CAB in neonates and identify an appropriate initial dosing regimen to rapidly achieve therapeutic levels using mechanistic PBPK modelling.

4.2 Methodology

This study is based on virtual patients; therefore, no ethical approval was required.

The PBPK model was designed in SimBiology version 5.8, a product of MATLAB R2018a (MathWorks, Natick, MA, USA 2018). [58] Virtual patients between 0 – 28 days were simulated. Neonatal maturation characteristics and a description of physiological and anatomical growth data were incorporated where appropriate. The model was based on the following assumptions: (1) well-stirred compartments with instant distribution of the drug; (2) no absorption of the drug from the colon; and (3) the model is blood flow limited.

4.2.1 Anatomy

Equations describing the basic anatomy and physiology of neonates have been previously described in Chapter 2 and were implemented in the neonatal PBPK model. The adult PBPK model was constructed using physiological and anatomical equations previously defined in the literature [69].

4.2.2 Plasma Protein Binding

Plasma protein binding of drugs in neonates was calculated using a previously combined database on age-related changes in plasma albumin and α_1-acid glycoprotein. [65] The unbound fraction of drug was estimated using the following equation (29): [66]

$$\mathrm{fu_{Paediatric}} = \frac{1}{1 + \frac{(1 - \mathrm{fu_{Adult}}) \times [\mathrm{P}]_{\mathrm{Paediatric}}}{[\mathrm{P}]_{\mathrm{Adult}} \times \mathrm{fu_{Adult}}}} \quad (29)$$

4.2.3 Metabolism

4.2.3.1 Ontogeny of UGT1A1 and UGT1A9

The ontogeny profile of UGT1A1 has been described by previously in Chapter 2 and detailed below in equation 30; a polynomial equation describing the fraction of UGT1A1 present in neonates in relation to the adult abundance. Due to insufficient data on neonatal UGT1A9 expression, the maturation profile was assumed to be identical to UGT1A1 ontogeny (equation 30). [65]

$$\mathrm{UGT1A1} = (-5 \times 10^{-10} \times \mathrm{Age}^4) + (-5 \times 10^{-7} \times \mathrm{Age}^3) - (0.0002 \times \mathrm{Age}^2) + (0.0203 \times \mathrm{Age}) + 0.0305 \quad (30)$$

4.2.4 Modelling Cabotegravir Clearance

The clearance of cabotegravir is majorly facilitated by UGT1A1 (67%), with smaller contributions from UGT1A9 (33%) and renal elimination (<1%) [111]. Intrinsic clearance values derived from *in vitro* experiments were used to scale UGT1A1 and UGT1A9 clearance. In the absence of literature data, UGT1A9 ontogeny was assumed to follow the same maturation profile as UGT1A1. Renal clearance of cabotegravir in neonates was not included in the final clearance calculation due to its relatively minor contribution (equation 31).

$$\mathrm{CL_{cabotegravir}} = \left(\mathrm{Clint_{U1A1+U1A9,adults}\ x\ Wliver\ x\ MPPGL\ xUGT1A1_{neonates}}\right) \quad (31)$$

Where $\mathrm{Clint_{U1A1+U1A9,\ adults}}$ is the sum of intrinsic clearance values of cabotegravir facilitated by UGT1A1 and UGT1A9 enzymes, $\mathrm{UGT1A1_{neonates}}$ is the fraction of UGT1A1 present in neonatal livers relative to the adult abundance, Wliver is the

neonatal liver weight, MPPGL is the neonatal microsomal protein per gram of liver and $CL_{cabotegravir}$ is the total clearance of cabotegravir in neonates expressed in L/h.

$CL_{cabotegravir}$ was then scaled using equation 32 to account for unbound fraction of drug in neonates (Fu) and neonatal hepatic vein blood flow (Q_{hv}).

$$CLh = \frac{(Q_{hv} \text{ x } Fu \text{ x } CL_{cabotegravir})}{(Q_{hv} + CL_{cabotegravir} \text{ x } Fu)} \quad (32)$$

4.2.5 Distribution

The volume of distribution was calculated using previously published equations and has been described in detail Chapter 2. [70]

4.2.6 Modelling IM administration

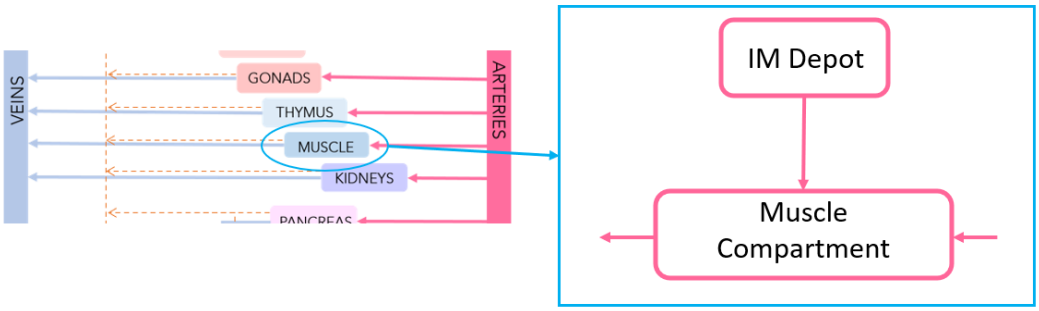

Figure 4.1 Schematic of intramuscular depot model.

The IM depot model was constructed by adding a further compartment (Figure 4.1) representing a proportion of the muscle the intramuscular injection is delivered to based on previous literature [72]. To model intramuscular drug release from the depot a previous population-PK study in which a two-compartment first-order absorption model was constructed to describe the absorption of long-acting, injectable cabotegravir, was used [58, 72]. Diffusion of drug from the IM compartment obeys first-order kinetics as described in Tegenge et al [118]. Based

on these findings, cabotegravir release rate in adults was assumed to be $4.5x10^{-4}$ h^{-1} [58, 72].

4.2.7 Model Simulations & Qualification

The qualified whole-body neonatal PBPK model described in Chapter 2 was modified to simulate cabotegravir in neonates in which the ontogeny of the key enzyme UGT1A1 was refined and validated using observed neonatal raltegravir clinical data [76]. For further validation of model input parameters, IM and oral cabotegravir were simulated in an adult PBPK model; observed, adult clinical data were used for comparison [119-121].

An 800 mg quarterly IM dose was simulated in the adult PBPK model. Clinical data concerning a 30 mg PO multiple-dose of cabotegravir [121] was used and simulated in the model for the oral validation. For each clinical scenario, simulations were run in 100 virtual patients and the mean AUC, maximum plasma concentration (C_{max}), minimum plasma concentration (C_{trough}) and CL were recorded for comparison against observed data.

4.2.7.1 Model Predictions

Several scenarios were modelled in healthy neonates with the aim of achieving plasma exposures 4-fold above the reported protein adjusted (PA) IC_{90} (4*$PAIC_{90}$: 0.664 µg/mL). To gain a better understanding on exposures in neonates, a range of IM doses from 10-25 mg were evaluated initially before moving forward with the dose that resulted in the most favourable PK in terms of target exposures. Since depot release in the neonate is unknown, simulations were performed using the adult release rate ($4.5x10^{-4}$) as well as with this parameter decreased and increased by 2, 5 and 10-fold. Several anatomical factors can affect the absorption and

dispersion of drug in neonates, including differences in muscle mass, composition, and vascularity. The possibility of an oral safety lead-in in conjunction with an IM injection was also explored in the model, simulating doses ranging from 0.5-1.5 mg in combination with a 20 mg IM dose.

4.2.7.2 Statistical Evaluation of the Model

The PBPK model was qualified by calculating the absolute average fold error (AAFE) and root mean squared error (RMSE) where appropriate. AAFE is a useful parameter to assess over or under-prediction of the model, values closer to 1 indicate a closer similarity with observed values. The RMSE calculates the error between the predicted value and the observed value. The model was assumed to be qualified if the predicted values fell within the following criteria: with AAFE < 2 and RMSE < 1 as per convention for the approach [10]. The absolute differences between simulated AUC, C_{max} and C_{trough} was also considered to evaluate the potential clinical relevance.

Table 4.1 Physiochemical properties of cabotegravir.

Property	Cabotegravir [58]
Molecular weight, g/mol	-
Log $P_{o:w}$	1.04
f_u	0.007
pK_a	10.04
R	0.5
Polar surface area, $Å^2$	99.2
Hydrogen bond donors	2
Caco-2 permeability, 10^{-6} cm/sec	NA
Clearance	NA
CL_{int} UGT1A9	2.2
CL_{int} UGT1A1	4.5
Solubility, mg/L	113

Abbreviations: CL_{int}, intrinsic clearance; log Po:w, partition coefficient between octanol and water; f_u, unbound fraction of drug; NA, not applicable; pKa, logarithmic value of the dissociation constant; R, blood-to-plasma ratio; Clearance, systemic clearance; UGT, uridine diphosphate glucuronosyltransferase ratio (µL/minute/mg of microsomal protein).

4.3 Results

4.3.1 Model Qualification

4.3.1.1 Oral Cabotegravir in Adults

The validation of cabotegravir in adults has been detailed in Table 4.2. Simulated mean PK parameters were within the acceptance criteria and deviated from observed data by an average of 16.5%, with mean AUC, C_{max}, C_{trough} and CL values falling within -9.6%, -22.8%, +0.21% and +33.3% of clinical data, respectively.

Table 4.2 Summary of oral cabotegravir qualification in adults.

PK characteristic	Clinical*	Simulated*	AAFE
AUC (mg.h/L)	146	132	1.106
C_{max} (mg/L)	8.1	6.25	1.296
C_{trough} (mg/L)	4.7	4.71	1.002
T_{max} (h)	3	4	1.333

Abbreviations: *Values shown as geometric mean; Cmax, maximum plasma concentration; AUC, area under curve over 24 hours, Ctrough, minimum plasma concentration; T_{max}, time taken to reach maximum concentrations; AAFE, absolute average fold error.

4.3.1.2 IM Cabotegravir in Adults

The validation of cabotegravir in adults has been detailed in Table 4.3. Simulated PK parameters were within the 2-fold acceptance criteria with mean AUC, C_{max}, C_{trough}

and CL values within +19.6%, +16.4%, +19.1% and +9.6% of observed clinical data, respectively. The simulated PK profile yielded an AAFE and RMSE value of 1.166 and 0.440, respectively, and has been presented in Figure 4.2.

Table 4.3 Summary of IM cabotegravir qualification in adults.

PK characteristic	Clinical*	Simulated*	AAFE
AUC (mg.h/L)	4467	5341	1.196
C_{max} (mg/L)	3.3	3.84	1.164
C_{trough} (mg/L)	1.075	1.28	1.191
CL (L/h)	0.249	0.273	1.096
Abbreviations: *Values shown as geometric mean; Cmax, maximum plasma concentration; AUC, area under curve over 24 hours, Ctrough, minimum plasma concentration; CL, total systemic clearance; AAFE, absolute average fold error.			

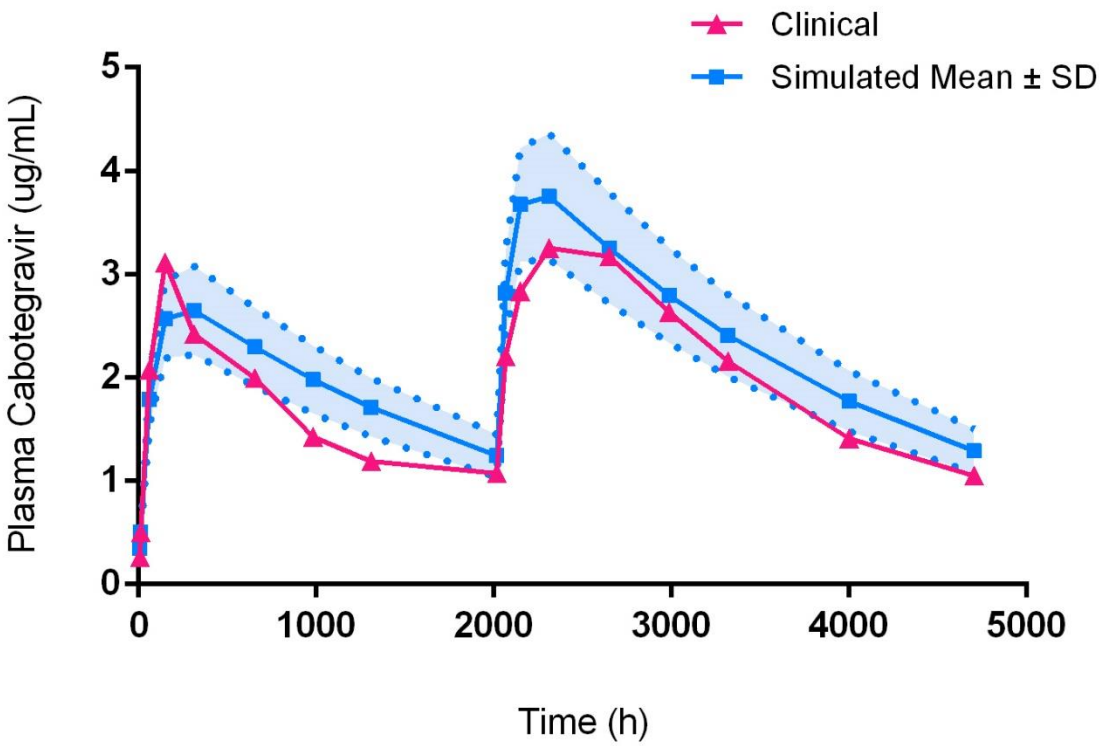

Figure 4.2 PBPK qualification of IM cabotegravir in adults (800 mg Q3mo dose).

4.3.2 IM Cabotegravir in Neonates

Initial simulations of cabotegravir in neonates suggested a 20 mg IM dose generated PK in keeping with target exposures, with C_{trough} values greater than the 4-fold $PAIC_{90}$ value (1.2 µg/mL vs 0.664 µg/mL). Further simulations were run with the 20 mg IM dose with several release rates. Early cabotegravir concentrations and time to achieve target concentrations were sensitive to the IM release rate. The initial simulations of IM cabotegravir suggested that a delay of 35 hours (Regimen 1, Table 1) is required to reach target concentrations if the infant cabotegravir release rate is identical to adults. To overcome this lag a single dose oral lead-in of cabotegravir was simulated (Regimen 8, Table 1).

Table 4.4 PK summary of cabotegravir dosing regimens in neonates.

Regimen	Dose	Release rate	Lag time to plasma concentration ≥4*PAIC$_{90}$ (h)	C_{max} (mg/L)	C_{trough} (mg/L)	$AUC_{0\text{-}28d}$ (mg*h/L)	AUCav (mg*h/L)
1	20 mg IM CAB on Day 0	Adult*	35	2.55	1.20	1218.2	43.5
2	20 mg IM CAB on Day 0	0.1x Adult	-	0.28	0.15	134.9	4.8
3	20 mg IM CAB on Day 0	0.2x Adult	-	0.53	0.28	260.5	9.3
4	20 mg IM CAB on Day 0	0.5x Adult	77	1.33	0.70	646.6	23.1
5	20 mg IM CAB on Day 0	2x Adult	17	4.69	1.80	2150.6	76.8

6	20 mg IM CAB on Day 0	5x Adult	7	10.06	2.21	4176.7	149.2
7	20 mg IM CAB on Day 0	10x Adult	4	15.85	1.90	5923.4	211.6
8	20 mg IM CAB & 0.8 mg PO CAB on Day 0	Adult	4	4.69	1.08	1438.5	51.4
Abbreviations: *Adult release rate = $4.5x10^{-4}$, 4*$PAIC_{90}$: 0.664 ug/mL; C_{max}, maximum plasma concentration; C_{trough}, minimum plasma concentration; AUC_{0-28d}, area under the curve over 28-days; AUCav, average daily concentration.							

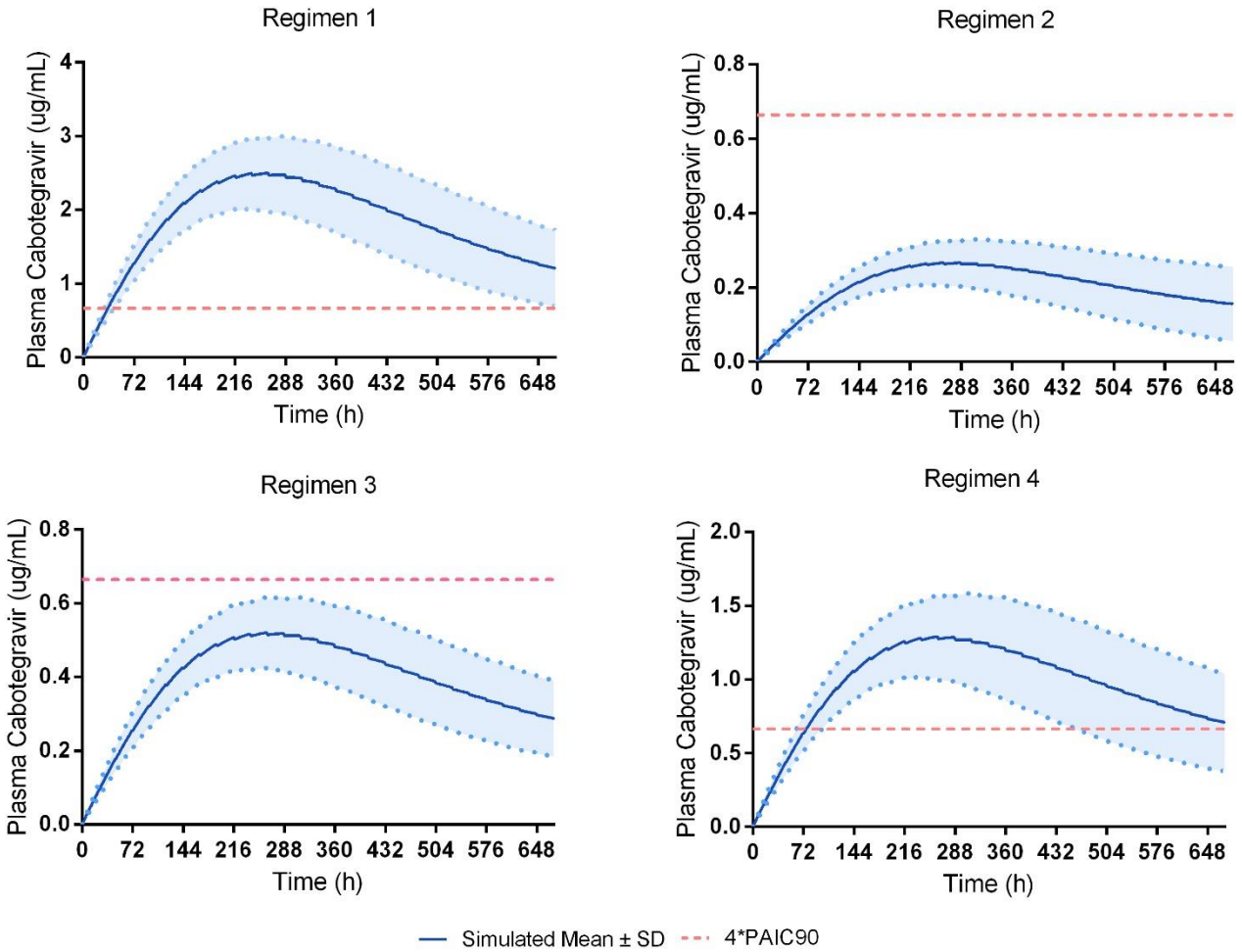

Figure 4.3 Simulated PK profiles of IM cabotegravir in neonates (Regimens 1-4) with 4*$PAIC_{90}$ therapeutic cut-off (0.664 µg/mL).

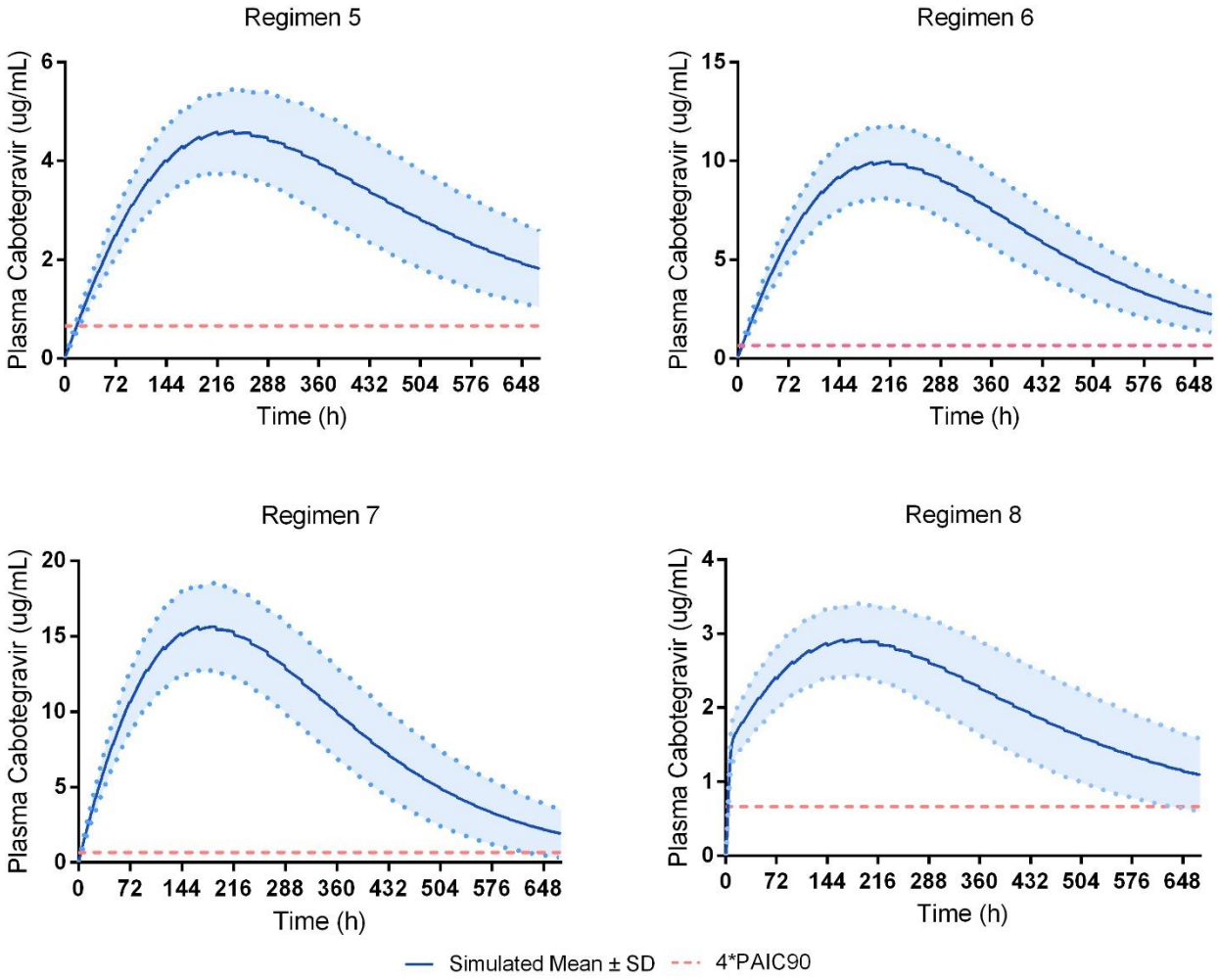

Figure 4.4 Simulated PK profiles of IM cabotegravir in neonates (Regimens 5-8) with 4*$PAIC_{90}$ therapeutic cut-off (0.664 µg/mL).

4.4 Discussion

Antiretroviral prophylaxis can considerably decrease the risk of infants acquiring HIV through perinatal transmission. The duration of treatments is dependent upon the length of breastfeeding and maternal risk factors [100, 122]. However, the number of antiretrovirals available for treatment in neonates is only a few. Long-acting or extended-release nanoproducts of antiretrovirals hold the potential of simplifying treatment regimens while improving adherence in populations where poor adherence impedes successful treatment. Though long-acting formulations have many advantages their utility in sub-populations such as neonates is still in question. This study predicted the pharmacokinetics of injectable IM CAB in neonates.

The previously developed neonatal PBPK model [123] was modified to simulate cabotegravir in neonates. In the absence of cabotegravir clinical data in neonates, the drug-specific model input parameters were qualified using an adult PBPK model. Observed data on IM and oral cabotegravir in adults were available for the qualification: an 800 mg Q3mo administration and a 30 mg QD dose, respectively, these conditions were replicated in the model [111, 120]. The intrinsic values derived from literature were insufficient in their characterisation of clearance hence a scaling factor was applied, this scaling factor was carried through to the neonatal model. The model succeeded in capturing both pharmacokinetic profiles of oral and IM LA cabotegravir in adults with values of AAFE falling within the acceptance criteria (<2 fold). The mean simulated pharmacokinetic parameters, AUC, C_{max} and C_{trough} also fell within the qualification criteria with an average percentage difference of 16.5% and 16.2% from clinical data for both oral and IM cabotegravir respectively.

Lack of data on neonatal characteristics make it inherently difficult to characterise certain parameters such as enzyme and transporter ontogenies, in such instances,

assumptions were made in the neonatal model. Cabotegravir is mainly metabolised by UGT1A1 with minor contributions from UGT1A9 [109]. The ontogeny of UGT1A1 was previously validated using the probe substrate raltegravir as described in Chapter 2, however, limited data were available for the characterisation of UGT1A9 expression in neonates. Due to inadequate data, it was assumed UGT1A9 had an identical maturation profile to UGT1A1 but considering the minor role UGT1A9 plays in cabotegravir metabolism, its subsequent effect on the PK profile was assumed to be minimal. Furthermore, cabotegravir is highly bound to plasma proteins (>99%), a cause for concern is its impact on bilirubin to albumin binding and the risk of neonates developing kernicterus from elevated levels of bilirubin in blood leading to bilirubin neurotoxicity [124]. The effect of cabotegravir on bilirubin displacement from albumin has not yet been studied and therefore was not considered by the model. Previous studies on the in vitro assessment of bilirubin displacement of integrase inhibitors, raltegravir [125] and dolutegravir [126], concluded that the extent of bilirubin displacement was not clinically significant, however this would need evaluating further *in vivo* for the long-acting formulation of cabotegravir.

Drugs can be transferred from mother to fetus transplacentally. Transplacental transfer of drugs is known to occur through passive diffusion, facilitated diffusion, active transport and other processes [127]. Maternal-fetal transfer of ARVs contributes to the prevention of perinatal HIV transmission however deducing the safety profile of drugs in fetuses is extremely challenging. Women who become pregnant while on long-acting drugs are advised to discontinue treatment. Nevertheless, washout PK data of drugs in newborns can be useful in determining elimination kinetics and can be used in neonatal model development to inform dose selection as has been demonstrated in Chapter 3 with dolutegravir. The transfer of

cabotegravir via breastmilk has not been considered in the model. Breastfed infants can be a cause for concern. The necessity of breastfeeding in resource limited countries to avoid infant mortality has been well established [100, 122]; pregnant women are likely to be receiving ART and maternal transfer of these drugs can pose a challenge. Studies on the kinetics of breastmilk transfer of long-acting cabotegravir are not yet available and would be necessary to understand infant exposures.

Despite limitations, the model predicted the PK of cabotegravir in neonates. 100 virtual patients were simulated to account for population variability. The simulations for cabotegravir were run for a duration of 28 days, covering the neonatal period (Table 4.3). Initially, three IM doses ranging from 10-25 mg were evaluated in the model with the adult release rate. The 20 mg IM dose yielded the most favorable outcome in terms of PK and target concentrations hence this dose was carried forward for further evaluation of release rates. As the release rate of the long-acting cabotegravir formulation is unknown in neonates this parameter was decreased and increased by 2, 5 and 10-fold to assess its impact on the PK. Decreases in the release rate showed an increase in lag time to target plasma concentration (>4*PAIC90) and lower concentrations in plasma (Regimens 2-4, Table 4.3), where release rate was 10-fold lower than the adult value, the resulting PK was 10-fold lower (Regimen 2, Table 4.3). Conversely, increasing the release rate decreased the time taken to reach target concentrations and, overall, increased plasma concentrations significantly (Regimens 5-7, Table 4.3). Taking these simulations into consideration, if release rates differ in neonates, dose adjustments may not only be significant, but necessary. The initial simulations also suggested a lag to reach target concentrations was present (≥ 35 hours), this delay could have serious implications in practice as neonates are most vulnerable in the first hours of life. Given the apparent differences

in composition of tissue and muscle mass in neonates compared to adults [54, 55], a delay in absorption following IM administration is somewhat anticipated and could be the result of reduced muscle blood flow, muscle mass and muscular contractions, all of which contribute to the overall dispersion of the drug [55]. To overcome this lag, oral doses were simulated in the neonatal model following validation in an adult PBPK model. A range of oral doses were explored in neonatal model, with a 0.8 mg dose yielding the most promising PK, this dose was then simulated in conjunction with the 20 mg intramuscular injection (Regimen 8, Table 4.3). Results from the simulations suggest an oral dose in conjunction with an IM dose can overcome the delay to reach target concentrations.

Assuming the cabotegravir depot release rate in neonates is the same as observed in adults, the simulations suggest a 20mg IM injection alongside a single dose of oral cabotegravir both initiated on day 0, is suitable to achieve target exposure (>4*$PAIC_{90}$). However, since the effect of neonatal physiology on the depot release rate is unknown, observational data are needed to delineate the depot release rate in neonates and establish an appropriate neonatal cabotegravir dosing regimen. Early evaluation of the application of long-acting formulations for neonatal use can provide significant knowledge and help support their development.

CHAPTER 5

DDI PBPK Model Development for Moderate Inducers

Contents

5.1 Introduction

The current standard of care for HIV treatment is highly active antiretroviral therapy (HAART) which involves a combination of multiple ARVs taken simultaneously to suppress HIV replication [128]. Since the introduction of combination therapy, mortality and morbidity in PLWH has considerably decreased [40]. However the resulting immunodeficiency from HIV, make patients susceptible to co-infections [129]. Concurrent morbidities are a systemic result of HIV/AIDS that require the use of additional medicines to treat, consequently increasing the chances of drug-drug interactions (DDI) in people living with HIV (PLWH) [129]. A DDI between two or more drugs can compromise the effectiveness of treatment or result in toxicity [130]; if a dose adjustment is required, a relevant change in drug concentration occurs or the co-medication is resulting in toxicity the DDIs has clinical significance [130]. Common co-infections in PLWH include tuberculosis (TB), hepatitis B, hepatitis C and malaria. TB remains the leading cause of death among PLWH [129].

The majority of DDIs remain unstudied during drug development due to the sheer volume of possible interactions and ethical constraints associated with high-risk DDIs. However, the importance of studying potential interactions is widely recognised, and as a result, a great deal of the PBPK models submitted to the US Food and Drug Administration (FDA) are regarding DDI prediction [131, 132]. During drug development clinical DDI studies are routinely focused on strong inducers and inhibitors evaluating the worst-case scenarios with fewer data regarding moderate and weak interactions, resulting in multiple DDIs with poor characterisation. The magnitude of induction/inhibition on victim drugs can be simulated via PBPK modelling, using *in vitro* metabolism data and *in vivo* studies for model qualification [132]. PBPK models have previously been developed for the

quantitative prediction of potential interactions and to evaluate whether they can be safely managed with dose adjustments [132-134].

Bictegravir is a novel selective and potent HIV-1 integrase inhibitor and doravirine is non-nucleoside reverse transcriptase inhibitor [94, 135]. Both drugs have limited clinical experience in DDIs. Rifabutin is a well characterised moderate inducer used for the treatment of TB and is commonly administered in PLWH, thus was used to develop a moderate inducer PBPK model.

5.2 Methodology

A whole-body adult PBPK model was applied to predict the pharmacokinetic parameters of moderate drug-drug interactions between bictegravir and rifabutin (BIC/RFB) and doravirine and rifabutin (DOR/RFB). All PBPK models were developed in Simbiology v5.8, a product of Matlab 2018a (MathWorks, Natick, MA, USA; 2018). 100 male and female virtual patients aged between 18-60 years were simulated for each DDI scenario. Physicochemical and biological drug properties, *in vitro* and *in vivo*, were used to simulate BIC, DOR, and RFB [88, 94-96, 136]. Parameter estimation was carried out via curve fitting where data was not available.

5.2.1 Anatomy

Male and female virtual patients aged between 18-60 years were simulated in the model. Data from the National Center for Health Statistics were used to define key characteristics, body weight and body mass index (BMI). These characteristics were used to determine body surface area and height, described in equations 33 and 34, respectively. [56]

$$BSA = \text{Weight}^{0.425} \times \text{Height}^{0.725} \times 0.007184 \quad (33)$$

$$\text{Height} = \text{Weight}/\text{BMI} \quad (34)$$

5.2.2 Tissue and organ weights

Organ and tissue weights were derived allometrically using height, weight, BMI, and age equations (Table 5.1). [56]

Table 5.1 Equations to calculate organ/tissue weights in the PBPK model using allometric scaling methods.

Organ/Tissue	Model equations
Adipose	((((1.20*BMI)+(0.23*Age)-16.2)*Weight)/100) ± 0.041
Blood	3.33*BSA-0.81 ± 0.1
Bones	exp(0.0689+2.67*log(Height)) ± 0.166
Brain	0.405*exp(-Age/629)*(3.68-2.68*exp(-Age/0.89)) ± 0.084
Gonads	(3.3+53*(1-(exp((-Age/17.5)^5.4)))/1000 ± 0.049
Heart	exp(-2.502+2.13*log(Height)) ± 0.069
Kidneys	exp(-2.306+1.93*log(Height)) ± 0.14
Liver	exp(-0.6786+1.98*log(Height)) ± 0.028
Lungs	exp(-2.092+2.1*log(Height)) ± 0.195
Intestines	exp(-1.351+2.47*log(Height)) ± 0.049
Muscle	0.93*Weight-Total weight
Pancreas	exp(-3.431+2.43*log(Height)) ± 0.245
Remaining	exp(-0.072+1.95*log(Height) ± 0.049
Skin	exp(1.64*BSA-1.93) ± 0.049
Stomach	exp(-3.266+2.45*log(Height)) ± 0.0965
Spleen	exp(-3.123+2.16*log(Height)) ± 0.156

Thymus	14*((7.1-6.1*exp(-Age/11.9))*((0.14+0.86*exp(-Age/10.3))))/1000 ± 0.049
Total Weight	Lungs + Heart + Bones + Kidneys + Stomach + Intestines + Spleen + Pancreas + Liver + Remaining + Brain + Skin +Blood + Adipose + Thymus + Gonads
Age expressed in years, BMI in kg/m^2, height in m, weight in kg and BSA in m^2.	

5.2.3 Blood Flow

Blood flows to each organ were represented as a fraction of the total cardiac output, (Table 5.2).

Table 5.2 Fraction of organ blood flow relative to total cardiac output

Organ/Tissue	Fraction of total cardiac output
Adipose	0.052
Bones	0.042
Gonads	0.01
Brain	0.11
Hepatic Vein	0.32
Hepatic Artery	0.12
Kidneys	0.175
Intestines	0.05

Muscle	0.19
Lungs	0.025
Pancreas	0.05
Skin	0.06
Spleen	0.05
Stomach	0.05
Remaining tissue	0.01
Portal Vein	0.2
Blood flows expressed in L/h. Cardiac output = 15 x Weight$^{0.75}$.	

5.2.4 Intestinal Absorption

Absorption was represented in the PBPK model using the CAT model described in Chapter 2 (Figure 2.1) [61] which considers a small intestine transit time of 3.3 hours and a stomach transit time of 0.5 hours [61]. The ordinary differential equations 35-43 (ODE) detailed herein were used to describe rates of change to the amount of drug in the gastrointestinal tract for each of the nine compartments.

Stomach compartment:

$$\frac{dA_{U,ST}}{dt} = -K_s \, x \, A_{U,ST} - K_D \, x \, A_{U,ST} \tag{35}$$

$$\frac{dA_{D,ST}}{dt} = -K_s \, x \, A_{D,ST} + K_D \, x \, A_{U,ST} \tag{36}$$

Small intestinal compartment:

$$\frac{dA_{U,SI}}{dt} = K_s \, x \, A_{U,ST} - K_t \, x \, A_{U,SI} - K_D \, x \, A_{U,SI} \quad (37)$$

$$\frac{dA_{D,SI}}{dt} = K_s \, x \, A_{D,ST} + K_D \, x \, A_{U,SI} - K_a \, x \, A_{D,SI} \, x \, C_{SOL,SI} \quad (38)$$

$$\frac{dA_{ABS,SI}}{dt} = K_a \, x \, C_{SOL,SI} x \, A_{D,SI} \quad (39)$$

Small intestinal compartments 2-7:

$$\frac{dA_{U,SIi}}{dt} = K_t \, x \, A_{U,SIi-1} - K_t \, x \, A_{U,SIi} - K_D \, x \, A_{U,SIi} \quad (40)$$

$$\frac{dA_{D,SIi}}{dt} = K_t \, x \, A_{D,SIi-1} - K_t \, x \, A_{D,SIi} + K_D \, x \, A_{U,SIi} - K_a \, x \, A_{D,SIi} \, x \, C_{SOL,SIi} \quad (41)$$

$$\frac{dA_{ABS,SIi}}{dt} = K_a \, x \, C_{SOL,SIi} x \, A_{D,SIi} \quad (42)$$

Colon Compartment:

$$\frac{dA_{CO}}{dt} = K_t \, x \, A_{U,SI7} - K_t \, x \, A_{D,SI7} - K_C \, x \, A_{CO} \quad (43)$$

5.2.5 Metabolism

Doravirine is extensively metabolised by cytochrome P450 3A4 (CYP3A4) and bictegravir metabolised by CYP3A4 (fm = 0.5) and UDP glucuronosyltransferase 1 family, polypeptide A1 (UGT1A1 – fm = 0.5) [88, 136].

5.2.5.1 Intestinal Metabolism

Equation 44 was used to calculate the clearance of drugs by the gut (CLgut). *In vitro* data on intrinsic clearance (CL_{int}), adult abundance of CYP3A4 enzyme (Ab_{CYP3A4}) and unit scaling factors were incorporated in the final calculation.

$$CLgut\ (L/h)\ = \frac{CL_{int}\ x\ Ab_{CYP3A4}\ x\ 1000\ x\ 60}{1000000} \quad (44)$$

The scaling of *in vitro* intrinsic clearance to adult systemic clearance has been outlined in Chapter 2.

5.2.6 Distribution

The volume of distribution was calculated using previously published *in silico* models and has been described in Chapter 2. Adult tissue composition parameters comprising water, phospholipids, and neutral lipids, have been highlighted in Table 5.3 and were used to calculate drug distribution. [70]

Table 5.3 Composition of tissues in adults

Organ/tissue	Water	Phospholipids	Neutral Lipids
Adipose	0.180	0.0020	0.790
Bone	0.439	0.0011	0.074
Brain	0.770	0.0565	0.051
Gut	0.718	0.0163	0.049
Heart	0.758	0.0166	0.012
Kidney	0.783	0.0162	0.021
Liver	0.751	0.0252	0.035

Lung	0.811	0.0090	0.003
Muscle	0.760	0.0072	0.024
Skin	0.718	0.0111	0.028
Spleen	0.788	0.0198	0.020
Plasma	0.945	0.0023	0.004
Fractions based on average adult weight, 70 kg.			

5.2.7 Induction modelling

5.2.7.1 CYP3A4 Induction Model

Rifabutin moderately induces CYP3A4. Induction equations for CYP3A4 were derived from a previously published model [133].

5.2.7.2 Model Equations

Induction (Ind) via CYP3A4 was estimated using equation 45. Where E_{max}, EC_{50} and I_h represent the maximum induction, concentration of inducer producing 50% of E_{max} and the concentration of inducer in the liver, respectively.

$$Ind = 1 + \frac{E_{max}\ x\ I_h}{EC_{50} + I_h} \quad (45)$$

Rifabutin was assumed to have minimal effect on UGT1A1 induction based on literature data [137]; information regarding the induction potential of RFB on UGT enzymes is sparse. A study on the induction effects of RFB on long-acting

cabotegravir implemented a 1.3-fold increase in clearance accounting for RFB induced clearance in order to predict the resulting PK [138, 139].

5.2.8 Model Simulations and Qualification

5.2.8.1 Qualification of Plasma PK

The plasma PK of doravirine, bictegravir and rifabutin were qualified in the PBPK model using observed clinical data prior to simulating drug-drug interactions to ensure input data could sufficiently characterise drugs. The input parameters have been summarised in Table 5.4.

100 virtual patients were simulated for each modelling scenario. A 100 mg once daily (QD) dose of orally administered DOR was simulated in the model and mean AUC, C_{max} and C_{trough} values were recorded for comparison [136]. The concentration-time profile was also compared against clinical data. For BIC, a 50 mg QD oral dose [94] was simulated and mean PK parameters were recorded for comparison. A 300 mg QD dose of orally administered RFB was also simulated; two sets of clinical PK data were available for comparison of mean PK parameters and a concentration-time profile.

The AAFE and RMSE (where applicable) were calculated as a measure of model validation, with AAFE values < 2 and RMSE values < 1 passing qualification [10].

5.2.8.2 Qualification of Moderate DDIs

Clinical data on DDIs routinely evaluate the magnitude of an interaction by calculating the geometric mean ratios of drug PK with and without inducer/inhibitor, with a result of 1 equating to no effect on the drug PK. For the qualification of moderate interactions of DOR/RFB, a 100/300 mg QD dose was simulated in the model and for BIC/RFB, a 75/300 mg QD dose was simulated based on observed

data. To subsequently evaluate the predictive performance of the substrate PBPK models for the effect of a UGT1A1 and CYP3A4 inducer, mean ratios were calculated assessing the effect on AUC, C_{max} and C_{min} using equations 46-48, for comparison against clinical data [88, 136].

$$AUC_R = AUC_{with\ inducer}/AUC_{without\ inducer} \quad (46)$$

$$C_{max,R} = C_{max,with\ inducer}/C_{max,without\ inducer} \quad (47)$$

$$C_{min,R} = C_{min,with\ inducer}/C_{min,without\ inducer} \quad (48)$$

A more stringent criteria than usual (<2 fold) was applied in the qualification of models, with models assumed qualified if ratios were ± 30 % of observed data and AAFEs were within 1.5-fold. As DDI model validation is tiered, single drug models must pass qualification first, followed by the validation of each DDI. To reduce model uncertainty a stricter criterion than usual was selected for the validation of the full DDI models.

Table 5.4 Physicochemical and biological properties of rifabutin, doravirine and bictegravir.

Property	Rifabutin [140-142]	Doravirine [135, 136]	Bictegravir [94-96, 143]
Molecular weight, g/mol	847.0	425.8	449.4
Log $P_{o:w}$	3.2	2.19	2.7
f_u	0.29	0.24	0.01
pK_a	6.9	9.47	9.8
R	0.6	0.9	0.64
Polar surface area, $Å^2$	209	98	99.2
Hydrogen bond donors	5	1	2
Caco-2 permeability, 10^{-6} cm/sec	95 nm/s	-	14.8
Clearance	48.3[A]	6.36[A]	621.9 [B]
CL_{int} CYP3A4	0.514	0.11	7.71×10^{-4}
CL_{int} UGT1A1	-	-	NA
Solubility, mg/L	190	11.5	62.3

$E_{max,CYP3A4}$	3.4	-	-
$EC_{50,CYP3A4}$, µm	0.3	-	-
Abbreviations: A, L/h; B, mL/h; CLint, intrinsic clearance; CYP, cytochrome P450 (µL/minute/pmol); log Po:w, partition coefficient between octanol and water; NA, not applicable; pKa, logarithmic value of the dissociation constant; R, blood-to-plasma drug ratio; UGT, uridine diphosphate glucuronosyltransferase (µL/minute/10^6); E_{max}, maximum induction of CYP3A4 measured in fold change; EC_{50}, concentration of CYP3A4 inducer producing 50% of $E_{max.}$			

5.3 Results

The PBPK models were initially validated using observed plasma PK on orally administered DOR, BIC and RFB alone before the prediction of DDIs.

5.3.1 Doravirine

Initial simulations of DOR in the PBPK model yielded AAFE values greater than 1.5-fold consequently failing qualification criteria, for this reason the parameter Vss was fitted in the model using the clinical data. Upon applying a correction factor to Vss, DOR plasma PK was successfully predicted by the model with AAFE values falling within the 1.5-fold acceptance criteria with C_{max} generating the highest AAFE value of 1.168 (Table 5.5). The concentration-time profile was also in good agreement with literature data (Figure 5.1), with the profile yielding AAFE and RMSE values of 1.131 and 0.188, respectively.

Table 5.5 Summary of observed and simulated PK parameters of a 100 mg QD dose of orally administered DOR.

PK Variable	Clinical	Simulated	AAFE
AUC (mg*h/L)	17.5	16.3	1.071
C_{max} (mg/L)	1.226	1.05	1.168
C_{trough} (mg/L)	0.384	0.427	1.112

Abbreviations: AUC, area under curve over 24 hours; C_{max}, maximum plasma concentration; C_{trough}, minimum plasma concentration; AAFE, absolute average fold error.

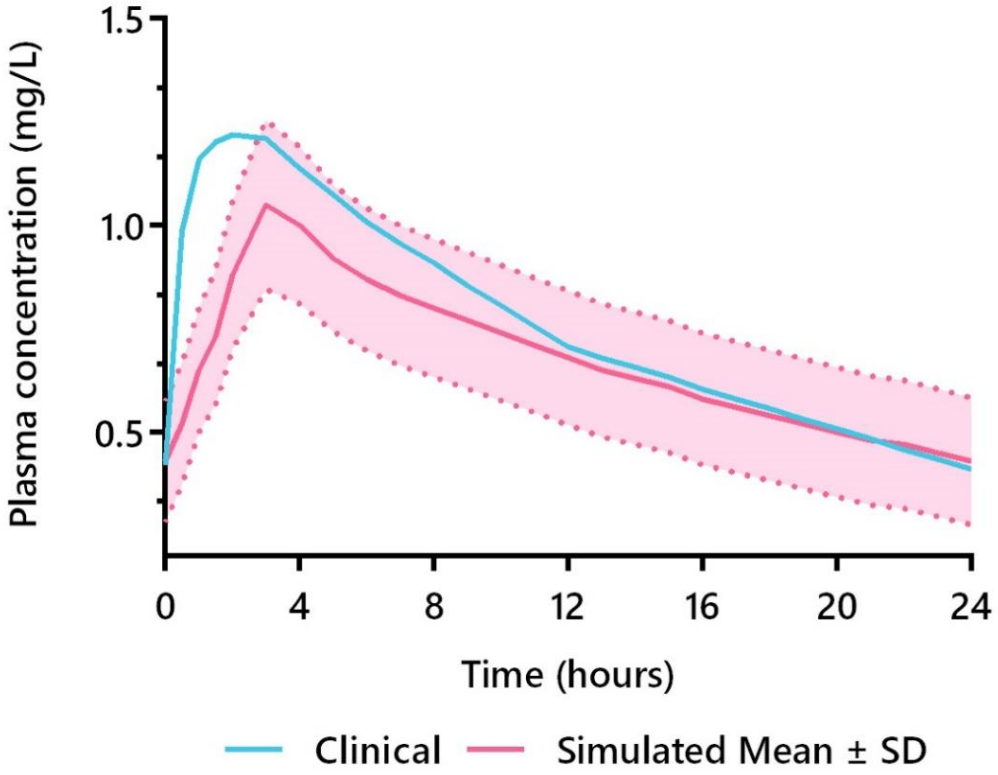

Figure 5.1 Simulated and observed concentration time profile of orally administered DOR 100 mg QD. Blue solid line represents observed clinical data (mg/L), pink solid line and shaded area represents simulated mean plasma concentration ± standard deviation (mg/L).

5.3.2 Bictegravir

Adjustments on the Vss were made in the model for better characterisation of PK parameters and clinical data was used to guide the level of correction applied to this parameter. Following adjustments, BIC PK were successfully predicted by the model with AAFE values of mean PK parameters well within the 1.5-fold acceptance criteria (Table 5.6).

Table 5.6 Summary of observed vs simulated PK parameters of a 50 mg QD dose of orally administered BIC.

PK Variable	Clinical	Simulated	AAFE
AUC (mg*h/L)	102	103.7	1.016
C_{max} (mg/L)	6.15	6.10	1.008
C_{trough} (mg/L)	2.61	2.75	1.054
CL (L/h)	0.622	0.695	1.117

Abbreviations: AUC, area under curve over 24 hours; C_{max}, maximum plasma concentration; C_{trough}, minimum plasma concentration; CL, total systemic clearance; AAFE, absolute average fold error.

5.3.3 Rifabutin

A 300 mg QD dose of orally administered RFB was simulated in the PBPK model and the resulting PK has been outlined in Table 5.7 and 5.8.

Comparison against clinical data yielded AAFE values within the 2-fold acceptance criteria. Both sets of clinical PK parameters passed qualification; the concentration-time profile has been illustrated in Figure 5.2, simulated profiles generated an AAFE and RMSE value of 1.370 and 0.084, respectively.

Table 5.7 Summary of observed and simulated PK parameters of a 300 mg QD dose of orally administered RFB.

PK Variable	Clinical	Simulated	AAFE
AUC (mg*h/L)	5.03	6.37	1.266
C_{max} (mg/L)	0.522	0.472	1.106
T_{max} (h)	4	3	1.333
Abbreviations: AUC, area under curve over 24 hours; C_{max}, maximum plasma concentration; T_{max}, time to reach maximum plasma concentration; AAFE, absolute average fold error.			

Table 5.8 Summary of observed and simulated PK parameters of a 300 mg QD dose of orally administered RFB.

PK Variable	Clinical	Simulated	AAFE
AUC (mg*h/L)	6.19	6.37	1.029
C_{max} (mg/L)	0.461	0.472	1.024
CL (L/h)	48.3	39.6	1.219

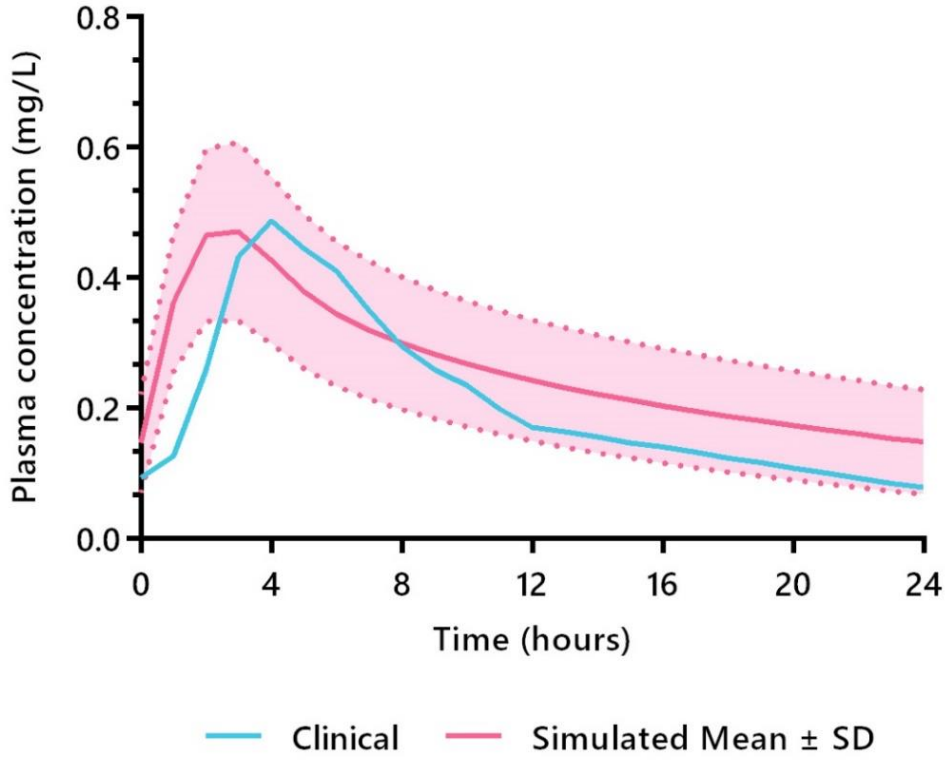

Figure 5.2 Simulated versus observed concentration time profiles of RFB 300 mg QD. Blue solid line represents observed clinical data (mg/L), pink solid line and shaded area represents simulated mean plasma concentration ± standard deviation (mg/L).

5.3.4 DOR/RFB Drug-Drug Interaction

Following successful validation of both DOR and RFB alone, a combination dose of 100-300 mg of DOR/RFB was simulated in the model. Simulated mean AUC, C_{max} and C_{min} values were recorded to calculate the mean ratio (Table 5.9).

The percentage difference between simulated mean ratios and clinical ratios for AUC, C_{max} and C_{min} were +21.4, -16.4% and +22.2%, respectively. The resulting AAFEs for AUC, C_{max} and C_{min} were 1.179, 1.240 and 1.250, respectively.

Table 5.9 Summary of predicted DDI between DOR/RFB in moderate DDI PBPK model.

PK variable	DOR 100 mg QD (simulated)	DOR 100 mg/RFB 300 mg QD (simulated)	Mean Simulated Ratio	Clinical Ratio
AUC (mg*h/L)	9.08	5.67	0.62	0.50
C_{max} (mg/L)	0.58	0.49	0.84	0.99
C_{min} (mg/L)	0.25	0.10	0.40	0.32

5.3.5 BIC/RFB Drug-Drug Interaction

Following successful validation of BIC, a combination dose of 75-300 mg of BIC-RFB was simulated in the model. Simulated mean AUC, C_{max} and C_{min} values were recorded to calculate the mean ratio (Table 5.10). The percentage difference between simulated mean ratios and clinical ratios for AUC, C_{max} and C_{min} were -7.8%, -7.2% and -2.2%, respectively. The resulting AAFEs for AUC, C_{max} and C_{min} were 1.081, 1.075 and 1.023, respectively. Simulated data were in good agreement with literature values.

Table 5.10 Summary of predicted DDI between BIC/RFB in moderate DDI PBPK model.

PK variable	BIC 75 mg QD (simulated)	BIC 75 mg/RFB 300 mg QD (simulated)	Mean Simulated Ratio	Clinical Ratio
AUC (mg*h/L)	83.75	56.31	0.67	0.62
C_{max} (mg/L)	5.14	4.40	0.86	0.80
C_{min} (mg/L)	2.35	1.05	0.45	0.44

5.4 Discussion

An adult PBPK model was developed by defining the physiological and anatomical characteristics using mathematical equations. The PBPK model was qualified for virtual adults aged between 18-60 years. Data on the anatomy and physiology of the target population was readily available and derived from existing literature. The model was qualified prior to running simulations with all blood flows, organ/tissue weights and volumes within the acceptance criteria (< 2-fold).

For the qualification of the CYP3A4 induction, each drug was initially validated in the model alone, prior to running drug-drug interaction simulations to evaluate model performance. In order for bictegravir and doravirine to pass model qualification criteria, modifications on the volume of distribution were made. Observed data were used to scale the correction factor to be applied on Vss in the PBPK model and the AAFE was used as a qualitative measure of model performance, a narrower criteria were used (within 1.5-fold) to minimise the error in prediction when validating the DDI model . Following modifications, the model successfully predicted the AUC, C_{max} and C_{min} of orally administered BIC, DOR and RFB alone, with AAFE's falling within 1.5-fold criteria and ratios within 30% of observed values. The induction of CYP3A4 was evaluated in the model using a previously established model assessing the inducing and inhibitory effects of efavirenz on several CYP substrates [133]. The number of studies on moderate and weak DDIs in comparison to strong DDIs is few as clinical studies for DDIs tend to focus on worst case scenarios.

Moderate drug-drug interactions are of clinical relevance as in some cases dose adjustments are necessary for treatment efficacy. BIC, as demonstrated in this chapter serves as an example, BIC is usually administered as a 50 mg dose,

however, in combination with RFB the dose is increased to 75 mg to compensate for the induction effects . Throughout the literature, inhibition, and induction of CYP enzymes has been widely studied therefore input data concerning E_{max} and EC_{50} for the perpetrator drug RFB on CYP3A4 were readily available in the literature. However, knowledge on the effect of inducers and inhibitors on non-cyp enzymatic pathways is less well characterised. The difficulty in modelling UGT-mediated DDIs is reflected in the lack of models and clinical studies available, of the data that is available majority are focused on the inhibition of these enzymes [144, 145]. Callegari *et al* recently developed a PBPK model to evaluate the inhibitory effects of mefenamic acid (MFA) on UGT enzymes [144]. They evaluated the DDI following co-administration of ertuglifozin (a UGT substrate) with MFA and qualified the model using clinical DDI data involving MFA and dapaglifozin. Dapaglifozin served as a probe substrate which has a similar metabolic profile to ertuglifozin in order to predict the DDI between MFA and ertuglifozin. The successfully qualified model predicted an AUC_R of 1.51 when MFA is co-administered with ertuglifozin. [144]

The only data that was available at the time of the study for UGT1A1 enzyme was the fold change in mRNA expression for UGT1A1 [137], data on EC_{50} values were not obtainable. In the instance that input data for the model is unavailable, it is common practice to estimate parameters using observed clinical data [144, 146]. To begin estimating the EC_{50} value for rifabutin for UGT1A1, a probe substrate that is entirely cleared by UGT1A1 would be necessary along with data on its co-administration with RFB to support the optimisation of this parameter. Raltegravir is metabolised solely by UGT1A1 and clinical data for both raltegravir alone and with rifabutin was available for model verification, however, the clinical PK that was available was itself conflicted, with greater exposures for AUC and C_{max} recorded in the presence of the inducer [137]. For this reason, the EC_{50} could not be estimated using these methods.

More recently, a study evaluating the inducing effects of rifabutin on oral cabotegravir was published [138], based on this study Han *et al* [139] assumed a 1.3-fold increase in clearance for long-acting (LA) cabotegravir (CAB) and implemented this value in a PPK model to predict the effect of rifabutin on LA CAB. Simulations were run for modified and unmodified regimens of LA CAB co-administered with RFB, in 500 virtual patients. The unmodified regimen resulted in 90-92% of simulated subjects achieving plasma concentrations above the target cut-off (0.65 µg/mL) following subsequent injections, suggesting moderate induction via RFB [139]. To overcome this, switching to a monthly injection of CAB was suggested when co-administering with rifabutin. Going forward, it may be worth applying a 1.3-fold induction on the UGT-facilitated clearance of BIC to evaluate the magnitude of induction on UGT1A1.

Although BIC is equally metabolised by CYP3A4 and UGT1A1, predictions of the interaction between RFB were still made and data on UGT1A1 induction was not included due to the abovementioned limitations and paucity of information. Taking into account the minor effect RFB had on RAL and CAB [137-139], it was assumed the magnitude of induction on UGT1A1 enzyme was less pronounced than on CYP3A; this rationale is supported by the model predictions, with clinical versus simulated ratios generating a less than 10% difference. There was a minor trend to underestimate the magnitude of interaction for BIC, which could be owed to the exclusion of UGT1A1 induction.

The DDI PBPK model only considers liver induction, rifabutin is known to induce P-glycoprotein (P-gp) transporters. P-gp are efflux transporters that play a role in the absorption, distribution, and elimination of certain compounds. Developing models that can characterise the magnitude of transporter DDIs are often met with complexities and several issues impede the ability to evaluate this through

modelling, few of which include, the lack of specific transporter substrates for *in vitro* characterisation, the need for validated *in vitro* assays to evaluate induction and the lack of clinical studies assessing the effect of P-gp related DDIs, all of which are essential to support PBPK model development. Although DOR is a P-gp substrate, its absorption has been attributed to its good permeability properties and P-gp is thought to play a relatively minor role [147], P-gp is also present in the intestine, however, induction has previously been reported to be of a weaker magnitude relative to CYP3A [147]. Based on this data and the given limitations, transporter and intestinal DDIs were not considered by the model.

As discussed previously, the current PBPK model is adequate to estimate the DDI of moderate inducer rifabutin. Bearing in mind the above-mentioned limitations the model successfully predicted the induction of CYP3A4 for both DOR and BIC and simulations were well within the acceptance criteria. Based on these simulations, the increased 75 mg dose of BIC is enough to overcome the effects of induction by RFB. As for the DOR/RFB DDI, the exposure of 100 mg DOR is significantly reduced, simulations would suggest either increasing the dose or reducing the frequency between doses (e.g Q12h) could result in target PK.

Clinical management of DDIs remains a challenge in the care and treatment of PLWH. The application of PBPK modelling to support drug development and discovery is now well recognised, more specifically, the application of models to predict DDIs has gained regulatory endorsement from the FDA, EMA and PMDA [131, 146]. Considering majority of the PBPK models developed in recent years have been focused on enhancing the management of CYP-related DDIs, there is considerable potential in the modelling of UGT-related and transporter-related DDIs. Although more research on this topic needs to be done for the effective translation of *in vitro* data in PBPK modelling, with a heavy focus on the neglected

areas that have been previously stated. A topic worth evaluating further is dose-dependent induction of moderate inducers, dexamethasone is a known moderate inducer of CYP3A and experiences dose-dependent induction [148]. With dose-dependent induction the magnitude of the interaction can be heightened and often underestimated [148].

CHAPTER 6

Mechanistic Modelling for the Evaluation of ARV Penetration in Lymphatic Tissues

Contents

6.1 Introduction

Lymphoid tissues (LT) are one of the primary sites of HIV replication. Antiretroviral (ARV) therapy results in the effective inhibition of viral replication in peripheral blood, however, HIV reservoirs can persist in different tissues. HIV reservoirs are a group of immune cells that are infected with HIV (latent stage) but are not actively producing new virus [149]. Continuing viral replication has previously been linked with sub-therapeutic concentrations of ARV drugs in the LT and LT can represent a reservoir of inducible virus [48, 150]. Understanding the degree in which ARVs penetrate LT could be pivotal in optimising therapy and reducing the latent reservoir [149, 151].

The lymphatic system plays an essential role in the homeostasis of tissue fluid, absorption of fats and nutrients and immunological response [152]. The lymphatics comprise a one-way transport system via a network of vessels and lymph nodes act as filtering ducts. Lymph is the fluid that circulates throughout the body and forms as interstitial fluid drains into the lymphatic capillaries [47]; it comprises white blood cells, majority of which are lymphocytes (B cells and T cells) that help protect the body from infections.

The majority of PBPK models that have previously incorporated lymphatic physiology have mainly been developed to evaluate the pharmacokinetics (PK) of biotherapeutics such as monoclonal antibodies (mAbs) [153-156] as large proteins mostly enter the lymphatic system. The PK mechanisms of macromolecules differ to that of small molecules, hence, to model macromolecules, sub-compartmentalisation of tissue compartments into intracellular, endosomal, interstitial, and vascular compartments is necessary to capture the non-uniform and permeability-limited distribution of these compounds [155, 156]. Shah and Betts

[155] developed such a PBPK model to characterise the plasma and tissue PK of nonspecific or antigen specific mAbs in mice and evaluated the scale-up potential of the model by characterising the plasma PK of mAbs in mouse, rat, monkey and humans. MAb entered endosomal space via pinocytosis and on and off rates were used to describe the interaction between FcRn and mAb. The PBPK model was similarly built by sub-dividing compartments and successfully characterised tissue and plasma PK of different mAbs with a common set of estimated parameters [155].

Lymphatic PBPK models for small molecules have not yet been developed, however in disease areas like HIV, other infections and cancer, it may be beneficial to understand treatment efficacy within these tissues. The objective of this chapter was to incorporate lymphatic physiology in a whole-body PBPK model to describe the penetration of ARVs in LT.

6.2 Methodology

Mechanistic adult PBPK models were developed in Simbiology v5.8, a product of Matlab 2018a (MathWorks, Natick, MA, USA; 2018) to predict the pharmacokinetic parameters and lymphatic penetration of raltegravir and efavirenz. Virtual cohorts comprising 100 male and female patients aged between 18-60 years were simulated in models for each drug. Alterations to the lymphatic system due to disease state were not considered by the model as simulated patients were considered 'healthy'.

6.2.1 Anatomy

The anatomy of the adult PBPK model has previously been highlighted in Chapter 5.

6.2.2 Tissue and organ weights and volumes

Organ and tissue weights were derived allometrically using height, weight, BMI, and age equations as described in Chapter 5; Table 5.1.

Values of the physiological parameters used to describe lymphatics in the PBPK model have been detailed in Table 6.1. Interstitial volumes for organs and tissues were derived from literature and implemented in the model for each interstitial compartment. Vascular volumes were defined as a fraction of the total organ/tissue volume based on literature data [154].

6.2.3 Blood and Lymph flow

Blood flows to each organ was represented as a fraction of the total cardiac output, listed in Chapter 5; Table 5.2.

Lymph flow has been reported to be 500 times lower than the blood flow to the given organ [152] hence blood flows to each tissue or organ was divided by 500 to derive the lymph flow.

6.2.4 Intestinal Absorption

Absorption was represented in the PBPK model using the CAT model described in Chapter 2. Ordinary differential equations (ODE) were used to describe transit of drug through the gastrointestinal tract and have been described in detail in Chapter 5.

6.2.5 Metabolism

6.2.5.1 Raltegravir and Efavirenz

Raltegravir is majorly metabolised by the UGT1A1 enzyme. Intrinsic clearance data on the metabolism of RAL by UGT1A1 was used to scale clearance.

Efavirenz is metabolised by CYP2B6, CYP2A6, CYP3A4, CYP1A2 and CYP3A5. Systemic clearance data was used to calculate clearance in the PBPK model.

6.2.6 Distribution

The volume of distribution was calculated using previously published *in silico* models and has been described in Chapters 2 & 5.

6.2.7 Model structure

Figure 6.1 details a schematic diagram of the lymphatic PBPK model structure. For the lymphatic model, each compartment was further divided into vascular, interstitial and tissue sub-compartments as shown in Figure 6.2. The model is set up such that the arterial blood compartment receives blood from the lung compartment and distributes blood to all vascular compartments. Each vascular compartment is

connected to its respective tissue and interstitial fluid compartment. Lymph from all the organs is delivered to a central lymph node compartment via the efferent lymph supply from the interstitial compartments. Lymph flow is then delivered to the venous compartment from the lymph node, completing the circuit. Physiological parameters such as lymphatic flow, interstitial fluid and vascular volumes etc. were used to characterise the physiology of the lymphatic system.

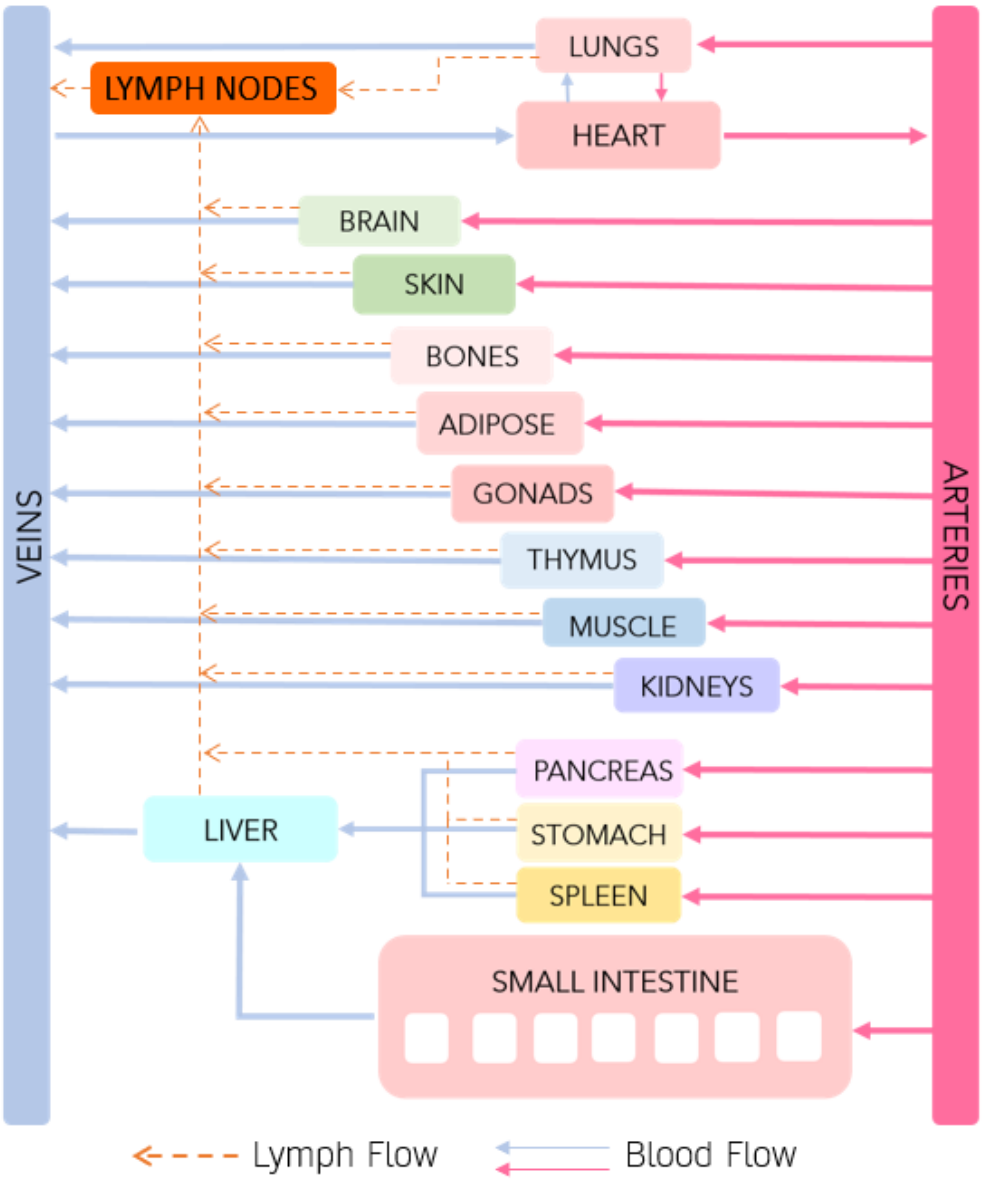

Figure 6.1 Schematic diagram of lymphatic PBPK model.

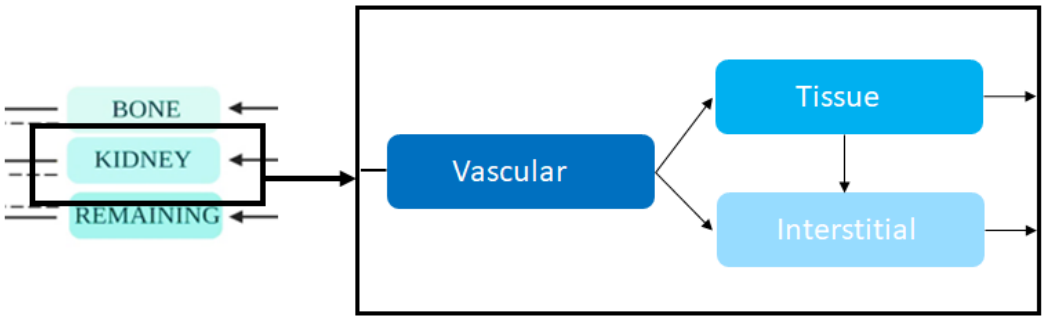

Figure 6.2 Structure of how organ/tissue compartments are further divided to describe movement of drug through lymphatics.

6.2.7.1 Model parameters

Based on previous lymphatic PBPK models [153, 155], a vascular and lymphatic reflection coefficient were incorporated in the model to describe the level of resistance provided to compounds by the vascular endothelial cells and lymphatic openings, respectively. For vascular reflection coefficients, the physiologic upper limits of pore size of different blood capillaries was previously reviewed, based on this, the vascular coefficients for heart, muscle, lung, skin, adipose and gut was set to 0.95; for kidney, spleen and pancreas, the value was set to 0.9; the value for bone, liver and spleen was set to 0.85 and for the brain the value was set to 0.99 a priori [155].

The lymphatic reflection coefficient was derived from a previously published study [157] on the effect of molecular weight on the lymphatic absorption of compounds. This was determined by measuring the cumulative recovery of four compounds in lymph following administration [157]. The data suggested a linear relationship between the weight of a drug and the proportion of dose absorbed by the lymphatics. Equation 49 represents the lymphatic recovery based on molecular weight, which was extrapolated from the literature using the Plotdigitizer tool (plotdigitizer.sourceforge.net) (Figure 6.3).

$$\text{Lymph recovery} = 0.00003 \text{ x Molecular weight} + 0.0404 \quad (49)$$

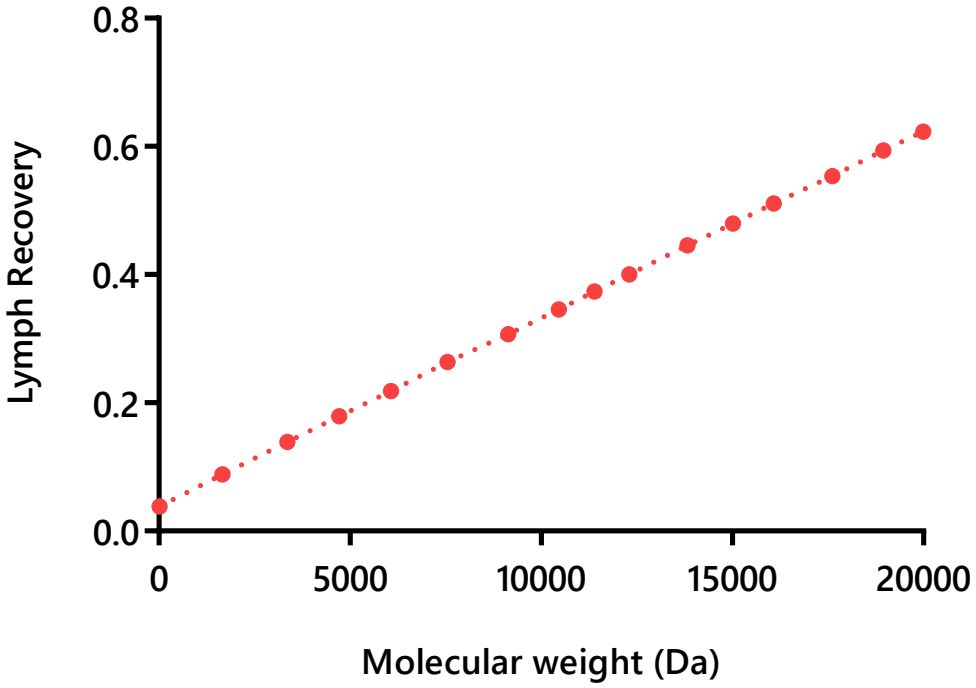

Figure 6.3 Linear correlation between molecular weight and lymph recovery. The curve drawn is the best fit calculated via linear regression and is defined as: Lymph recovery = 0.00003 x Molecular weight + 0.0404, with a correlation coefficient *r* of 0.99.

6.2.7.2 Model equations

Drug enters the vascular compartment via the arterial blood supply ($Q_{arterial}$) (Equation 50). The movement of drug from the vascular compartment to the interstitial compartment considers lymph flow to the organ (LF_{organ}), the concentration of drug in the vascular compartment ($C_{vascular}$), volume of the arterial compartment (V_{artery}), the fraction of drug unbound and the blood to plasma ratio (B:P) and has been detailed in Equation 51.

$$A_{vascular} = Q_{arterial}\, x\, C_{arterial} \quad (50)$$

$$A_{ISF} = LF_{organ} x\, (C_{vascular} / V_{vascular}) x\, fu\, x\, B{:}P \quad (51)$$

$$LF_{organ}\, x\, (C_{organ}/V_{organ})\, x\, fu_t \quad (52)$$

$$LF_{organ}\, x\, (C_{ISF}/V_{ISF}) \quad (53)$$

Equation 52 reflects movement of drug from the tissue compartment (C_{organ}) to the interstitial compartment via the lymph flow and considers the fraction of unbound drug in tissue (fu_t). Equation 53 describes the movement of drug from the interstitial compartment to the central lymph node compartment, where C_{ISF} is the concentration of drug in the interstitial fluid and V_{ISF} is the volume of ISF. Movement of drug from the tissue compartments back to the venous blood flow were modified from the whole-body adult PBPK model by subtracting the lymph flow from the venous blood flow (Q_{organ}) (Equation 54), where T:P is the tissue to plasma ratio and C_{veinal} is the concentration of drug in the veinal compartment.

$$(((Q_{organ} - LF_{organ})\, x\, C_{organ}\, x\, (fu/T{:}P)) - ((Q_{organ} - LF_{organ})\, x\, C_{veinal}) \quad (54)$$

$$A_{LN} \div 3 \quad (55)$$

$$\frac{dA_{LymphNode}}{dt} = \left(\sum LF_{organ} x\, C_{ISF}\right) - (A_{LN} \div 3) \quad (56)$$

The amount of drug leaving the lymph node was defined in the model as the amount of drug in the lymph nodes (A_{LN}) divided by the time taken for drug to transit from

lymph to systemic circulation; 3 hours [156]. Differential Equation 56 calculates the amount of drug in the lymph node ($A_{LymphNode}$) considering the total sum of Equation 52 for all organs and subtracting it by the amount of drug leaving the lymph node compartment (Equation 55).

Table 6.1 Physiological parameters for lymphatic PBPK model. [153-155]

Organ/Tissue	Interstitial volume (L)	Vascular volume (defined as a fraction of total organ volume)
Heart	0.0488	0.042
Lungs	0.300	0.185
Muscle	3.910	0.027
Skin	1.125	0.050
Adipose	2.289	0.031
Bone	1.891	0.050
Brain	0.261	0.050
Liver	0.429	-
Spleen	0.0443	0.050
Pancreas	0.018	0.050
Remaining	0.277	0.050
Kidney	0.0498	0.070
Gut	0.1624	0.050

Stomach	0.277	0.050
Gonads	0.277	0.050
Parameters based on average adult weighing 70 kg.		

6.2.8 Model Simulations and Qualification

Experimental *in vitro* data was utilised as input data in the model to simulate the pharmacokinetic profiles of raltegravir and efavirenz (Table 6.2). The PBPK model was qualified against available literature data [158] describing the tissue: plasma penetration ratio (LT: P) of both these drugs in humans. In these studies, human lymph node tissue and plasma were collected from deceased patients from tissue banks and concentrations of the drugs were measured by LC-MS/MS. LT: P in the PBPK model was assessed by running simulations for 30 days to evaluate lymph accumulation and then dividing lymph node and plasma areas under the concentration time curves (Equation 57).

$$LT{:}P = AUC_{Lymph}/AUC_{Plasma} \quad (57)$$

The percentage difference between observed and simulated ratios were calculated as a measure of model performance, with predictions ±30% of observed data passing model qualification. The AAFE was also calculated with a more stringent qualification criteria of 1.5-fold. As the predictions were based on a comparison of ratios, the qualification criteria were tightened to reduce the error and further improve predictions.

The plasma PK parameters for each drug were also compared to literature data [159, 160] to ensure model modifications did not negatively impact predictions of plasma concentration. Clinical data on a 400 mg twice daily dose (BID) of RAL was used for qualification and for EFV a 600 mg once daily dose was simulated in the model. 100 virtual patients aged between 18-60 years were simulated and the mean AUC, C_{max} and C_{trough} were recorded for comparison against observed data.

The PBPK model was qualified by calculating the absolute average fold error (AAFE). AAFE is a useful parameter to assess over or under-prediction of the model, values closer to 1 indicate a closer similarity with observed values [10].

Table 6.2 Physicochemical properties of raltegravir and efavirenz.

Property	Raltegravir [73]	Efavirenz [72]
Molecular weight, g/mol	445.2	316
Log $P_{o:w}$	0.58	4.60
f_u	0.17	0.02
pK_a	6.67	12.52
R	0.60	0.74
Polar surface area, $Å^2$	150	38.33
Hydrogen bond donors	3	1
Caco-2 permeability, 10^{-6} cm/sec	6.6	2.5
Clearance (L/kg)	NA	9.4 [161]
CL_{int} CYP3A4	NA	0.007
CL_{int} UGT1A1	12.4	NA
Solubility, mg/L	70000 [74]	93

Abbreviations: A, L/h; CLint, intrinsic clearance; CYP, cytochrome P450 (µL/minute/pmol); log Po:w, partition coefficient between octanol and water; NA, not applicable; pKa, logarithmic value of the dissociation constant; R, blood-to-plasma drug ratio; UGT, uridine diphosphate glucuronosyltransferase (µL/minute/10^6).

6.3 Results

6.3.1 Plasma PK qualification

6.3.1.1 Efavirenz

A 600 mg once daily dose of efavirenz was simulated in the model for comparison against literature data. The PK parameters (highlighted in Table 6.3), AUC, C_{max} and C_{trough} were within the acceptance criteria for model qualification, with a maximum AAFE value of 1.311.

Table 6.3 PBPK qualification of a 600 mg QD dose of efavirenz; summary of predicted versus observed pharmacokinetic parameters.

PK characteristic	Clinical	Predicted	AAFE
AUC (mg*h/L)	58.14	65.02 (32)	1.118
Cmax (mg/L)	4.076	3.25 (20)	1.254
Ctrough (mg/L)	1.77	2.32 (50)	1.311

AUC, area under curve over 24 hours; C_{max}, maximum plasma concentration and C_{trough}, minimum plasma concentration.

6.3.1.2 Raltegravir

A 400 mg BID of raltegravir was simulated in the PBPK model for comparison against clinical data. The resulting PK parameters have been outlined in Table 6.4. AUC_{12}, C_{max} and C_{trough} were within model qualification acceptance criteria, with simulations generating a maximum AAFE value of 1.583.

Table 6.4 PBPK qualification of a 400 mg BID dose of raltegravir; summary of predicted versus observed pharmacokinetic parameters.

PK characteristic	Clinical*	Predicted*	AAFE
AUC_{12} (mg*h/L)	7.076 (27)	11.2 (17)	1.583
Cmax (mg/L)	2.519 (25)	2.275 (23)	1.107
Ctrough (mg/L)	0.071 (35)	0.072 (27)	1.014
*Data shown as geometric mean (%CV). AUC_{12}, area under curve over 12 hours; C_{max}, maximum plasma concentration and C_{trough}, minimum plasma concentration.			

6.3.2 Lymph PK qualification

6.3.2.1 Efavirenz and Raltegravir

Simulations for a 600 mg QD dose of efavirenz and a 400 mg BID dose of raltegravir were run for a duration of 30 days to evaluate accumulation in lymph. The PK curve for both raltegravir and efavirenz flattened by day 10, to ensure both drugs had reached steady state concentrations simulations were run for a 30-day period. The average daily plasma and lymph concentrations were calculated by dividing the total AUC over 30 days.

Figure 6.4 Average daily concentrations (mg*h/L) of efavirenz and raltegravir in plasma and lymph. Lighter bars represent plasma concentrations and darker bars represent lymph concentrations, with actual values highlighted within the table.

The lymph to plasma tissue penetration ratios were calculated by dividing lymph concentrations by plasma concentrations. The resulting ratios have been detailed (Figure 6.5), with percentage differences of -4.8% and -14.6% of observed data for raltegravir and efavirenz, respectively. The AAFEs were 1.049 and 1.157 for RAL and EFV, respectively. The model successfully passed all qualification criteria.

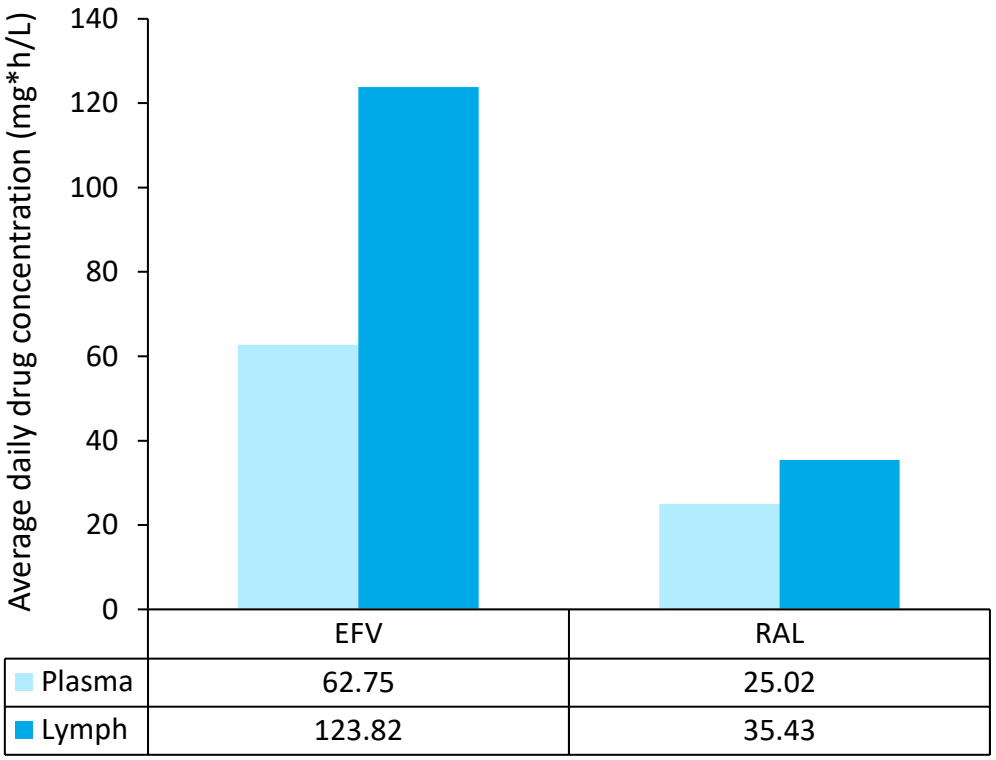

	EFV	RAL
Plasma	62.75	25.02
Lymph	123.82	35.43

Figure 6.5 Observed and simulated Lymph: Plasma tissue penetration ratios of RAL and EFV. Lighter bars represent observed data and darker bars represent simulated data with values highlighted within table.

6.4 Discussion

Although substantial progress has been made in the treatment of HIV, with combination ARV therapy proving highly effective, curing the virus still remains a major challenge. Residual levels of viremia can be detected in most patients on continuous therapy and if treatment is interrupted, rapid viral rebound occurs [162]. The reservoir comprises resting $CD4^+$ memory T cells that harbour latent HIV-1 and routinely evade immune surveillance due to their quiescent nature, because of this the reservoir has a relatively long lifespan, hindering prospects of a cure. Progression in the quantification of the latent reservoir has been pivotal in establishing the stability of the reservoir. Lymphoid tissues represent a primary site of HIV replication [163]. Continuing viral replication has been linked with sub-therapeutic concentrations of ARV drugs in the lymphoid tissues [48]. Knowledge on treatment efficacy in these areas can help optimise therapy and support future HIV eradication strategies.

A whole-body adult PBPK model was modified to simulate drug penetration and distribution in the lymphoid tissues. Several parameters were used to describe the physiology of the lymphatic system, all of which were derived from existing literature. Interstitial fluid volumes were readily available for most organs besides the stomach, gonads, and remaining tissue, in this instance, the remaining unaccounted interstitial fluid was divided equally among organs. Vascular volumes for all organs and tissues were readily available in the literature and were represented in the model as a fraction of total organ volume [154]. The physiology of the lymphatic system is considerably complex, around 500-600 lymph nodes [152] are present throughout the body and to replicate this *in silico* is a challenge. To lessen the computational burden and reduce model complexity the lymph nodes

were represented as a single compartment in the model, where the effluent lymph supply from all interstitial compartments was collected and then transferred to the systemic circulation. This technique has been used in previous PBPK models that have incorporated lymphatics [153-156]. Coefficients to describe the level of resistance provided by the lymphatic and vascular endothelium were incorporated in the model based on previous model structures. During model development, these parameters were explored, and it was found that both coefficients had very little to no influence on the outputs. This could possibly be explained by the differences observed in the mechanisms of transport of small molecules versus large molecules in the body. As these parameters had very little influence on model outputs, they were removed from the equations.

Observed data on oral raltegravir and efavirenz were used for the qualification of the model. To ensure the addition of lymphatic compartments did not alter the predictions for plasma PK, plasma concentrations of each drug were also validated. Mean AUC, C_{max} and C_{trough} were within the 2-fold acceptance criteria with efavirenz and raltegravir yielding a maximum AAFE value of 1.311 and 1.583, respectively. To assess the model's capability in predicting the lymph penetration of both drugs, observed data concerning the lymph to plasma ratio were used. Observed data on penetration of ARVs in lymph are generally sparse and of those few studies that have been conducted, an overall consensus on a method to quantify drug exposure in such tissues is lacking with results often being opposed [164, 165]. Some studies have investigated concentrations in lymph node mononuclear cells [48] whereas others have used tissue homogenate [165]. As such, minimal data was available for the qualification of the model with only one human plasma sample available for RAL. The data that was used involved studying samples from human lymph node tissue of deceased PLWH who had been adherent to ARVs to allow for better

characterisation via LC-MS/MS [158]. The tissue samples were homogenised prior to analysis. The study measured concentrations of several ARVs in plasma and lymph node tissue to calculate ratios; both EFV and RAL were chosen for model development due to the availability of input and clinical data.

Simulations in the models were run on healthy individuals and did not account for disease state or altered disposition. Interestingly, the same aforementioned study explored the effect of viral infection on antiretroviral penetration in the lymph nodes of human, mice, rats, and non-human primates and concluded no differences were found in any of the species and so the effects of diseases state were thought to be minimal. A limitation of the model was the absence of transporter ontogenies and their influence on distribution of compounds in lymph, however, Burgunder *et al* [158] also found few predictive relationships between drug transporter expression and ARV LT: P. It has been suggested distribution of small compounds in lymph nodes occurs through passive diffusion-based processes [158]. Considering such data is sparse and often limited; transporter expression was not included in the model due to the minimal effect it was suggested to have on penetration ratios [158].

Although the model had its limitations it successfully passed validation criteria. Model predictions were in good agreement with literature values (within 30%); the simulated ratios for efavirenz and raltegravir were 1.9 and 1.41, respectively. Efavirenz was found to have a greater penetration ratio than raltegravir in the literature as well as the model. A previous study evaluating the bioavailability of antiretrovirals in lymphoid tissues in mice observed key physicochemical parameters such as pKa, lipophilicity (logP), protein binding and ionisation influenced the magnitude of penetration [166]. This finding is in keeping with the model data presented herein and the literature data used to qualify the model [158].

According to the study, efavirenz experienced the highest penetration and exhibits greater pKa, logP and hydrophobicity in comparison to other drugs studied (pKa, EFV: 12.52 > RAL: 6.67; LogP, EFV: 4.6 > RAL: 0.58; hydrophobicity (based on water solubility) EFV: 93 mg/L < RAL: 70000 mg/L.) To increase model reliability & performance, it would be worth qualifying the model with additional ARVs from different classes and for further analysis on the aforementioned parameters that have been found to influence distribution.

Integration of a PBPK model, like the one described in this chapter, with a dynamic model can provide important information on treatment efficacy. Dynamic models describing viral kinetics can be combined into this modelling framework providing a mechanistic description of drug and drug effects on a cellular or tissue level. Models of HIV dynamics have been used extensively over the years to quantify the level of HIV infection and efficacy of therapies [167-169]. Jilek *et al* [169] quantified the intrinsic antiviral activity of ARV drug combinations, where the level of inhibition at clinically relevant concentrations was used to assess the inhibitory potential of various 2 and 3-drug regimens. Similar models are constantly being improved and developed further. PBPK models can generate data on tissue-specific concentrations which can be used as input data for dynamic models, therefore an integrated PBPK-PD framework can represent a valuable, informative tool for the enhancement of HIV therapy and rationalise strategy for the HIV cure.

The development and incorporation of the lymphatic system in a PBPK model can be particularly useful in several disease states. Cancer is a leading cause for deaths worldwide, responsible for almost 10 million deaths in 2020 [170]. It has been found that the lymphatics are a primary site of solid tumour metastases [171] and therapies targeting this area continue to be developed [172]. Evaluating the efficacy of

existing and new cancer therapies in lymphoid tissues can prove pivotal in treatment success and to minimise the formation of metastases.

In this chapter, a PBPK model to characterise the ARV content in lymphoid tissues was successfully developed. The lymphatics play a crucial role in the pathology of HIV. Lymphoid organs such as the lymph nodes, spleen, and gut-associated lymphoid tissue (GALT) are major sites in viral replication. Determining drug exposures in these tissues can help optimise treatment and maximise efficacy.

CHAPTER 7

General Discussion

7.1 Special population PBPK modelling: Neonates

The number of new infections has significantly decreased over the years following HAART, however, focus now needs to shift to the many overlooked areas of HIV. Treatment in vulnerable populations including patients with co-morbidities, children and infants, pregnant women, and the elderly requires optimisation. A number of ARV guidelines recommend initiating therapy in all adults living with HIV at any CD4 cell count [40, 41].

The benefits of initiating ARV therapy shortly after birth may include prevention of infection in at-risk infants and early viral suppression in those infants who are infected, compared to deferring therapy until the abovementioned clinical criteria are met [97]. The term 'early' has varying definitions, with ART routinely initiated in infants between 2-6 months of life. Although breastfeeding increases the risk of infection in newborns it has enormous benefits for health and is recommended by WHO [98]. Initiating ART in the first hours of life is met with numerous challenges from limited scientific knowledge to ethical and logistical difficulties. As there are only a few ARVs with adequate neonatal PK and safety data with formulations suitable for use in neonates, the need for more potent alternatives is essential for effective early treatment and prophylaxis [100].

PBPK modelling, as described throughout this thesis, represents a bottom-up approach that requires *in vitro, in vivo,* and physicochemical information as input data to generate simulations of various clinical scenarios. Where a biological system e.g., human, non-human primates, rats, mice etc. is described using mathematical equations. Drug-related processes such as absorption, distribution, metabolism, and elimination are also represented using mathematical descriptions and predictive models. Clinical trials are typically conducted in healthy patients aged

between 18-35 years old, with a poor representation of special populations. Since gaining regulatory acceptance there have been several instances in which PBPK modelling has been successfully used, with most impact on informing drug-labels, few of which have been highlighted (Table7.1).

Company	Drug/ Drug Name	Drug Label – Clinical Pharmacology Review
Janssen	Rilpivirine HCl/Edurant	https://www.accessdata.fda.gov/drugsatfda_docs/nda/2011/202022Orig1s000ClinPharmR.pdf
Astrazeneca	Olaparib/Lynparza	https://www.accessdata.fda.gov/drugsatfda_docs/nda/2014/206162Orig1s000ClinPharmR.pdf
Novartis	Ceritinib/Zykadia	https://www.accessdata.fda.gov/drugsatfda_docs/nda/2014/205755Orig1s000ClinPharmR.pdf https://www.ema.europa.eu/en/documents/product-information/zykadia-epar-product-information_en.pdf
Janssen	Simeprevir/Olysio	https://www.accessdata.fda.gov/drugsatfda_docs/nda/2013/205123Orig1s000ClinPharmR.pdf

These are just some of the cases in which PBPK modelling has been used to either inform drug labels on unstudied scenarios or in place of clinical trials. Initially PBPK modelling was routinely carried out for DDI evaluation, but as regulatory acceptance is increasing the applications for PBPK have also increased in other areas and fields such as special-population modelling, drug formulation modelling, modelling as an alternative to animal testing in cosmetics industries etc.

Chapters 2-4 demonstrate how the above-mentioned principles of PBPK modelling can be applied to help inform knowledge gaps in the absence of empirical data. A whole-body neonatal PBPK model was built using anthropometric equations derived from the literature. Following extensive validation of anatomical and

physiological characteristics, the PK of integrase inhibitors, DTG and BIC were predicted in Chapter 3. All models were successful in passing the 2-fold qualification criteria. The potential of neonatal prophylaxis and treatment using long-acting integrase inhibitor CAB was explored in Chapter 4. Long-acting (LA) or extended-release nanoproducts of antiretrovirals hold the potential of simplifying treatment regimens while improving adherence in populations where poor adherence impedes successful treatment. LA formulations have many advantages, including, reducing the frequency of dosing and in regard to neonates, hold the potential of a single administration for the duration of the neonatal period.

While the models were effective in predicting drug PK, a number of limitations arose during development. A reoccurring problem when modelling special populations is the paucity of data available concerning physiological changes. Previously developed neonatal PBPK models faced with this limitation have taken similar approaches [52, 65], though not ideal, where data in neonates is lacking adult values are implemented and on occasion allometrically scaled. There is a high reliance on input data and the quality of this data often reflects the quality of generated simulations. The sparsity of data on developmental changes in transporter expression represents another challenge in special-population modelling. Transporters facilitate the movement of drugs and are crucial in ADME research. Replicating this parameter *in silico* without sufficient, quantifiable data is inherently difficult therefore data on transporters was not included in the models. Previously developed neonatal PBPK models faced with this limitation have taken similar approaches [52, 65], though not ideal, where data in neonates is lacking adult values are implemented and on occasion allometrically scaled. To further improve model predictions, a mechanistic understanding on the ontogenies and activities of transporters in neonates would be advantageous. Another consideration when

modelling in neonates is maternal transfer of drug through breast milk or placenta. Pregnant women with HIV infection are expected to start or already be receiving treatment which involves a combination of ARVs. As breastfeeding is encouraged, a cause for concern in breastfed neonates is maternal transfer of these drugs. Although maternal transfer has not been considered in our models, this data can be generated using a mechanistic PBPK model detailing the physiology of the maternal-fetal complex and equations to characterise movement of drug across placental barriers. Previous models have been successful in characterising breastmilk and placental transfer, with input data such as milk: plasma ratios key in generating predictions [173].

A lack of *in vivo* data to aid in the qualification of ADME processes also poses a problem, the number of clinical studies carried out in neonates are relatively few. Of the data that is available, studies are usually conducted on a small number of patients with sparse sampling. When conducting predictive modelling studies, validation is an integral part of the process which establishes confidence in model predictions. Qualification criteria of PBPK models is wide-ranging, PK parameters such as Cmax, AUC, Tmax etc., clearance or concentration-time plots can be used to evaluate a model's performance. Validating predictions against concentration-time profiles can be considered the 'gold-standard', however, when working with such populations where data sampling is sparse, using concentration-time profiles may not always be an option.

The data generated in Chapters 3 and 4 can be used to support the rationale of future ARV studies in neonates and clinical trials can be conducted in a confirmatory manner rather than exploratory. Publishing these data led to some valuable peer review which were crucial in the applicability of the DTG model. It was made clear that there were formulation restrictions that surrounded DTG (5 mg dispersible

tablets) and upon discovering this, each regimen was accordingly tailored to these restrictions. The necessity for a bridge between clinicians, industry professionals and academic researchers is ever important in producing meaningful data. The employment of this modelling technique earlier on in drug discovery and development stages can prove advantageous in avoiding restrictions like the ones highlighted here and facilitate in the design of potential clinical trials.

7.2 DDIs in PLWH

Given the previously outlined advances in HIV therapy, a byproduct of which is increased life expectancy, comorbidities continue to complicate treatment. For patients who are adherent to treatment, HIV has become manageable, however, many PLWH require additional medication for concomitant diseases such as hypertension, diabetes, cardiovascular diseases etc. The majority of DDIs remain unstudied during drug development due to the sheer volume of possible interactions and ethical constraints associated with high-risk DDIs. The magnitude of induction and/or inhibition on victim drugs can be simulated via PBPK modelling, using *in vitro* metabolism data and *in vivo* studies for model qualification as has been demonstrated in Chapter 5 of this thesis [132]. An adult PBPK model was developed by defining the physiological and anatomical characteristics using mathematical equations. The PBPK model was qualified for virtual adults aged between 18-60 years. Data on the anatomy and physiology of the target population was readily available and derived from existing literature. The model was qualified prior to running simulations with all blood flows, organ/tissue weights and volumes within the acceptance criteria (< 2-fold). The induction model was successfully built and predictions of DDIs between moderate inducer rifabutin, with doravirine and bictegravir were within the acceptance criteria.

One of the major limitations of our approach was the lack of *in vitro* data available on non-cyp enzymes, *in vitro* assays concerning CYPs have been developed and well characterised over the years, however, UGTs and other non-cyp enzymatic pathways remain widely overlooked. For this reason, it was not possible to evaluate the induction effect of rifabutin on the UGT-mediated clearance of bictegravir. Given the importance of UGT enzymes, there is great potential for PBPK modelling of UGT-related DDIs and optimisation of *in vitro* experiments for this non-cyp enzymatic pathway should be prioritised to enhance and improve PBPK DDI studies.

Modelling the effect of transporters also remains a challenge with limited knowledge on their effect on key ADME processes. Developing models that can characterise the magnitude of transporter DDIs are often met with complexities and several issues impede the ability to evaluate this through modelling, including, the lack of specific transporter substrates for *in vitro* characterisation, the need for validated *in vitro* assays to evaluate induction and the lack of clinical studies assessing the effect of P-gp related DDIs, all of which are essential to support PBPK model development. Quantification of these parameters *in vitro* can lead to a better representation of the mechanisms underpinning DDIs and further improve model reliability.

Clinical management of DDIs remains a challenge in the care and treatment of PLWH. The application of PBPK modelling to support drug development and discovery is well recognised, more specifically, the application of models to predict DDIs has gained regulatory endorsement from the FDA, EMA and PMDA [131, 146]. Considering majority of the PBPK models developed in recent years have been focused on enhancing the management of CYP-related DDIs, there is considerable potential in the modelling of UGT-related and transporter-related DDIs. Although more research on this topic needs to be done for the effective translation of *in vitro*

data in PBPK modelling, with a heavy focus on the neglected areas that have been previously stated.

7.3 Lymphatic penetration of ART

Early initiation of ART to reduce residual viremia, optimising treatments in special populations and optimising treatment to avoid the likelihood of adverse drug-drug interactions all hold great potential to advance the current status of HIV treatment, however, finding a cure remains paramount. Although substantial progress has been made in the treatment of HIV, with combination ARV therapy proving highly effective, curing the virus remains a major challenge. ART inhibits viral replication effectively but does not eradicate the virus. Residual levels of viremia can be detected in most adherent patients on therapy and if treatment is interrupted, rapid viral rebound occurs [162]. Rebound viremia stem from reservoirs which comprise resting $CD4^+$ memory T cells that harbour latent HIV-1 and routinely evade immune surveillance due to their quiescent nature, because of this the reservoir has a relatively long lifespan, hindering any prospects of a cure. Previous modelling studies have suggested over 70 years of ART would be necessary to eliminate the reservoir using only ART. Progression in the quantification of the latent reservoir has been pivotal in establishing the stability of the reservoir. Lymphoid tissues represent a primary site of HIV replication [163]. Continuing viral replication has been linked with sub-therapeutic concentrations of ARV drugs in the lymphoid tissues [48]. Knowledge on treatment efficacy in these areas can help design therapy and support future HIV eradication interventions.

Typical models investigating distribution and kinetics of small molecules do not describe or include lymphatic physiology. Most PBPK models that have lymphatic physiology incorporated within them are often used to represent large molecules

such as monoclonal antibodies (mAb). There are significant differences in the ADME processes of large and small molecules, with the lymphatic system heavily influencing large molecule distribution. The incorporation of the lymphatic system in our model was structured around these existing models, with exception to mechanisms that were specific to large molecules. In Chapter 6, a whole-body adult PBPK model was modified to simulate drug penetration and distribution in the lymphoid tissues. Several parameters were used to describe the physiology of the lymphatic system, all of which were derived from existing literature. Dividing the standard compartments of an adult PBPK model into interstitial, vascular and tissue required additional input data which was readily available in the literature [154]. The physiology of the lymphatic system is considerably complex, around 500-600 lymph nodes [152] are present throughout the body and to replicate this *in silico* was a challenge, to lessen the computational burden and reduce model complexity the lymph nodes were represented as a single compartment in our models, where the effluent lymph supply from all interstitial compartments was collected and then transferred to the systemic circulation, this technique has been used in previous PBPK models that have incorporated lymphatics [153-156]. The simplification of complex systems like lymphatics represents an area in modelling that can be further improved for a better characterisation of key processes however the availability of such data is limited as well as the capability of modelling software's.

Validation of the model also represented a challenge with few data on lymphatic distribution of antiretrovirals. Considering the lymphatics represents an appealing target for therapy the lack of translatable data concerning treatment efficacies within these tissues is lacking. RAL and EFV were used for the validation as they represent two different classes of antiretrovirals, and sufficient data was available for these

drugs. For further refinement of model parameters, validating against multiple ARVs of different classes could improve the overall performance of the model.

Integration of this lymphatic PBPK model, with a dynamic model can provide important information on treatment efficacy. Dynamic models describing viral kinetics can be combined into this modelling framework providing a mechanistic description of drug and drug effects on a cellular or tissue level. Models of HIV dynamics have been used extensively over the years to quantify the level of HIV infection and efficacy of therapies [167-169]. PBPK models can generate data on tissue-specific concentrations which can be used as input data for dynamic models, therefore an integrated PBPK-PD framework can represent a valuable, informative tool for the enhancement of HIV therapy and rationalise strategy for the HIV cure.

7.4 Conclusion

Before a potential treatment reaches the stages of a clinical trial it must undergo numerous approval stages during which it is subjected to various research studies and the process can take several years. Once a certain level of safety, efficacy and toxicity has been established the treatment is put forward for animal studies before studying in humans, should the outcome be positive. However, this entire process is met with several limitations, from the length of approval to the type of populations being investigated. PBPK modelling can effectively evaluate hard-to-study clinical scenarios prior to direct evaluation and provide valuable insight which cannot be easily gained. The overall aim of this thesis was to explore and develop several mechanistic PBPK models to help support the optimisation of ART and design/inform future clinical studies. Where logistical, methodological, and ethical constraints hinder or complicate the ability to evaluate certain clinical scenarios, PBPK modelling proves an advantageous tool for deducing vital information.

Bibliography

[1] L.A. Bauer, Applied clinical pharmacokinetics, Third edition. ed., McGraw-Hill Medical, New York, 2014.

[2] M. Rowland, T.N. Tozer, Clinical pharmacokinetics : concepts and applications, 3rd ed., Williams & Wilkins, Baltimore, 1995.

[3] I. Nestorov, Whole body pharmacokinetic models, Clin Pharmacokinet, 42 (2003) 883-908.

[4] S.A. Peters, A.L. Ungell, H. Dolgos, Physiologically based pharmacokinetic (PBPK) modeling and simulation: applications in lead optimization, Curr Opin Drug Discov Devel, 12 (2009) 509-518.

[5] H.M. Jones, I.B. Gardner, K.J. Watson, Modelling and PBPK simulation in drug discovery, AAPS J, 11 (2009) 155-166.

[6] H.M. Jones, K. Mayawala, P. Poulin, Dose selection based on physiologically based pharmacokinetic (PBPK) approaches, AAPS J, 15 (2013) 377-387.

[7] H.M. Jones, M. Dickins, K. Youdim, J.R. Gosset, N.J. Attkins, T.L. Hay, I.K. Gurrell, Y.R. Logan, P.J. Bungay, B.C. Jones, I.B. Gardner, Application of PBPK modelling in drug discovery and development at Pfizer, Xenobiotica, 42 (2012) 94-106.

[8] E.M. Agency, Guideline on the reporting of physiologically based pharmacokinetic (PBPK) modelling and simulation, Committee for Medicinal Products for Human Use (CHMP), 2018.

[9] S.A. Peters, H. Dolgos, Requirements to Establishing Confidence in Physiologically Based Pharmacokinetic (PBPK) Models and Overcoming Some of the Challenges to Meeting Them, Clin Pharmacokinet, 58 (2019) 1355-1371.

[10] K. Abduljalil, T. Cain, H. Humphries, A. Rostami-Hodjegan, Deciding on success criteria for predictability of pharmacokinetic parameters from in vitro studies: an analysis based on in vivo observations, Drug Metab Dispos, 42 (2014) 1478-1484.

[11] I. Poggesi, M.S. Benedetti, R. Whomsley, S. Le Lamer, M. Molimard, J.B. Watelet, Pharmacokinetics in special populations, Drug Metab Rev, 41 (2009) 422-454.

[12] C. Perry, G. Davis, T.M. Conner, T. Zhang, Utilization of Physiologically Based Pharmacokinetic Modeling in Clinical Pharmacology and Therapeutics: an Overview, Curr Pharmacol Rep, (2020) 1-14.

[13] H. Koffler, Fetal and neonatal physiology, Clin Obstet Gynecol, 24 (1981) 545-553.

[14] J. Grijalva, K. Vakili, Neonatal liver physiology, Semin Pediatr Surg, 22 (2013) 185-189.

[15] M. Sulemanji, K. Vakili, Neonatal renal physiology, Semin Pediatr Surg, 22 (2013) 195-198.

[16] I.E. Templeton, N.S. Jones, L. Musib, Pediatric Dose Selection and Utility of PBPK in Determining Dose, AAPS J, 20 (2018) 31.

[17] R. Michelet, J.V. Bocxlaer, A. Vermeulen, PBPK in Preterm and Term Neonates: A Review, Curr Pharm Des, 23 (2017) 5943-5954.
[18] M. Chetty, M.P. Danckwerts, A. Julsing, Prediction of the exposure to a 400-mg daily dose of efavirenz in pregnancy: is this dose adequate in extensive metabolisers of CYP2B6?, Eur J Clin Pharmacol, 76 (2020) 1143-1150.
[19] K. Abduljalil, A. Pansari, M. Jamei, Prediction of maternal pharmacokinetics using physiologically based pharmacokinetic models: assessing the impact of the longitudinal changes in the activity of CYP1A2, CYP2D6 and CYP3A4 enzymes during pregnancy, J Pharmacokinet Pharmacodyn, 47 (2020) 361-383.
[20] A.A. Mangoni, S.H. Jackson, Age-related changes in pharmacokinetics and pharmacodynamics: basic principles and practical applications, Br J Clin Pharmacol, 57 (2004) 6-14.
[21] F. Stader, H. Kinvig, M.A. Penny, M. Battegay, M. Siccardi, C. Marzolini, Physiologically Based Pharmacokinetic Modelling to Identify Pharmacokinetic Parameters Driving Drug Exposure Changes in the Elderly, Clin Pharmacokinet, 59 (2020) 383-401.
[22] A.L. Ammirati, Chronic Kidney Disease, Rev Assoc Med Bras (1992), 66Suppl 1 (2020) s03-s09.
[23] D. Schuppan, N.H. Afdhal, Liver cirrhosis, Lancet, 371 (2008) 838-851.
[24] L. Zhou, X. Tong, P. Sharma, H. Xu, N. Al-Huniti, D. Zhou, Physiologically based pharmacokinetic modelling to predict exposure differences in healthy volunteers and subjects with renal impairment: Ceftazidime case study, Basic Clin Pharmacol Toxicol, 125 (2019) 100-107.
[25] S.B. Howell, Clinical applications of a novel sustained-release injectable drug delivery system: DepoFoam technology, Cancer J, 7 (2001) 219-227.
[26] D. Ramyadevi, P. Sandhya, Dual sustained release delivery system for multiple route therapy of an antiviral drug, Drug Deliv, 21 (2014) 276-292.
[27] C. Flexner, A. Owen, M. Siccardi, S. Swindells, Long-acting drugs and formulations for the treatment and prevention of HIV infection, Int J Antimicrob Agents, 57 (2021) 106220.
[28] S. Swindells, M. Siccardi, S.E. Barrett, D.B. Olsen, J.A. Grobler, A.T. Podany, E. Nuermberger, P. Kim, C.E. Barry, A. Owen, D. Hazuda, C. Flexner, Long-acting formulations for the treatment of latent tuberculous infection: opportunities and challenges, Int J Tuberc Lung Dis, 22 (2018) 125-132.
[29] S.R. Kumar, C.H. Mehta, U.Y. Nayak, Long-Acting Formulations: A Promising Approach for the Treatment of Chronic Diseases, Curr Pharm Des, 27 (2021) 876-889.
[30] N. Cottura, A. Howarth, R.K.R. Rajoli, M. Siccardi, The Current Landscape of Novel Formulations and the Role of Mathematical Modeling in Their Development, J Clin Pharmacol, 60 Suppl 1 (2020) S77-S97.

[31] A. Engelman, P. Cherepanov, The structural biology of HIV-1: mechanistic and therapeutic insights, Nat Rev Microbiol, 10 (2012) 279-290.
[32] D.S. Goodsell, Illustrations of the HIV life cycle, Curr Top Microbiol Immunol, 389 (2015) 243-252.
[33] K.A. Meulendyke, J.D. Croteau, M.C. Zink, HIV life cycle, innate immunity and autophagy in the central nervous system, Curr Opin HIV AIDS, 9 (2014) 565-571.
[34] C.B. Wilen, J.C. Tilton, R.W. Doms, HIV: cell binding and entry, Cold Spring Harb Perspect Med, 2 (2012).
[35] E.O. Freed, HIV-1 gag proteins: diverse functions in the virus life cycle, Virology, 251 (1998) 1-15.
[36] W.S. Hu, S.H. Hughes, HIV-1 reverse transcription, Cold Spring Harb Perspect Med, 2 (2012).
[37] K.D. Jayappa, Z. Ao, X. Yao, The HIV-1 passage from cytoplasm to nucleus: the process involving a complex exchange between the components of HIV-1 and cellular machinery to access nucleus and successful integration, Int J Biochem Mol Biol, 3 (2012) 70-85.
[38] M.S. Dahabieh, E. Battivelli, E. Verdin, Understanding HIV latency: the road to an HIV cure, Annu Rev Med, 66 (2015) 407-421.
[39] P.A. Volberding, S.G. Deeks, Antiretroviral therapy and management of HIV infection, Lancet, 376 (2010) 49-62.
[40] J.S. Eggleton, S. Nagalli, Highly Active Antiretroviral Therapy (HAART), StatPearls, Treasure Island (FL), 2021.
[41] P. Erb, M. Battegay, W. Zimmerli, M. Rickenbach, M. Egger, Effect of antiretroviral therapy on viral load, CD4 cell count, and progression to acquired immunodeficiency syndrome in a community human immunodeficiency virus-infected cohort. Swiss HIV Cohort Study, Arch Intern Med, 160 (2000) 1134-1140.
[42] N. Sluis-Cremer, D. Arion, M.A. Parniak, Molecular mechanisms of HIV-1 resistance to nucleoside reverse transcriptase inhibitors (NRTIs), Cell Mol Life Sci, 57 (2000) 1408-1422.
[43] J.J. Kessl, N. Jena, Y. Koh, H. Taskent-Sezgin, A. Slaughter, L. Feng, S. de Silva, L. Wu, S.F. Le Grice, A. Engelman, J.R. Fuchs, M. Kvaratskhelia, Multimode, cooperative mechanism of action of allosteric HIV-1 integrase inhibitors, J Biol Chem, 287 (2012) 16801-16811.
[44] Y. Pommier, A.A. Johnson, C. Marchand, Integrase inhibitors to treat HIV/AIDS, Nat Rev Drug Discov, 4 (2005) 236-248.
[45] V. Briz, E. Poveda, V. Soriano, HIV entry inhibitors: mechanisms of action and resistance pathways, J Antimicrob Chemother, 57 (2006) 619-627.
[46] J.A. Este, A. Telenti, HIV entry inhibitors, Lancet, 370 (2007) 81-88.
[47] J.W. Breslin, Y. Yang, J.P. Scallan, R.S. Sweat, S.P. Adderley, W.L. Murfee, Lymphatic Vessel Network Structure and Physiology, Compr Physiol, 9 (2018) 207-299.

[48] C.V. Fletcher, K. Staskus, S.W. Wietgrefe, M. Rothenberger, C. Reilly, J.G. Chipman, G.J. Beilman, A. Khoruts, A. Thorkelson, T.E. Schmidt, J. Anderson, K. Perkey, M. Stevenson, A.S. Perelson, D.C. Douek, A.T. Haase, T.W. Schacker, Persistent HIV-1 replication is associated with lower antiretroviral drug concentrations in lymphatic tissues, Proc Natl Acad Sci U S A, 111 (2014) 2307-2312.
[49] E.M.B. Scholz, A.D.M. Kashuba, The Lymph Node Reservoir: Physiology, HIV Infection, and Antiretroviral Therapy, Clin Pharmacol Ther, 109 (2021) 918-927.
[50] C. Kline, J. Ndjomou, T. Franks, R. Kiser, V. Coalter, J. Smedley, M. Piatak, Jr., J.W. Mellors, J.D. Lifson, Z. Ambrose, Persistence of viral reservoirs in multiple tissues after antiretroviral therapy suppression in a macaque RT-SHIV model, PLoS One, 8 (2013) e84275.
[51] D.F. Clarke, M. Penazzato, E. Capparelli, T.R. Cressey, G. Siberry, N. Sugandhi, M. Mirochnick, W.H.O.P.A.W. Group, Prevention and treatment of HIV infection in neonates: evidence base for existing WHO dosing recommendations and implementation considerations, Expert Rev Clin Pharmacol, 11 (2018) 83-93.
[52] S. Bjorkman, Prediction of drug disposition in infants and children by means of physiologically based pharmacokinetic (PBPK) modelling: theophylline and midazolam as model drugs, Br J Clin Pharmacol, 59 (2005) 691-704.
[53] S. Haddad, C. Restieri, K. Krishnan, Characterization of age-related changes in body weight and organ weights from birth to adolescence in humans, J Toxicol Environ Health A, 64 (2001) 453-464.
[54] G.L. Kearns, S.M. Abdel-Rahman, S.W. Alander, D.L. Blowey, J.S. Leeder, R.E. Kauffman, Developmental pharmacology--drug disposition, action, and therapy in infants and children, N Engl J Med, 349 (2003) 1157-1167.
[55] K. Allegaert, M. van de Velde, J. van den Anker, Neonatal clinical pharmacology, Paediatr Anaesth, 24 (2014) 30-38.
[56] S. Bosgra, J. van Eijkeren, P. Bos, M. Zeilmaker, W. Slob, An improved model to predict physiologically based model parameters and their inter-individual variability from anthropometry, Crit Rev Toxicol, 42 (2012) 751-767.
[57] A. Smits, P. De Cock, A. Vermeulen, K. Allegaert, Physiologically based pharmacokinetic (PBPK) modeling and simulation in neonatal drug development: how clinicians can contribute, Expert Opin Drug Metab Toxicol, (2018) 1-10.
[58] R.K.R. Rajoli, D.J. Back, S. Rannard, C.F. Meyers, C. Flexner, A. Owen, M. Siccardi, In Silico Dose Prediction for Long-Acting Rilpivirine and Cabotegravir Administration to Children and Adolescents, Clin Pharmacokinet, 57 (2018) 255-266.
[59] World Health Organization, The WHO Child Growth Standard.
[60] W.E.U. Finkbeiner, P. C; Davis, R. L, Autopsy Pathology: A Manual and Atlas, 2nd ed.2009.

[61] L.X. Yu, G.L. Amidon, A compartmental absorption and transit model for estimating oral drug absorption, Int J Pharm, 186 (1999) 119-125.
[62] A.R. Maharaj, A.N. Edginton, Examining Small Intestinal Transit Time as a Function of Age: Is There Evidence to Support Age-Dependent Differences among Children?, Drug Metab Dispos, 44 (2016) 1080-1089.
[63] M. Gertz, A. Harrison, J.B. Houston, A. Galetin, Prediction of human intestinal first-pass metabolism of 25 CYP3A substrates from in vitro clearance and permeability data, Drug Metab Dispos, 38 (2010) 1147-1158.
[64] D. Sun, H. Lennernas, L.S. Welage, J.L. Barnett, C.P. Landowski, D. Foster, D. Fleisher, K.D. Lee, G.L. Amidon, Comparison of human duodenum and Caco-2 gene expression profiles for 12,000 gene sequences tags and correlation with permeability of 26 drugs, Pharm Res, 19 (2002) 1400-1416.
[65] T.N. Johnson, A. Rostami-Hodjegan, G.T. Tucker, Prediction of the clearance of eleven drugs and associated variability in neonates, infants and children, Clin Pharmacokinet, 45 (2006) 931-956.
[66] P.J. McNamara, J. Alcorn, Protein binding predictions in infants, AAPS PharmSci, 4 (2002) E4.
[67] S.J. Miyagi, A.C. Collier, The development of UDP-glucuronosyltransferases 1A1 and 1A6 in the pediatric liver, Drug Metab Dispos, 39 (2011) 912-919.
[68] Z.E. Barter, J.E. Chowdry, J.R. Harlow, J.E. Snawder, J.C. Lipscomb, A. Rostami-Hodjegan, Covariation of human microsomal protein per gram of liver with age: absence of influence of operator and sample storage may justify interlaboratory data pooling, Drug Metab Dispos, 36 (2008) 2405-2409.
[69] M. Siccardi, A. Olagunju, K. Seden, F. Ebrahimjee, S. Rannard, D. Back, A. Owen, Use of a physiologically-based pharmacokinetic model to simulate artemether dose adjustment for overcoming the drug-drug interaction with efavirenz, In Silico Pharmacol, 1 (2013) 4.
[70] P. Poulin, F.P. Theil, Prediction of pharmacokinetics prior to in vivo studies. II. Generic physiologically based pharmacokinetic models of drug disposition, J Pharm Sci, 91 (2002) 1358-1370.
[71] D.K. Bhatt, A. Mehrotra, A. Gaedigk, R. Chapa, A. Basit, H. Zhang, P. Choudhari, M. Boberg, R.E. Pearce, R. Gaedigk, U. Broeckel, J.S. Leeder, B. Prasad, Age- and Genotype-Dependent Variability in the Protein Abundance and Activity of Six Major Uridine Diphosphate-Glucuronosyltransferases in Human Liver, Clin Pharmacol Ther, (2018).
[72] R.K. Rajoli, D.J. Back, S. Rannard, C.L. Freel Meyers, C. Flexner, A. Owen, M. Siccardi, Physiologically Based Pharmacokinetic Modelling to Inform Development of Intramuscular Long-Acting Nanoformulations for HIV, Clin Pharmacokinet, 54 (2015) 639-650.
[73] D.M. Moss, M. Siccardi, D.J. Back, A. Owen, Predicting intestinal absorption of raltegravir using a population-based ADME simulation, J Antimicrob Chemother, 68 (2013) 1627-1634.

[74] National Center for Biotechnology Information, PubChem Database. Raltegravir, CID=54671008.
[75] E. Jacqz-Aigrain, C. Wood, I. Robieux, Pharmacokinetics of midazolam in critically ill neonates, Eur J Clin Pharmacol, 39 (1990) 191-192.
[76] A.E. Clarke DF, Chain A, Cababasay M, Wang J, Teppler H, et al. , IMPAACT P1110 : Raltegravir Pharmacokinetics and Safety in HIV-1 exposed neonates: Dose-finding study, Conference on Retroviruses and Opportunistic InfectionsBoston, 2017.
[77] D.F. Clarke, E.P. Acosta, M.L. Rizk, Y.J. Bryson, S.A. Spector, L.M. Mofenson, E. Handelsman, H. Teppler, C. Welebob, D. Persaud, M.P. Cababasay, J. Wang, M. Mirochnick, A.C.T.P.S.T. International Maternal Pediatric Adolescent, Raltegravir pharmacokinetics in neonates following maternal dosing, J Acquir Immune Defic Syndr, 67 (2014) 310-315.
[78] UNAIDS, 2019 GLOBAL HIV STATISTICS 2020.
[79] T. Horvath, B.C. Madi, I.M. Iuppa, G.E. Kennedy, G. Rutherford, J.S. Read, Interventions for preventing late postnatal mother-to-child transmission of HIV, Cochrane Database Syst Rev, (2009) CD006734.
[80] A. Violari, M.F. Cotton, D.M. Gibb, A.G. Babiker, J. Steyn, S.A. Madhi, P. Jean-Philippe, J.A. McIntyre, C.S. Team, Early antiretroviral therapy and mortality among HIV-infected infants, N Engl J Med, 359 (2008) 2233-2244.
[81] U.S. Department of Health and Human Services: AIDSinfo, Guidelines for the Use of Antiretroviral Agents in Pediatric HIV Infection., 2018.
[82] E.D. Deeks, Bictegravir/Emtricitabine/Tenofovir Alafenamide: A Review in HIV-1 Infection, Drugs, 78 (2018) 1817-1828.
[83] A.H. Gaur, M.F. Cotton, C.A. Rodriguez, E.J. McGrath, E. Helstrom, A. Liberty, E. Natukunda, P. Kosalaraksa, K. Chokephaibulkit, H. Maxwell, P. Wong, D. Porter, S. Majeed, M.S. Yue, H. Graham, H. Martin, D.M. Brainard, C. Pikora, Fixed-dose combination bictegravir, emtricitabine, and tenofovir alafenamide in adolescents and children with HIV: week 48 results of a single-arm, open-label, multicentre, phase 2/3 trial, Lancet Child Adolesc Health, 5 (2021) 642-651.
[84] A.E. Ruel T, Singh R, Alvero C, Fenton T, George K, et al., Pharmacokinetic and 4-week safety/efficacy of dolutegravir (S/GSK1349572) dispersible tablets in HIV-infected children aged 4 weeks to <6 years: results from IMPAACT P1093, International Workshop on HIV Pediatrics 2018.
[85] M.J. Reese, P.M. Savina, G.T. Generaux, H. Tracey, J.E. Humphreys, E. Kanaoka, L.O. Webster, K.A. Harmon, J.D. Clarke, J.W. Polli, In vitro investigations into the roles of drug transporters and metabolizing enzymes in the disposition and drug interactions of dolutegravir, a HIV integrase inhibitor, Drug Metab Dispos, 41 (2013) 353-361.
[86] U.S Food & Drug Administration, FDA Label TIVICAY- Dolutegravir sodium tablet, 2014.
[87] U.S.F.D. Administration, 204790 Dolutegravir Clinpharm PREA, (2016).

[88] U.S Food & Drug Administration, FDA Label BIKTARVY (bictegravir, emtricitabine and tenofovir alafenamide), 2018.
[89] National Center for Biotechnology Information, PubChem Database, Dolutegravir, CID=54726191.
[90] G. Malhotra, K. Joshi, J. Ghosalkar, P. Raut, Pharmaceutical Compositions JUSTIA Patents, 2017.
[91] K.R. Wajima T, Pharmacokinetic / pharmacodynamic Modeling and Long-term Simulation of Dolutegravir (DTG ,S/GSK1349572) in Integrase Resistant Patients with a Simple Viral Dynamic Model, Population Approach Group Europe (PAGE-meeting)Greece, 2011.
[92] I.H. Song, J. Borland, P.M. Savina, S. Chen, P. Patel, T. Wajima, A.F. Peppercorn, S.C. Piscitelli, Pharmacokinetics of Single-Dose Dolutegravir in HIV-Seronegative Subjects With Moderate Hepatic Impairment Compared to Healthy Matched Controls, Clin Pharmacol Drug Dev, 2 (2013) 342-348.
[93] U.S.F.D. Administration, Dolutegravir Clinical Pharmacology Review, FDA, 2012.
[94] European Medicines Agency, Biktarvy, INN:bictegravir / emtricitabine / tenofovir alafenamide, public assessment report. EMA/293559/2018., 2018.
[95] N.C.f.B. Information, PubChem Compound Summary for CID 90311989, Bictegravir., (2021).
[96] Drugbank, Bictegravir DB11799, 2021.
[97] M.F. Cotton, S. Holgate, A. Nelson, H. Rabie, C. Wedderburn, M. Mirochnick, The last and first frontier--emerging challenges for HIV treatment and prevention in the first week of life with emphasis on premature and low birth weight infants, J Int AIDS Soc, 18 (2015) 20271.
[98] World Health Organization, WHO Guidelines on HIV and Infant Feeding 2010.
[99] World Health Organization, Consolidated guidelines on the use of antiretroviral drugs for treating and preventing HIV infection: recommendations for a public health approach. Second edition.
[100] U.S. Department of Health and Human Services: AIDSinfo, Antiretroviral Management of Newborns with Perinatal HIV Exposure or Perinatal HIV, 2018.
[101] S. Chen, P. St Jean, J. Borland, I. Song, A.J. Yeo, S. Piscitelli, J.P. Rubio, Evaluation of the effect of UGT1A1 polymorphisms on dolutegravir pharmacokinetics, Pharmacogenomics, 15 (2014) 9-16.
[102] H. Li, J.N. Lampe, Neonatal cytochrome P450 CYP3A7: A comprehensive review of its role in development, disease, and xenobiotic metabolism, Arch Biochem Biophys, 673 (2019) 108078.

[103] R. Kobbe, S. Schalkwijk, G. Dunay, J.M. Eberhard, U. Schulze-Sturm, B. Hollwitz, O. Degen, M. Teulen, A. Colbers, D. Burger, Dolutegravir in breast milk and maternal and infant plasma during breastfeeding, AIDS, 30 (2016) 2731-2733.
[104] N. Mulligan, B.M. Best, J. Wang, E.V. Capparelli, A. Stek, E. Barr, S.L. Buschur, E.P. Acosta, E. Smith, N. Chakhtoura, S. Burchett, M. Mirochnick, I.P.P. Team, Dolutegravir pharmacokinetics in pregnant and postpartum women living with HIV, AIDS, 32 (2018) 729-737.
[105] J.Z. Byczkowski, J.C. Lipscomb, Physiologically based pharmacokinetic modeling of the lactational transfer of methylmercury, Risk Anal, 21 (2001) 869-882.
[106] M.A. Verner, P. Ayotte, G. Muckle, M. Charbonneau, S. Haddad, A physiologically based pharmacokinetic model for the assessment of infant exposure to persistent organic pollutants in epidemiologic studies, Environ Health Perspect, 117 (2009) 481-487.
[107] F. Partosch, H. Mielke, R. Stahlmann, U. Gundert-Remy, Exposure of Nursed Infants to Maternal Treatment with Ethambutol and Rifampicin, Basic Clin Pharmacol Toxicol, 123 (2018) 213-220.
[108] E.D.G. Garessus, H. Mielke, U. Gundert-Remy, Exposure of Infants to Isoniazid via Breast Milk After Maternal Drug Intake of Recommended Doses Is Clinically Insignificant Irrespective of Metaboliser Status. A Physiologically-Based Pharmacokinetic (PBPK) Modelling Approach to Estimate Drug Exposure of Infants via Breast-Feeding, Front Pharmacol, 10 (2019) 5.
[109] C. Trezza, S.L. Ford, W. Spreen, R. Pan, S. Piscitelli, Formulation and pharmacology of long-acting cabotegravir, Curr Opin HIV AIDS, 10 (2015) 239-245.
[110] C.D. Andrews, W. Heneine, Cabotegravir long-acting for HIV-1 prevention, Curr Opin HIV AIDS, 10 (2015) 258-263.
[111] U.S Food & Drug Administration, FDA Label CABENUVA (cabotegravir extended-release injectable suspension; rilpivirine extended-release injectable suspension), 2020.
[112] P. Gardiner, L. Dvorkin, Promoting medication adherence in children, Am Fam Physician, 74 (2006) 793-798.
[113] J.P. McEvoy, Risks versus benefits of different types of long-acting injectable antipsychotics, J Clin Psychiatry, 67 Suppl 5 (2006) 15-18.
[114] T. Kishimoto, A. Robenzadeh, C. Leucht, S. Leucht, K. Watanabe, M. Mimura, M. Borenstein, J.M. Kane, C.U. Correll, Long-acting injectable vs oral antipsychotics for relapse prevention in schizophrenia: a meta-analysis of randomized trials, Schizophr Bull, 40 (2014) 192-213.
[115] A. Fortea, D. Ilzarbe, L. Espinosa, M. Solerdelcoll, C. de Castro, G. Oriolo, G. Sugranyes, I. Baeza, Long-Acting Injectable Atypical Antipsychotic Use in Adolescents: An Observational Study, J Child Adolesc Psychopharmacol, 28 (2018) 252-257.

[116] P. Jacob, S. Shere, J.V.S. Kommu, The use of first-generation long-acting injectable antipsychotics in children and adolescents-A retrospective audit from India, Asian J Psychiatr, 61 (2021) 102663.
[117] A. Markham, Cabotegravir Plus Rilpivirine: First Approval, Drugs, 80 (2020) 915-922.
[118] M.A. Tegenge, R.J. Mitkus, A physiologically-based pharmacokinetic (PBPK) model of squalene-containing adjuvant in human vaccines, J Pharmacokinet Pharmacodyn, 40 (2013) 545-556.
[119] D.A. Margolis, J. Gonzalez-Garcia, H.J. Stellbrink, J.J. Eron, Y. Yazdanpanah, D. Podzamczer, T. Lutz, J.B. Angel, G.J. Richmond, B. Clotet, F. Gutierrez, L. Sloan, M.S. Clair, M. Murray, S.L. Ford, J. Mrus, P. Patel, H. Crauwels, S.K. Griffith, K.C. Sutton, D. Dorey, K.Y. Smith, P.E. Williams, W.R. Spreen, Long-acting intramuscular cabotegravir and rilpivirine in adults with HIV-1 infection (LATTE-2): 96-week results of a randomised, open-label, phase 2b, non-inferiority trial, Lancet, 390 (2017) 1499-1510.
[120] R. Parasrampuria, S.L. Ford, Y. Lou, C. Fu, K.K. Bakshi, A.R. Tenorio, C. Trezza, W.R. Spreen, P. Patel, A Phase I Study to Evaluate the Pharmacokinetics and Safety of Cabotegravir in Adults With Severe Renal Impairment and Healthy Matched Control Participants, Clin Pharmacol Drug Dev, 8 (2019) 674-681.
[121] U.S Food & Drug Administration, FDA Label VOCABRIA (cabotegravir) tablets, for oral use, (2021).
[122] A.H. Krist, A. Crawford-Faucher, Management of newborns exposed to maternal HIV infection, Am Fam Physician, 65 (2002) 2049-2056.
[123] F. Bunglawala, R.K.R. Rajoli, M. Mirochnick, A. Owen, M. Siccardi, Prediction of dolutegravir pharmacokinetics and dose optimization in neonates via physiologically based pharmacokinetic (PBPK) modelling, J Antimicrob Chemother, 75 (2019) 640-647.
[124] P.A. Dennery, D.S. Seidman, D.K. Stevenson, Neonatal hyperbilirubinemia, N Engl J Med, 344 (2001) 581-590.
[125] D.F. Clarke, R.J. Wong, L. Wenning, D.K. Stevenson, M. Mirochnick, Raltegravir in vitro effect on bilirubin binding, Pediatr Infect Dis J, 32 (2013) 978-980.
[126] C.N. Schreiner, C.E. Ahlfors, R.J. Wong, D.K. Stevenson, D.F. Clarke, M. Mirochnick, In Vitro Study on the Effect of Maraviroc or Dolutegravir on Bilirubin to Albumin Binding, Pediatr Infect Dis J, 37 (2018) 908-909.
[127] G.M. Pacifici, R. Nottoli, Placental transfer of drugs administered to the mother, Clin Pharmacokinet, 28 (1995) 235-269.
[128] U.S. Department of Health and Human Services: AIDSinfo, Guidelines for the Use of Antiretroviral Agents in Adults and Adolescents Living with HIV, 2018.
[129] C.C. Chang, M. Crane, J. Zhou, M. Mina, J.J. Post, B.A. Cameron, A.R. Lloyd, A. Jaworowski, M.A. French, S.R. Lewin, HIV and co-infections, Immunol Rev, 254 (2013) 114-142.

[130] A.D. Rodrigues, Drug-drug interactions, 2nd ed., Informa Healthcare, New York, 2008.
[131] U.S Food & Drug Administration, Guidance for industry: physiologically based pharmokinetic analyses - format and content, (2018).
[132] X. Zhuang, C. Lu, PBPK modeling and simulation in drug research and development, Acta Pharm Sin B, 6 (2016) 430-440.
[133] C. Marzolini, R. Rajoli, M. Battegay, L. Elzi, D. Back, M. Siccardi, Physiologically Based Pharmacokinetic Modeling to Predict Drug-Drug Interactions with Efavirenz Involving Simultaneous Inducing and Inhibitory Effects on Cytochromes, Clin Pharmacokinet, 56 (2017) 409-420.
[134] D. Moj, N. Hanke, H. Britz, S. Frechen, T. Kanacher, T. Wendl, W.E. Haefeli, T. Lehr, Clarithromycin, Midazolam, and Digoxin: Application of PBPK Modeling to Gain New Insights into Drug-Drug Interactions and Co-medication Regimens, AAPS J, 19 (2017) 298-312.
[135] Drugbank, Doravirine; DB12301, 2018.
[136] U.S Food & Drug Administration, PIFELTRO™ (doravirine) tablets, 2018.
[137] D.M. Brainard, K. Kassahun, L.A. Wenning, A.S. Petry, C. Liu, J. Lunceford, N. Hariparsad, R. Eisenhandler, A. Norcross, E.P. DeNoia, J.A. Stone, J.A. Wagner, M. Iwamoto, Lack of a clinically meaningful pharmacokinetic effect of rifabutin on raltegravir: in vitro/in vivo correlation, J Clin Pharmacol, 51 (2011) 943-950.
[138] S.L. Ford, Y. Lou, N. Lewis, M. Kostapanos, R. D'Amico, W. Spreen, P. Patel, Effect of rifabutin on the pharmacokinetics of oral cabotegravir in healthy subjects, Antivir Ther, 24 (2019) 301-308.
[139] K.M. Han, D. Spreen, W. Ford, SL. , Impact of UGT Induction by Rifampin and Rifabutin on Cabotegravir Long-Acting Pharmacokinetics for HIV Pre-exposure Prophylaxis (PrEP) using Population Pharmacokinetic Modeling and Simulation, HIV Research for Prevention HIVR4P Virtual, 2021.
[140] Drugbank, Rifabutin DB00615, 2018.
[141] U.S Food & Drug Administration, MYCOBUTIN; Rifabutin capsules, USP, U.S Food & Drug Administration, 2014.
[142] B. Reinach, G. de Sousa, P. Dostert, R. Ings, J. Gugenheim, R. Rahmani, Comparative effects of rifabutin and rifampicin on cytochromes P450 and UDP-glucuronosyl-transferases expression in fresh and cryopreserved human hepatocytes, Chem Biol Interact, 121 (1999) 37-48.
[143] Pharmaceuticals and Medical Devices Agency (PMDA), BICTEGRAVIR/EMTRICITABINE/TENOFOVIR ALAFENAMIDE FIXED-DOSE COMBINATION (B/F/TAF FDC): Pharmacokinetics Written Summary, 2018.
[144] E. Callegari, J. Lin, S. Tse, T.C. Goosen, V. Sahasrabudhe, Physiologically-Based Pharmacokinetic Modeling of the Drug-Drug Interaction of the UGT Substrate Ertugliflozin

Following Co-Administration with the UGT Inhibitor Mefenamic Acid, CPT Pharmacometrics Syst Pharmacol, 10 (2021) 127-136.
[145] P. Aceves Baldo, J. Anzures-Cabrera, D. Bentley, In vivo evaluation of drug-drug interactions linked to UGT inhibition: the effect of probenecid on dalcetrapib pharmacokinetics, Int J Clin Pharmacol Ther, 51 (2013) 215-218.
[146] European Medicines Agency, Guideline on the reporting of physiologically based pharmacokinetic (PBPK) modelling and simulation, European Medicines Agency 2018.
[147] S.G. Khalilieh, K.L. Yee, R.I. Sanchez, R. Liu, L. Fan, M. Martell, H. Jordan, M. Iwamoto, Multiple Doses of Rifabutin Reduce Exposure of Doravirine in Healthy Subjects, J Clin Pharmacol, 58 (2018) 1044-1052.
[148] T.G. Jacobs, C. Marzolini, D.J. Back, D.M. Burger, Dexamethasone is a dose-dependent perpetrator of drug-drug interactions: implications for use in people living with HIV, J Antimicrob Chemother, 77 (2022) 568-573.
[149] A. Lafeuillade, Eliminating the HIV reservoir, Curr HIV/AIDS Rep, 9 (2012) 121-131.
[150] M.J. Churchill, S.G. Deeks, D.M. Margolis, R.F. Siliciano, R. Swanstrom, HIV reservoirs: what, where and how to target them, Nat Rev Microbiol, 14 (2016) 55-60.
[151] J.T. Kimata, A.P. Rice, J. Wang, Challenges and strategies for the eradication of the HIV reservoir, Curr Opin Immunol, 42 (2016) 65-70.
[152] M.A. Swartz, The physiology of the lymphatic system, Adv Drug Deliv Rev, 50 (2001) 3-20.
[153] K.L. Gill, I. Gardner, L. Li, M. Jamei, A Bottom-Up Whole-Body Physiologically Based Pharmacokinetic Model to Mechanistically Predict Tissue Distribution and the Rate of Subcutaneous Absorption of Therapeutic Proteins, AAPS J, 18 (2016) 156-170.
[154] E. Offman, C. Phipps, A.N. Edginton, Population physiologically-based pharmacokinetic model incorporating lymphatic uptake for a subcutaneously administered pegylated peptide, In Silico Pharmacol, 4 (2016) 3.
[155] D.K. Shah, A.M. Betts, Towards a platform PBPK model to characterize the plasma and tissue disposition of monoclonal antibodies in preclinical species and human, J Pharmacokinet Pharmacodyn, 39 (2012) 67-86.
[156] L. Zhao, P. Ji, Z. Li, P. Roy, C.G. Sahajwalla, The antibody drug absorption following subcutaneous or intramuscular administration and its mathematical description by coupling physiologically based absorption process with the conventional compartment pharmacokinetic model, J Clin Pharmacol, 53 (2013) 314-325.
[157] A. Supersaxo, W.R. Hein, H. Steffen, Effect of molecular weight on the lymphatic absorption of water-soluble compounds following subcutaneous administration, Pharm Res, 7 (1990) 167-169.
[158] E. Burgunder, J.K. Fallon, N. White, A.P. Schauer, C. Sykes, L. Remling-Mulder, M. Kovarova, L. Adamson, P. Luciw, J.V. Garcia, R. Akkina, P.C. Smith, A.D.M. Kashuba,

Antiretroviral Drug Concentrations in Lymph Nodes: A Cross-Species Comparison of the Effect of Drug Transporter Expression, Viral Infection, and Sex in Humanized Mice, Nonhuman Primates, and Humans, J Pharmacol Exp Ther, 370 (2019) 360-368.
[159] U.S.F.D. Administration, Isentress (raltegravir potassium) tablet label, (2011).
[160] U.S.F.D. Administration, Sustiva (efavirenz) tablets label, (2011).
[161] C. Csajka, C. Marzolini, K. Fattinger, L.A. Decosterd, J. Fellay, A. Telenti, J. Biollaz, T. Buclin, Population pharmacokinetics and effects of efavirenz in patients with human immunodeficiency virus infection, Clin Pharmacol Ther, 73 (2003) 20-30.
[162] N. Bachmann, C. von Siebenthal, V. Vongrad, T. Turk, K. Neumann, N. Beerenwinkel, J. Bogojeska, J. Fellay, V. Roth, Y.L. Kok, C.W. Thorball, A. Borghesi, S. Parbhoo, M. Wieser, J. Boni, M. Perreau, T. Klimkait, S. Yerly, M. Battegay, A. Rauch, M. Hoffmann, E. Bernasconi, M. Cavassini, R.D. Kouyos, H.F. Gunthard, K.J. Metzner, H.I.V.C.S. Swiss, Determinants of HIV-1 reservoir size and long-term dynamics during suppressive ART, Nat Commun, 10 (2019) 3193.
[163] N.M. Archin, D.M. Margolis, Emerging strategies to deplete the HIV reservoir, Curr Opin Infect Dis, 27 (2014) 29-35.
[164] L. Kinman, S.J. Brodie, C.C. Tsai, T. Bui, K. Larsen, A. Schmidt, D. Anderson, W.R. Morton, S.L. Hu, R.J. Ho, Lipid-drug association enhanced HIV-1 protease inhibitor indinavir localization in lymphoid tissues and viral load reduction: a proof of concept study in HIV-2287-infected macaques, J Acquir Immune Defic Syndr, 34 (2003) 387-397.
[165] C. Solas, A. Lafeuillade, P. Halfon, S. Chadapaud, G. Hittinger, B. Lacarelle, Discrepancies between protease inhibitor concentrations and viral load in reservoirs and sanctuary sites in human immunodeficiency virus-infected patients, Antimicrob Agents Chemother, 47 (2003) 238-243.
[166] S.R. Dyavar, N. Gautam, A.T. Podany, L.C. Winchester, J.A. Weinhold, T.M. Mykris, K.M. Campbell, Y. Alnouti, C.V. Fletcher, Assessing the lymphoid tissue bioavailability of antiretrovirals in human primary lymphoid endothelial cells and in mice, J Antimicrob Chemother, 74 (2019) 2974-2978.
[167] M.A. Boyd, N.M. Dixit, U. Siangphoe, N.E. Buss, M.P. Salgo, J.M. Lange, P. Phanuphak, D.A. Cooper, A.S. Perelson, K. Ruxrungtham, Viral decay dynamics in HIV-infected patients receiving ritonavir-boosted saquinavir and efavirenz with or without enfuvirtide: a randomized, controlled trial (HIV-NAT 012), J Infect Dis, 194 (2006) 1319-1322.
[168] S. Iwami, B.P. Holder, C.A. Beauchemin, S. Morita, T. Tada, K. Sato, T. Igarashi, T. Miura, Quantification system for the viral dynamics of a highly pathogenic simian/human immunodeficiency virus based on an in vitro experiment and a mathematical model, Retrovirology, 9 (2012) 18.
[169] B.L. Jilek, M. Zarr, M.E. Sampah, S.A. Rabi, C.K. Bullen, J. Lai, L. Shen, R.F. Siliciano, A quantitative basis for antiretroviral therapy for HIV-1 infection, Nat Med, 18 (2012) 446-451.

[170] E.M. Ferlay J, Lam F, Colombet M, Mery L, Pinero M, et al., Global Cancer Observatory: Cancer Today, (2020).
[171] T.P. Padera, E.F. Meijer, L.L. Munn, The Lymphatic System in Disease Processes and Cancer Progression, Annu Rev Biomed Eng, 18 (2016) 125-158.
[172] D.S. Spencer, A.S. Puranik, N.A. Peppas, Intelligent Nanoparticles for Advanced Drug Delivery in Cancer Treatment, Curr Opin Chem Eng, 7 (2015) 84-92.
[173] P. Mian, K. Allegaert, S. Conings, P. Annaert, D. Tibboel, M. Pfister, K. van Calsteren, J.N. van den Anker, A. Dallmann, Integration of Placental Transfer in a Fetal-Maternal Physiologically Based Pharmacokinetic Model to Characterize Acetaminophen Exposure and Metabolic Clearance in the Fetus, Clin Pharmacokinet, 59 (2020) 911-925.